BEHAVIORAL STUDIES OF THE ALCATOR C AND DOUBLET III FUSION MACHINE POWER SUPPLIES

by

N. E. Rasmussen
J. G. Kassakian

Electric Power Systems Engineering Laboratory
and
Plasma Fusion Center

School of Engineering
Massachusetts Institute of Technology

September 1979

This work was supported by the U. S. Department of Energy through the MIT Plasma Fusion Center.

PFC/RR-80-4

ABSTRACT

The use of very high power ac to dc thyristor rectifier type power converters as electromagnetic field energy sources for Tokamak fusion reactors results in unusual performance and design problems. In this study, physical scale models of two such power supplies are constructed at power levels approximately one-million times smaller than the actual systems, for purposes of simulation prior to full scale operation. Simulation results reveal certain undesirable aspects of power supply operation which were not previously appreciated. New analytical models are introduced which can be used to predict performance with improved accuracy.

TABLE OF CONTENTS

TABLE OF CONTENTS CONTINUED

TABLE OF CONTENTS CONTINUED

INTRODUCTION

Confinement and heating coils in large Tokamak type fusion reactors require high energy pulses of regulated dc power for durations of .5 to 2 seconds. To supply this power the use of dedicated variable frequency alternators becomes practical as Tokamak peak input power levels excede 100 megawatts. The rotational mass of the alternator is used as an energy storage device (flywheel) and rotational energy is electrically removed through the armature by operating the alternator into a Tokamak-loaded thyristor rectifier set.

The operation of large alternator-driven thyristor type power supplies presents many unusual performance and stability problems which have not been encountered before in power systems engineering.

Traditionally, multi-megawatt alternators are designed and specified for operation into balanced, three-phase loads whose impedance changes slowly when compared with the electrical alternator frequency. Operating such an alternator into a phase controlled thyristor rectifier set of comparable KVA rating causes the alternator to see a load impedance which changes dramatically over the course of a single ac cycle and which can give rise to step functions

of alternator load or power factor.

The general solution of the ac to dc converter performance problem is available for converters operating in the rectifier mode from simple reactive sources[1,2,3] and has been used by Preag[4] and others to design electric utility supplied Tokamaks. Unfortunately, these solutions are not adequate for use in systems in which the converter represents nearly the entire rated load of an alternator, since in this case the alternator cannot be represented as a simple reactive source. Behavior of multi-megawatt alternators under both steady state and transient loading can be determined from published models[5,6] using the machine specifications. These models must be extended to allow for power converter type loads, since the non-linear load presented to the alternator by the thyristor power converter gives rise to severe alternator waveform distortion.

A thyristor rectifier set is normally designed to be driven form a stiff (low reactance) ac source. When a rectifier set is supplied from an alternator of comparable KVA rating, the rectifier source can no longer be considered stiff and reactances associated with the alternator must be taken into account when determining the loaded dc rectifier output voltage. System performance can only be predicted and consequently a design can only be attempted when the alternator/rectifier interface is understood.

It is the purpose of this study to investigate phenomena at the alternator/rectifier interface including:

A) The effect of rapid rectifier phase control variations on internal alternator voltages and exciter control loops.

B) Inter-supply cross coupling resulting from simultaneous operation of two or more supplies from the same alternator.

C) The mechanisims responsible for alternator waveform distortion.

D) The effect of alternator waveform distortion on converter phase-referencing circuits.

The MIT Alcator C Tokamak and the General Atomic Doublet III Tokamak are both alternator driven and currently under construction (1979). In this study, physical scale models of the plasma confinement and ohmic heating supplies for both the Alcator C and Doublet III Tokamaks are constructed.

The practicality of the scale model technique, as applied to converter/alternator systems, has been succesfully demonstrated by Blake[7]. The models are constructed using a one kilowatt model alternator, two six-pulse phase controlled thyristor rectifier sets, a six-hundred joule model confinement coil, and a fifty-five joule model ohmic heating coil. The model alternator and coil parameters are adjusted to appropriate scaled values, and the two rectifier sets

are programmed to generate specified time functions of the scaled coil currents. The experimental work for this thesis was carried out in the MIT Electric Power Systems Engineering Laboratory, where an available model alternator[8,9] was modified to satisfy the requirements of this study.

In chapter I, the scale model of the MIT Alcator C power supply system is described, and the experimental results are presented. The development of chapter II is parallel to that of chapter I except in this case the General Atomic Doublet III power supply is simulated.

The results of the scale model of the Alcator C power supply revealed that the output capablilities of the design were below specification. Unfortunately, the scale model study could not be used to determine the relative importance of the various mechanisims which together resulted in the sub-specification performance. Consequently, in chapter III, a special computer model is developed to supply additional data for use in a performance analysis.

In chapter IV the results of the Alcator C simulations of chapters I and III are brought together and used to determine the reason for the sub-specification performance and find modifications which could be used to raise performance.

The results of the General Atomic Doublet III

simulation of chapter II revealed that dangerous transients of the alternator terminal voltage result from system operation. In chapter IV a simplified model is proposed to explain these transients. Also, modifications to the Doublet III system which can remove these transients are proposed.

In chapter V, fundamental performance limitations of regulated alternator driven phase controlled rectifier type power supplies are examined.

CHAPTER I

PHYSICAL SCALE MODEL OF ALCATOR C POWER SUPPLY SYSTEM

In this chapter, the physical scale model of the M.I.T. Alcator C power supply is described, and experimental results are presented. First, the actual Alcator C power supply is briefly described, along with the function that it is expected to perform. Next, the physical scale model is introduced, and correspondence between the model and the actual system is demonstrated. Finally, actual measurements from the model, in the form of oscillograms, are presented, from which the expected performance of the real Alcator C power supply is directly inferred.

1.1 System to be modelled

The basic Alcator C machine is composed of three coils, which provide magnetic fields for the confinement, ohmic heating, and equilibrium of the experimental plasma. Each of these coils is excited during an experiment using energy extracted from the rotational inertia of the rotor of a 225 MW 3-phase turbo-alternator. The energy is electrically extracted by operating the alternator in the conventional manner, the alternator output being stepped down by a pulse-rated transformer group to supply the Alcator C coils via a combination of thyristor rectifier sets.

At the end of an experiment, a significant fraction of the lost alternator rotational energy remains in the magnetic fields of the coils. Most of this energy is returned to the alternator by rectifier phase-controlled inversion, in which case the alternator is operated as a synchronous motor. All energy dissipated by coil resistance must be absorbed by the liquid nitrogen coil coolant. The amount of energy stored in the magnetic field of the TF coil is approximately 80 MJ during the experiment. If none of this energy were returned to the alternator, then over 400,000 liters of gaseous nitrogen would be generated by coolant vaporization after each experiment. Clearly, rapid, efficient inversion of the stored TF coil energy is desirable.

In this study, the interactions between the rectifier sets and the alternator are of primary interest. The alternator energy transfer associated with equilibrium supply operation is smaller than that associated with the heating or confinement supplies; additionally, the equilibrium supply does not operate at all during the critical charging of the confinement field, or during the time of peak alternator loading. Consequently, in this study, only the operations of the confinement (TF or Toroidal Field) and ohmic heating (OH) supplies are modelled, which constitute around 89% and 11%, respectively, of the peak alternator load.

The interconnections of the major parts of the Alcator C, TF and OH supplies are shown in figure 1-1. The specified

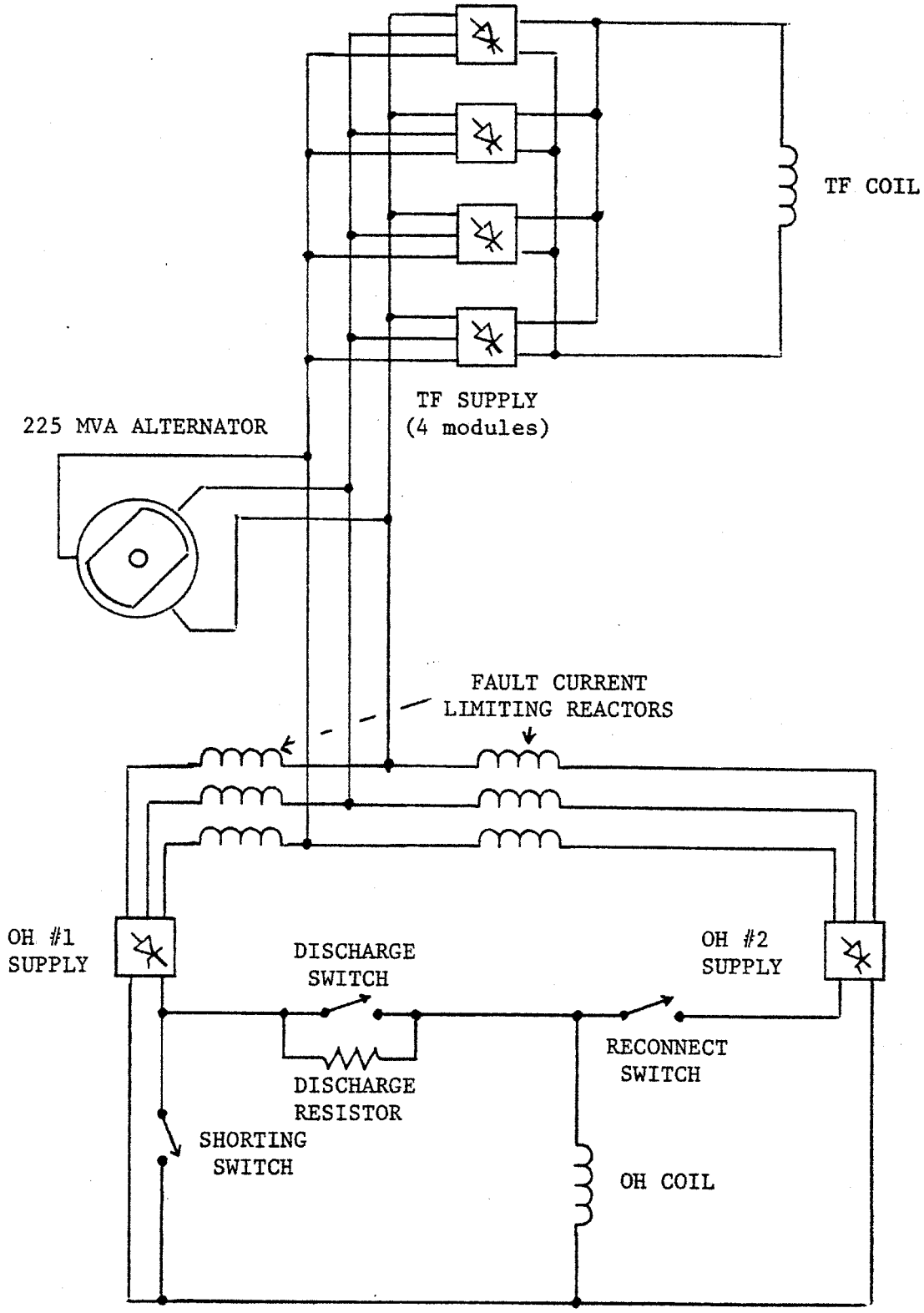

Figure 1-1: Interconnections of Alcator C power supply

time-functions of the TF and OH coil currents are shown in figures 1-2 and 1-3. The sequence of TF supply operations which give rise to the current profile of figure 1-2 is explained:

Phase 1: TF current ramp-up period. During this period, the TF supply rectifier set is operated without intentional phaseback, that is, in the simple rectifier mode. The TF supply output voltage jumps from a pre-phase 1 value of 0 Vdc to a value in the neighborhood of 1000 Vdc. As phase 1 continues, the current in the inductive TF coil rises, being accompanied by a steady decrease of the supply output voltage. The supply output voltage falls due to a combination of (A) voltage lost to the rectifier commutation reactance; (B) voltage lost to internal supply resistances; (C) voltage lost due to decay of the alternator speed; and (D) voltage lost due to decay of alternator flux. The fraction of the unloaded supply output voltage which is lost due to these effects approaches 40 to 50 percent as the end of phase 1 is approached.

Phase 2: TF current flat-top period. When the TF coil current reaches the preset value of 200 kA (lower preset values can also be used) the TF supply thyristor-rectifiers are operated with intentional phaseback. The phaseback is adjusted by a closed-loop feedback system in order to regulate the coil current at the preset value. The current is to be held constant despite the fall of the alternator voltage and variations of the real and imaginary

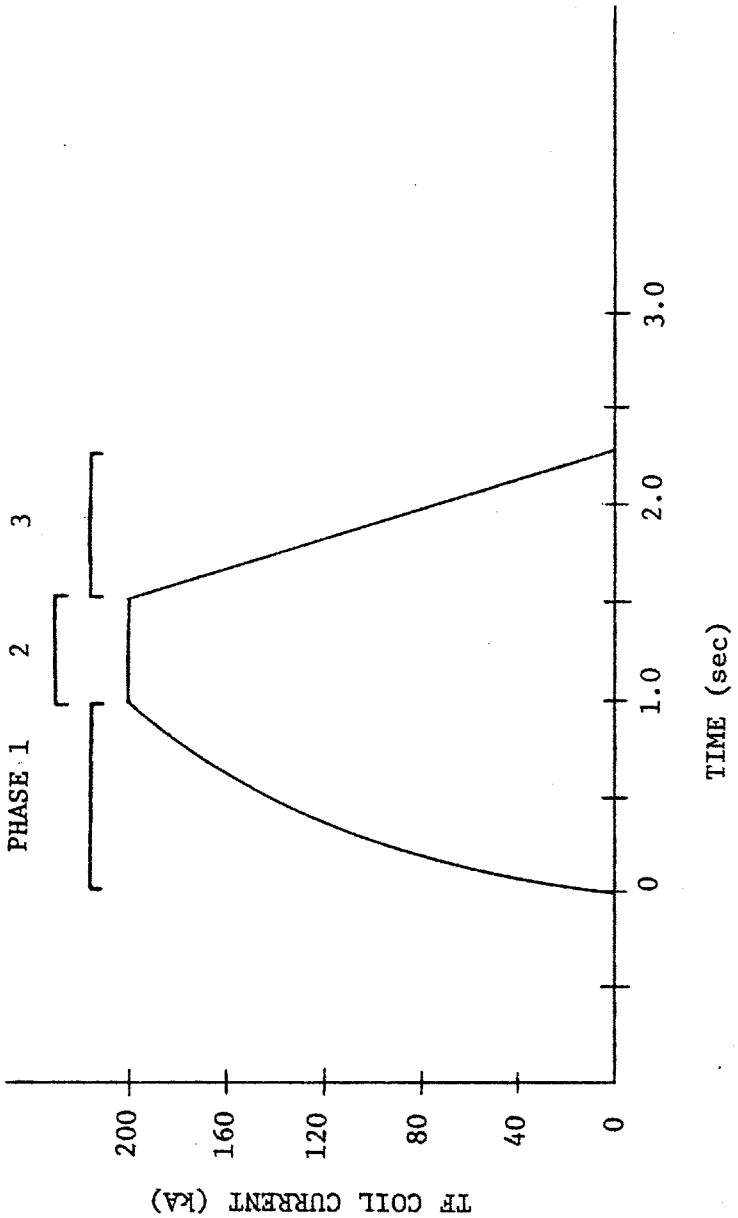

Figure 1-2: Alcator C TF coil current profile

parts of the TF coil impedance which result from coil heating and the generation of the experimental plasma. The duration of the flat-top period is adjustable, with a nominal value of .5 seconds.

Phase 3: TF current inversion period. When the flat-top period has ended, the rectifier set is phased back to delay angles greater than 90 degrees in order to invert the TF coil current. In this case, the dc coil voltage will be opposite in sign from the pre-phase 3 voltage, while coil induction forces the current to continue in the same direction. Consequently, the direction of power transfer is reversed, and energy is removed from the TF coil. The inversion voltage must be a carefully controlled function of the TF coil current during the current ramp-down, in order to guarantee successful rectifier commutation. Commutation failure causes the rectifier set to short-circuit, forcing the load current to decay at the natural load L/R time constant, dissipating the remaining stored magnetic energy as heat.

The sequence of OH supply operations which give rise to the current profile of figure 1-3 is explained:

Phase 1: OH coil ramp-up period. During this period, one half of the OH supply is connected across the OH coil and operated without phase-back. As in the TF coil ramp-up, the current in the inductive OH coil rises and is accompanied by falling supply output voltage.

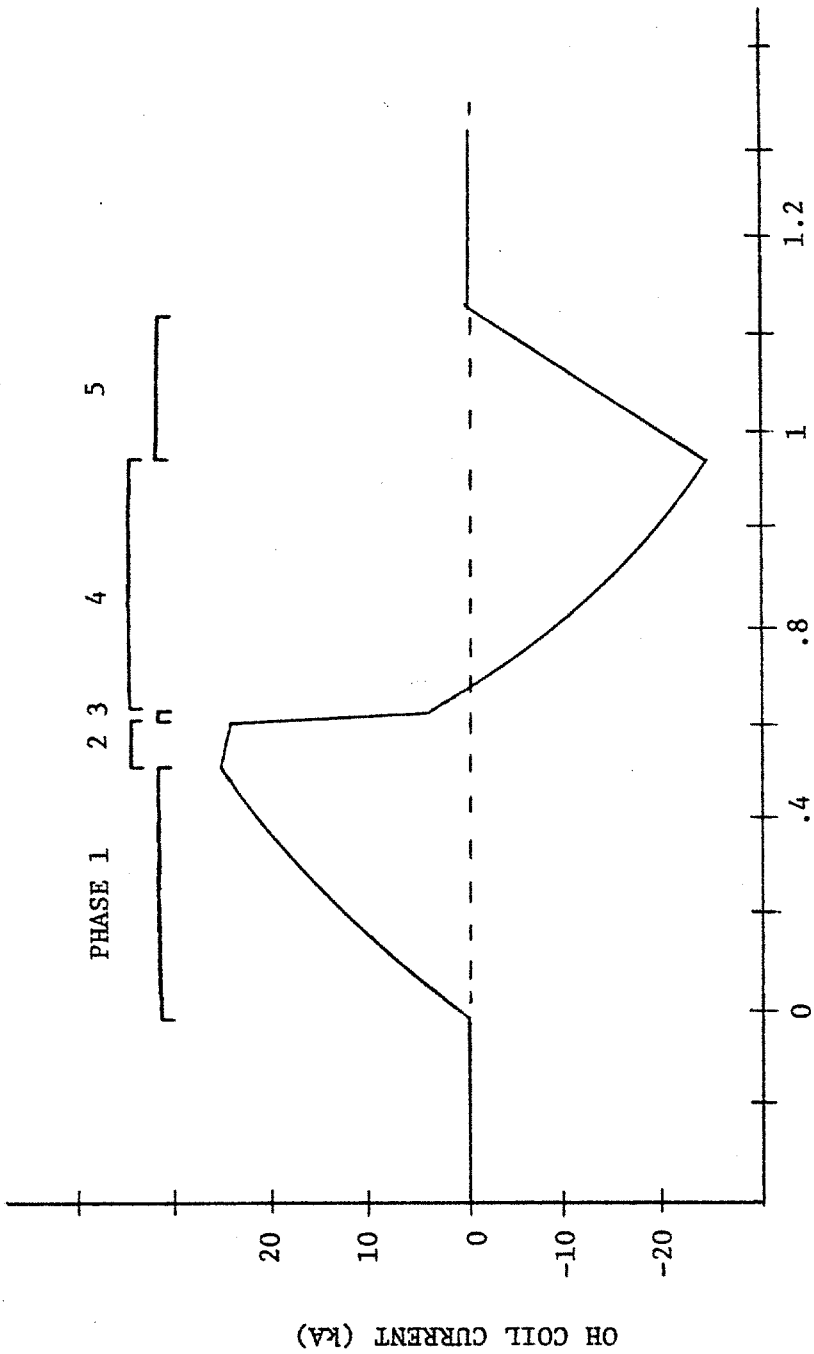

Figure 1-3: Alcator C OH coil current profile

Phase 2: OH coil crowbar period. When the OH coil current reaches approximately 25 kA, the supply is rapidly phased back to a slightly negative dc output voltage and is immediately shorted at the output with high current switch S1. At this point, the supply current goes to zero due to rectifier misfire, while the OH coil current continues to circulate through the crowbar switch, decaying at the natural OH coil L/R time constant. Once the OH supply current is known to be zero, the supply is disconnected by opening another switch, isolating the OH coil/crowbar switch loop.

Phase 3: OH coil discharge period. When the OH supply is safely disconnected, OH coil discharge is initiated. A resistor with a value of around 5 Ω is connected in parallel with the switch S2; when the switch is opened, signalling the beginning of the OH coil discharge period, the entire coil current of nearly 25 kA is forced to circulate through this resistor. The L/R time constant of this circuit is approximately 5 ms; consequently, the initial OH coil current decays rapidly.

Phase 4: Second OH coil ramp-up period. When the OH coil voltage falls to around 500 Vdc, the second half of the OH supply is connected across the coil using switch S3. The connection is such that the polarity of the rectifier output voltage is opposite to that used during the ramp-up of phase 1; therefore, the current ramps in the opposite direction. Timing of the entire OH supply

cycle is adjusted so that this second OH coil ramp-up period begins and ends with the TF flat-top period. During this phase, the OH supply may be operated with phaseback, in order to control the shape of the current ramp.

Phase 5: OH coil inversion period. At the end of the second OH current ramp, the experiment is over, and as in the TF case, significant energy remains in the OH coil. Again, much of this energy can be returned to the alternator to prevent coil heating by using phase-controlled inversion.

The first step in the construction of a physical scale model of a rectifier power supply is to represent the modeled system by a one line impedance diagram; the system of figure 1-1 can be reduced to the one line impedance diagram of figure 1-4. Next, the values of the impedances in the one line diagram are scaled. Finally, the scaled values are realized using actual components, and an operating model system is constructed.

1.2 Physical scale model scale factors

In theory, the relationship between a physical scale model and the modelled system is completely described by the so called "model scale factors". In this study, we are interested in the electrical behavior of the systems under investigation, and it is therefore necessary to define model scale factors for:

time, voltage, current, power, energy, and resistance

These scale factors must be selected in order that certain defining relationships are preserved by the actual/model system transformation, and these relationships can be reduced to:

energy = power x time
voltage = current x resistance
power = voltage^2/resistance

the model scale factors used in this study were selected in accordance with the following four constraints:

(A) The limited energy capacity (1/2 I^2L) of the available TF power supply inductive load model

(B) The fixed synchronous reactance of the available model alternator

(C) The constraint that the time scale factor be 1:1

(D) The practical constraint that the model power level be as high as possible, in order to avoid measurement and control errors due to thyristor holding current, thryistor forward voltage drop, and electromagnetic interference

These combined constraints on energy, reactance, and time are sufficient, when applied to the described defining relationships, to constrain all model scale factors.

The selected model scale factors for the Alcator C physical scale model are given in table 1, along with the actual and model values of the parameters required to describe the alternator, the supplies, and the loads. The required parameters include those from the one line impedance diagram of figure 1-4, as well as parameters commonly used to characterize the alternator.

In practice, the relationship between the model system and the actual system is not completely described by model scale factors, since some characteristics of the actual system are neglected, or represented by the model over limited regions of operation. Often, the operation of the modeled system is understood well enough, prior to modeling, to guarantee that the neglected characteristics will contribute tolerable, compensatable, or zero error. When prior knowledge of system operation is inadequate, justifications of model compromises are made by constructing the model and experimentally observing that the boundaries of unrepresented operational modes are not approached. In this study, these techniques have been used to verify model design. A complete design of a simple model reactor, for example, must address issues of saturation characteristic, resistance, core loss, insulation breakdown voltage, fusing current, capacitance, etc. However, in the descriptions of the Alcator C model subassemblies which follow, only those model limitations which significantly affect the experimental results are mentioned.

TABLE I

PARAMETERS OF ALCATOR C POWER SUPPLY SYSTEM MODEL

MODEL SCALE FACTORS (referred to alternator side of transformers):

POWER	1 MODEL WATT	CORRESPONDS TO	818,181 ACTUAL WATTS
VOLTAGE	1 MODEL VOLT	CORRESPONDS TO	90.6 ACTUAL VOLTS
CURRENT	1 MODEL AMP	CORRESPONDS TO	9021 ACTUAL AMPS
TIME	1 MODEL SEC	CORRESPONDS TO	1 ACTUAL SEC

ALTERNATOR PARAMETERS:

PARAMETER	ACTUAL VALUE	MODEL VALUE	COMMENT
X_d	1.41 pu	1.41 pu	synchronous reactance
X_d'	.265 pu	.26 pu	transient reactance
X_d''	.165 pu	.165 pu	subtransient reactance
T_{do}'	7.01 s	7.0 s	open circuit field τ
T_d'	1.09 s	1.1 s	short circuit field τ
H	2.36 s	2.36 s	inertia constant
V_{base}	14.4 kV	159 V	
I_{base}	9021 A	1.0 A	
P_{base}	225 MVA	275 VA	
f_{base}	60 hz	60 hz	

TF SUPPLY PARAMETERS:

Coil L	4.5 mH	114.5 H	
Coil R	2.2 mΩ	56 Ω	
X_{trans}	.28 pu	68.1 mH	pu on alternator base
R_{trans}	.3 mΩ	7.6 Ω	referred to load side
Turns Ratio	16:1	1:1	
$X_{ac\ bus}$	.05 pu	12 mH	pu on alternator base
$R_{dc\ bus}$	.5 mΩ	13.7 Ω	

OH SUPPLY PARAMETERS:

Coil L	13 mH	91.3 H	
Coil R	5 mΩ	35.1 Ω	
X_{trans}	2.42 pu	587 mH	pu on alternator base
R_{trans}	1.04 pu	95 Ω	
Turns Ratio	16.8:1	2:1	
$X_{cl\ react}$	.347 pu	84.3 mH	pu on alternator base
$R_{cl\ react}$	.046 pu	5.0 Ω	pu on alternator base

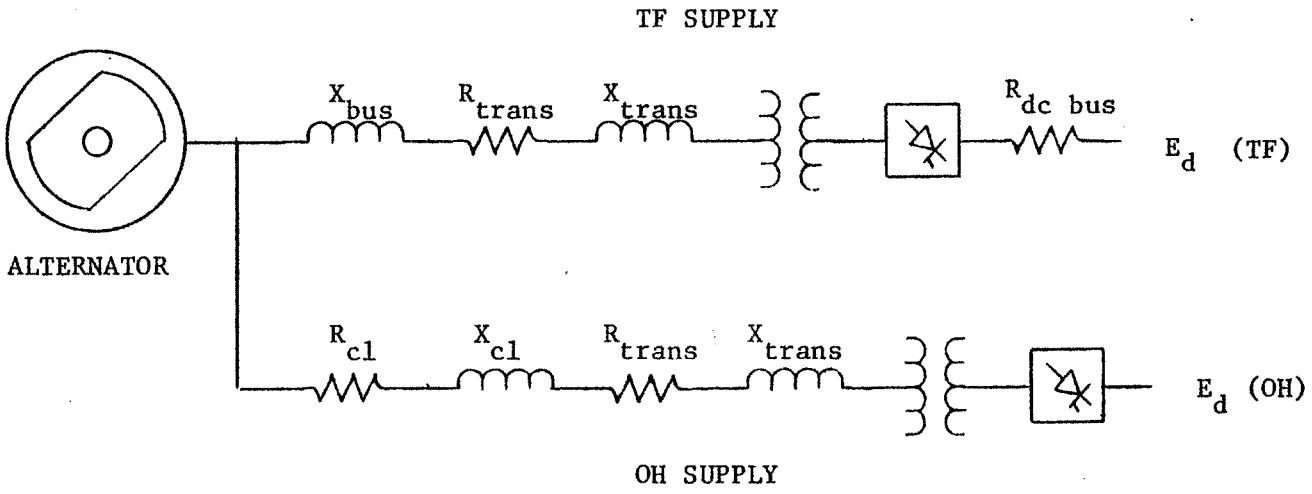

Figure 1-4: One line impedance diagram of Alcator C power supply

1.3 Physical scale model construction

Thy physical scale model of the Alcator C power supply system can be broken down into five basic subassemblies, which are:

(1) Model alternator
(2) Model TF supply
(3) Model TF supply load
(4) Model OH supply
(5) Model OH supply load

The interconnection of the subassemblies is illustrated in the model system diagram of figure 1-5. Functional descriptions for each of the five subassemblies are given in the following subsections. Detailed circuit descriptions are found in Appendix B.

1.3.1 Model alternator

Located in the MIT Electric Power Systems Laboratory are a unique group of small (approximately 1 kW) alternators. These alternators were constructed as accurate scale models of large turbo-generators used in the American Electric Power Company's system. In this study, we have chosen to modify one of these models in such a way that it can serve as a scale model of the G.E. alternator used in the Alcator C power supply. To this end, the time constants and per-unit reactances of the selected model alternator were adjusted, following the procedures outlined by Blake;[1] these procedures are summarized in the following paragraphs.

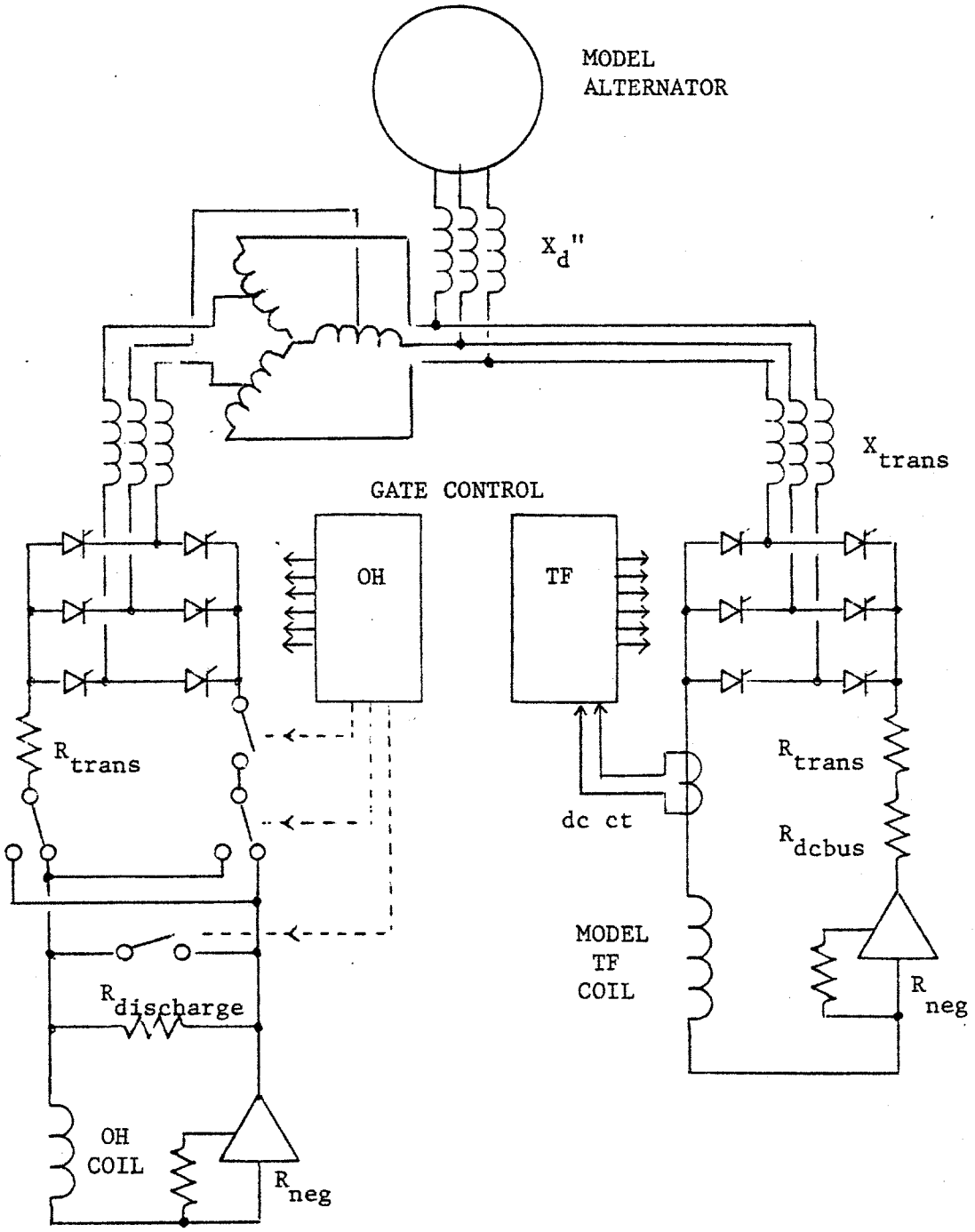

Figure 1-5: Alcator C scale model system diagram

It was determined that the synchronous reactance of the model alternator was the most difficult parameter to adjust, and consequently it was not modified. Since we desire the per-unit value of this impedance to correspond to the given Alcator C alternator value, our decision immediately fixes the base impedance of the model alternator. Combining this constraint with the one-to-one time scaling and the given maximum inductive load model energy, we find that the base power, current, and voltage are also specified (this follows from the requirement that the ratio of the alternator base power to the peak inductive load energy must be the same in both the model and actual systems). With this knowledge, the desired values of the model machine parameters can be computed.

The subtransient reactance (X_d'') of the unmodified model alternator is smaller than the required value; therefore external reactors are added at the alternator terminals to build up the subtransient reactance to the desired value.

The transient reactance (X_d') of the model alternator is adjusted to the required value by the addition of reactance in series with the rotor winding.

The open circuit transient time constant (T_d') is adjusted by changing the resistance in series with the rotor winding.

The inertia constant (H) of the unmodified model is much larger than the required value. Since the inertia constant is defined as the ratio of the stored rotational energy at

rated speed to the base power, it is necessary to decrease the rotational inertia of the machine. This is accomplished by making use of a dc motor which is attached to the model alternator rotor shaft. The torque supplied by this motor is made proportional to the rate of change of the rotor rotational speed by using a special circuit. Consequently, the motor serves as a brake when the alternator supplies power to the load, and the motor acts to increase rotor speed when the load supplies power to the alternator. In this way, the apparent rotational inertia of the alternator is decreased.

1.3.2 Model TF supply

The TF supply rectifier set model consists of six thyristors connected in the standard six-pulse rectifier configuration. The rectifier set is supplied from the ac bus (alternator output) through a rectifier transformer model. The model transformer turns ratio is selected to be one-to-one, allowing the rectifier transformer to be simply represented by its resistance and its leakage and magnetizing reactances; since the magnetizing current is much smaller than the peak (loaded) transformer input current, we replace the magnetizing branch of the transformer with an open circuit. The transformer, then, is represented by inductors with a value equal to the pu value of the leakage reactance of the actual transformer, the inductors being

connected in series with each of the three input phases to the rectifier bridge; and by a single resistance in series with the output of the rectifier bridge with a value equal to the pu value of the transformer resistance.

The model rectifier set is driven by a gate firing circuit which is capable of rectification, regulation, and inversion with load current controlled margin angle. The gate firing circuit is slave to a "profile generator" circuit which controls the sequence and timing of the three phases of TF supply operation (described in section 1.1). A dc current transformer senses the supply output for use by the gate firing circuits during the closed-loop regulation phase and the open-loop controlled inversion phase. Gate timing reference signals are derived from attenuated alternator terminal voltage.

An additional reactance is placed in series with each of the three ac input phases to the TF supply model to model the reactance of the ac bus which connects the supply to the alternator in the actual system.

1.3.3 Model TF supply load

The TF coil is represented by a simple L-R circuit. In order to determine load model component values, the actual TF coil parameters are expressed in pu on the alternator base, where in this case the base impedance is reflected to the secondary (load side) of the rectifier transformer.

The resulting pu values are then multiplied by the model base impedance to arrive at the load model values.

The available inductive load model is set to the proper value by adjusting the length of the inductor air-gap and selecting the appropriate inductor tap. Unfortunately, the model load resistance in this case is larger than the required value. To compensate for the excessive resistance, a negative resistor (refer to figure 1-5) is inserted in series with the load model. The negative resistor is gyrated using a floating, non-inverting, 150 Watt, broadband, dc coupled power amplifier. The connection of the load model, including the negative resistor, is shown in figure 1-5.

An additional resistance is used to connect the model TF supply to the load in order to model the resistance of the actual dc interconnection bus.

1.3.4 Model OH supply

The OH supply model consists of six thyristors connected in the six-pulse rectifier configuration, a rectifier transformer model, a model of the supply current limiting reactors, and an OH coil switching network.

Two OH supplies are used in the actual Alcator C system; however, in the mode of OH operation that we represent in this study (push-pull operation) the supplies are never operated simultaneously. Consequently, we have added relay switches in addition to those required in the actual

system in order to allow a single model supply to effectively "change positions" and perform the function of a twin-supply system.

The turns ratio for this model is selected to be 2:1 (step down) so that the required OH load inductance (a function of the turns ratio) lies in a conveniently simulated range. In particular, the large peak model OH coil voltage (20 kV in the actual system) was held below the 2 kV model OH coil design/test voltage by this turns ratio selection.

The reactance on the ac side of the rectifier in the actual OH supply consists of two parts; namely, the transformer reactance and the current limiting reactance. The total of these two reactances (in pu) must be equal in the model and actual systems. The reactances of the selected model transformers were supplemented by external reactors to raise the total model ac reactance to the required value.

The rectifier set is driven by a gate firing circuit which is capable of operation at preset open loop firing angles. The gate firing circuit is driven by a "profile generator" circuit which controls the sequence and timing of the five phases of OH supply operation (described in section 1.1). This profile generator also drives the OH coil switching network. The OH sequence is initiated by a command from the TF supply model in order that the TF and OH supplies operate in the prescribed time relationship.

In addition to the OH switching which is specified in the description of the five OH supply operational phases, a supply output reversal is performed during the crowbar (third) phase to accomplish the twin supply emulation described above. Conventional electro-mechanical relays are used for all switches in the OH switching network.

1.3.5 Model OH supply load

The OH coil is represented by a simple L-R circuit. The values of the components used in the model are determined as in the TF case (section 1.3.3) except that in this case the turns ratio of the model transformer must be taken into account. The pu value of the load, as viewed from the alternator through the transformer, must be the same in both the model and actual systems.

A 60 Joule model inductor was adjusted to the appropriate value. Unfortunately, the time constant of the model load was small due to excessive dc resistance. As in the TF case, a wideband dc coupled power amplifier was connected as a negative resistor and used to lower the effective resistance to the required value.

1.4 Scale model limitations

The scale model of the Alcator C power supply contains some compromises which may affect the accuracy of the simulation results. These inaccuracies are described in the following paragraphs.

The saturation characteristic of the alternator is not accurately modeled. This is due to the fact that the model scale foctors demanded that the model alternator be operated in a region of negligible saturation, whereas the actual alternator is rated to operate slightly into the curved region of the saturation characteristic. We conclude that errors of the measured supply performance due to this effect are negligible, although measurements of the alternator field current may contain significant errors. The alternator flux does decay considerably during the experiment, and therefore any errors due to lack of saturation become very small during the important flat-top period.

The model TF load inductor exhibits a "soft" saturation characteristic, with measurable saturation extending down to the physical scale model operating level. This saturation amounts to less than a 5% decrease in the effective value of the load inductance at the peak operating current level. This same inductor was used in the work of Blake,[7] however, in that study the inductor was operated at a 50% higher current level and the consequential saturation resulted in findings differing considerably from those of this study.

The resistance of the actual Alcator C TF coil will not be constant during the experiment, but will instead rise as a result of resistive heating from some nominal value to a projected 2.2 milliohms by the end of the flat-top period.

In this study, the projected worstcase value of 2.2 milliohms was assumed for the entire experiment. If the load resistance is substantially lower than this value near the end of the ramp-up period, then the rate of rise of the coil current during that time would be somewhat more rapid than predicted by the physical scale model.

1.5 Scale model tests of Alcator C power supply

The simulation results of the Alcator C physical scale model study are contained in the oscillograms of figures 1-6 through 1-15. The vertical scales represent actual Alcator values of the variables, and were computed using model scale factors. The TF coil voltages were recorded at the coil terminals (after the dc bus resistance) using a 60 Hz two-pole low-pass filter to remove ripple. The ac bus frequency was recorded using an alternator shaft driven tachometer. The slip of the induction motor (used for bringing the alternator up to speed between experiments) was assumed to be 2%. Constant field voltage alternator excitation was used during all experiments.

Figure 1-6: In this figure the TF coil current fails to reach the programmed 200 kA flat-top level; peak TF coil current is 183 kA at 1.7 seconds; initial alternator voltage is 14.6 kV (line to line).

Figure 1-7: With an initial alternator voltage increased to 15.8 kV, the TF coil current again fails to reach the

programmed 200 kA flat-top level; peak TF coil current is 195 kA at 1.6 seconds.

Figure 1-8: With an initial alternator voltage of 15.8 kV the TF coil current easily attains a programmed flat-top level of 150 kA; time to flat-top is .8 seconds while total pulse time is 2.5 seconds.

Figure 1-9: With an initial alternator voltage of 14.8 kV the TF coil current attains a programmed 175 kA flat-top level; in this case the pre-flat-top coil voltage is 590 Vdc, the time to flat-top is 1.2 seconds, and the total pulse duration is 2.75 seconds.

Figure 1-10: In this figure the inversion voltage profile of the TF supply has been programmed to minimize the inversion time (minimum margin angle); the initial alternator voltage is 16.6 kV, the pre-flat-top voltage is 775 Vdc, the time to flat-top is .9 seconds, and the total pulse time is 2.25 seconds.

Figure 1-11: In this figure the alternator frequency variations which accompany power supply operation are shown. The frequency at the end of the pulse is 48.5 Hz, corresponding to an overall alternator kinetic energy loss of 30.5%; inversion is optimized as in the previous case.

Figure 1-12: An expanded view of the TF coil current shows excellent regulation during the flat-top period (better than 1%) and fast settling time. The OH supply output voltage displays the characteristic droop during the two OH coil

ramp-up periods. In the actual Alcator C OH supply system, the two ramp-up periods are handled by different supplies, so that the curve in this figure can be thought of as the sum of the output voltages of the two supplies.

Figure 1-13: This figure shows the bus distortion immunity of the gate firing circuit of the Alcator C TF power supply; the gate firing circuit is required to derive sinusoidal reference voltages from the distorted ac bus voltage in order to determine timing of gate firings; the lack of discontinuities of the derived waveform insures stable rectifier triggering (nevertheless, we have found that the reference waveforms are not optimal, and this limitation is discussed in detail in chapter 5).

Figure 1-14: This figure illustrates the effects of commutation failure during the inversion period; commutation fails at a TF coil current of around 105 kA due to insufficient margin angle. Note that during a commutation failure the inversion voltage is reduced, prolonging the decay of the TF coil current. As the margin angle approaches the commutation overlap angle, rectifier commutation becomes erratic, and the supply output voltage jumps between the desired inversion voltage and zero, providing reduced average inversion voltage; this effect occurs between TF coil currents of 105 kA and 80 kA in the figure. When the margin angle is constantly less than the overlap angle, the average supply output voltage is zero, effectively crowbarring the load

current; this effect occurs between TF coil currents of 60 kA and 50 kA in the figure. In the latter case, the load current will decay at the natural L/R time constant of the TF coil. This condition must be remedied immediately by either (A) phasing forward the rectifier set or (B) crowbarring the entire rectifier set. If one of these steps is not taken, then the entire coil current will continue to circulate in one leg of the rectifier transformer, causing transformer saturation (which will appear as a dc side fault from the ac side). The thermal ratings of the thyristors and/or transformer may also be exceeded.

Figure 1-15: This figure serves to show the OH coil current profile which may result if the switch which initiates the OH coil discharge period fails to clear. The switch arc-over lasts for around .65 seconds, being finally extinguished when the OH coil current falls to 12 kA. The breakdown characteristics of the switch used in this study were not selected to match those of the switch used in the actual system, and therefore the exact shape of the decay of the OH coil current is not significant. Nevertheless, switch clearing must be guaranteed to prevent very high arc power dissipation.

1.6 Summary of Alcator C scale model tests

We have found that the Alcator C TF supply model is capable of generating the prescribed current profile using

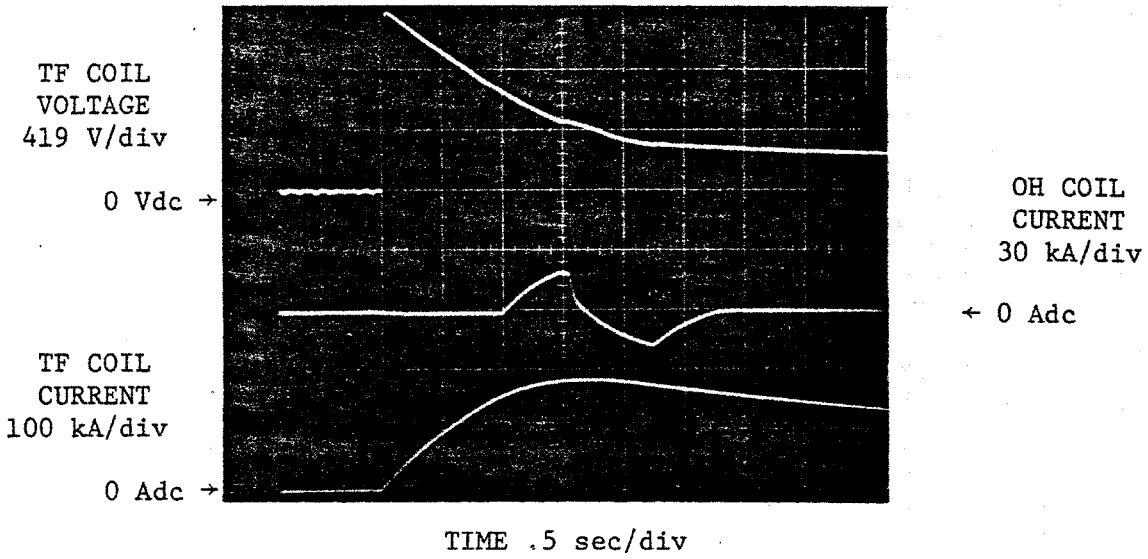

Figure 1-6: Oscillogram showing results from Alcator C power supply model tests; initial alternator voltage = 14.6 kV

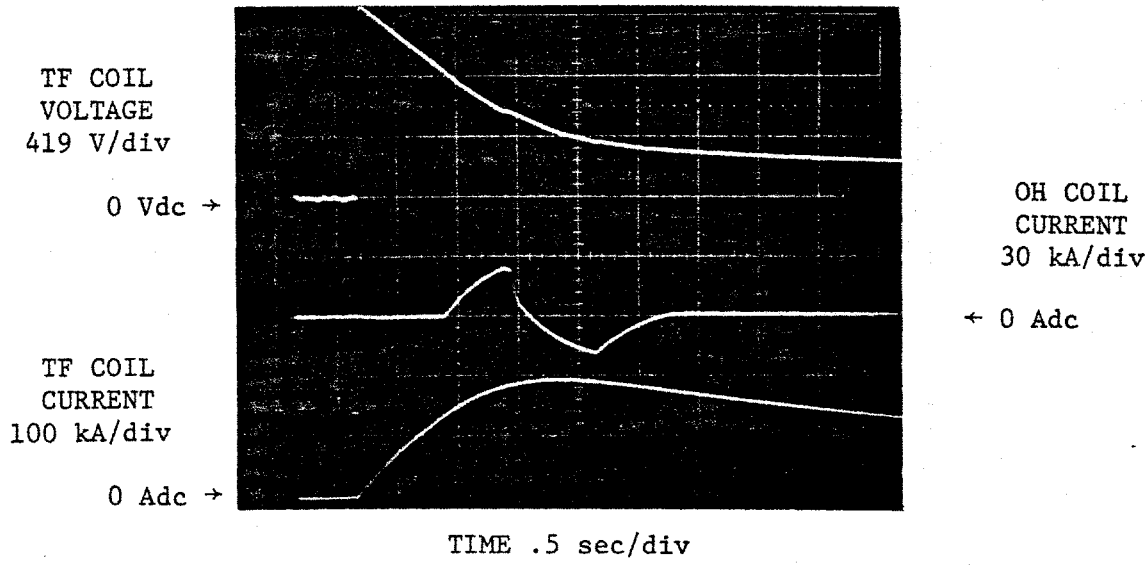

Figure 1-7: Oscillogram showing results from Alcator C power supply model tests; initial alternator voltage = 15.8 kV

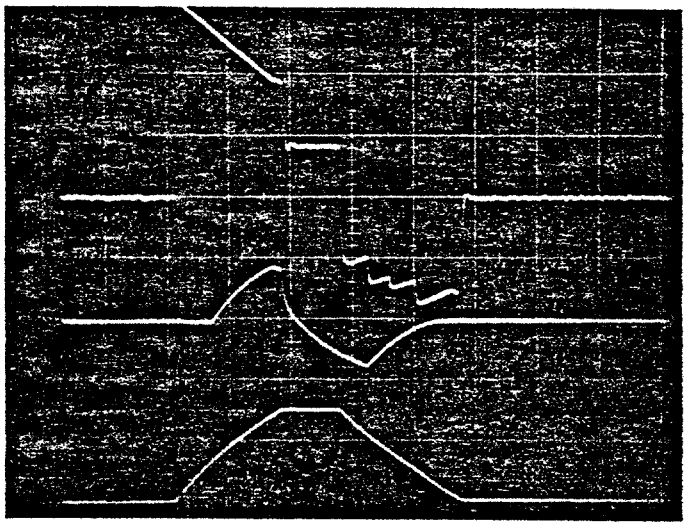

Figure 1-8: Oscillogram showing results from Alcator C power supply model tests; initial alternator voltage = 15.8 kV

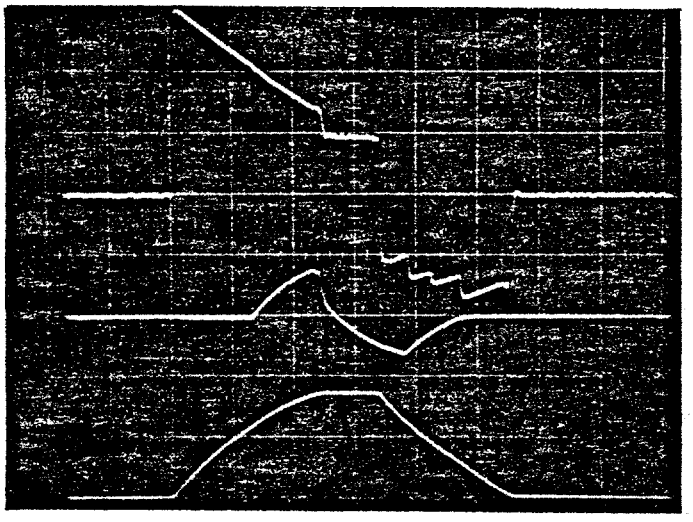

Figure 1-9: Oscillogram showing results from Alcator C power supply model tests; initial alternator voltage = 14.9 kV

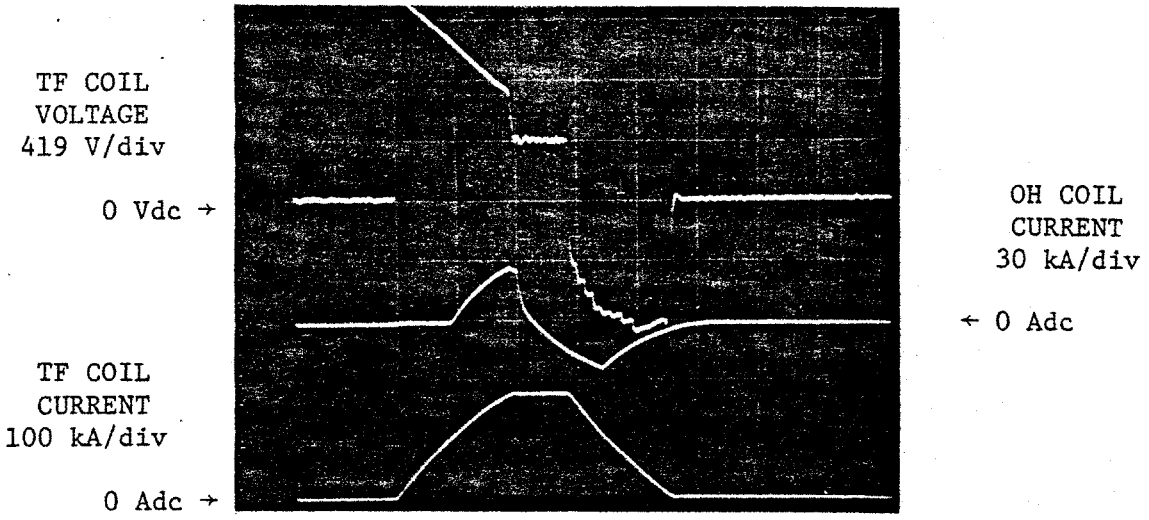

Figure 1-10: Oscillogram showing results from Alcator C power supply model tests; initial alternator voltage = 16.6 kV

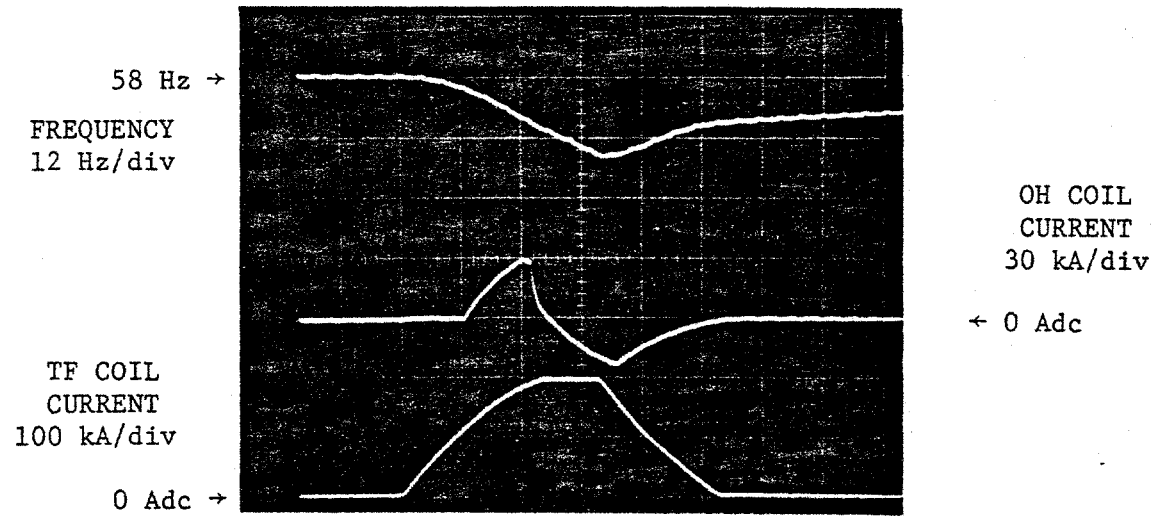

Figure 1-11: Oscillogram showing results from Alcator C power supply model tests; initial alternator voltage = 16.6 kV

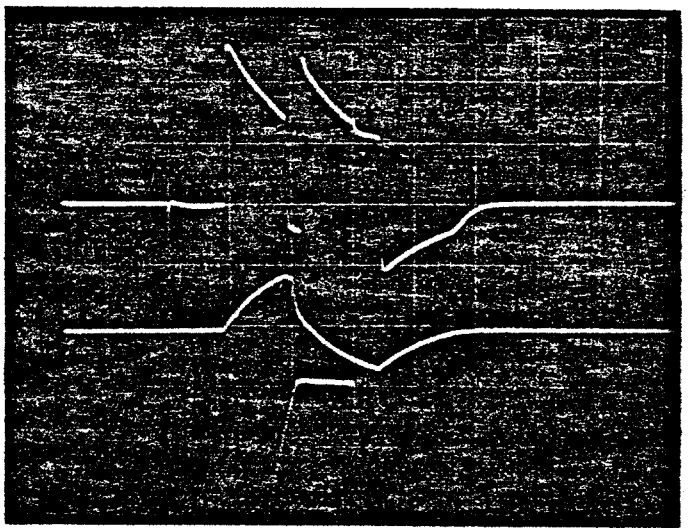

Figure 1-12: Oscillogram showing results from Alcator C power supply model tests; initial alternator voltage = 16.6 kV

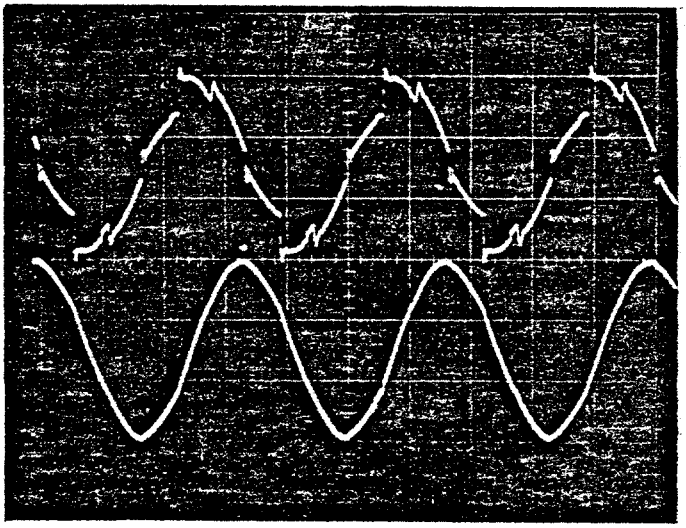

Figure 1-13: Oscillogram showing bus distortion immunity of gate firing circuit

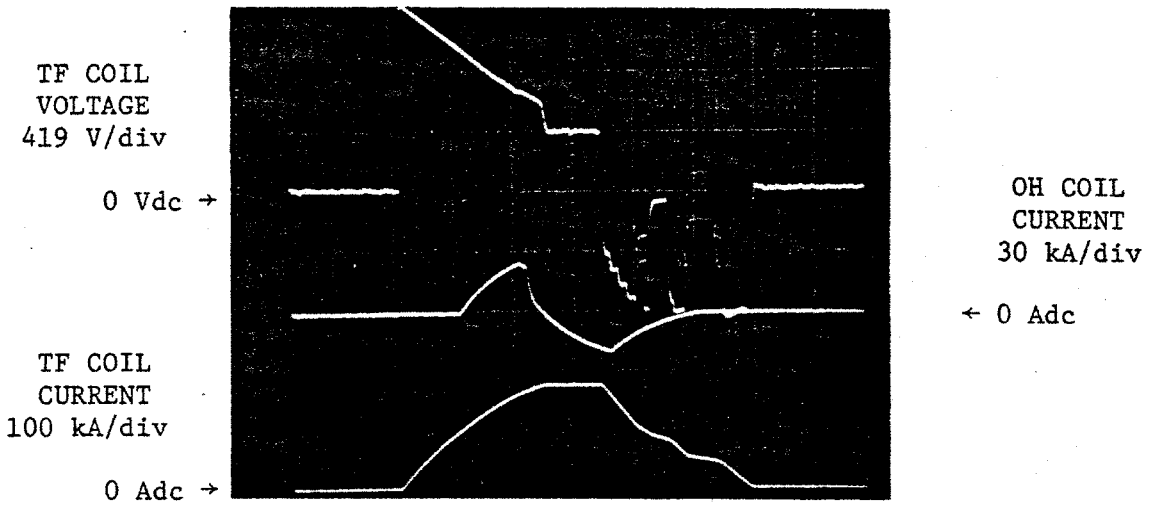

Figure 1-14: Oscillogram showing results from Alcator C power supply model tests; initial alternator voltage = 15.8 kV

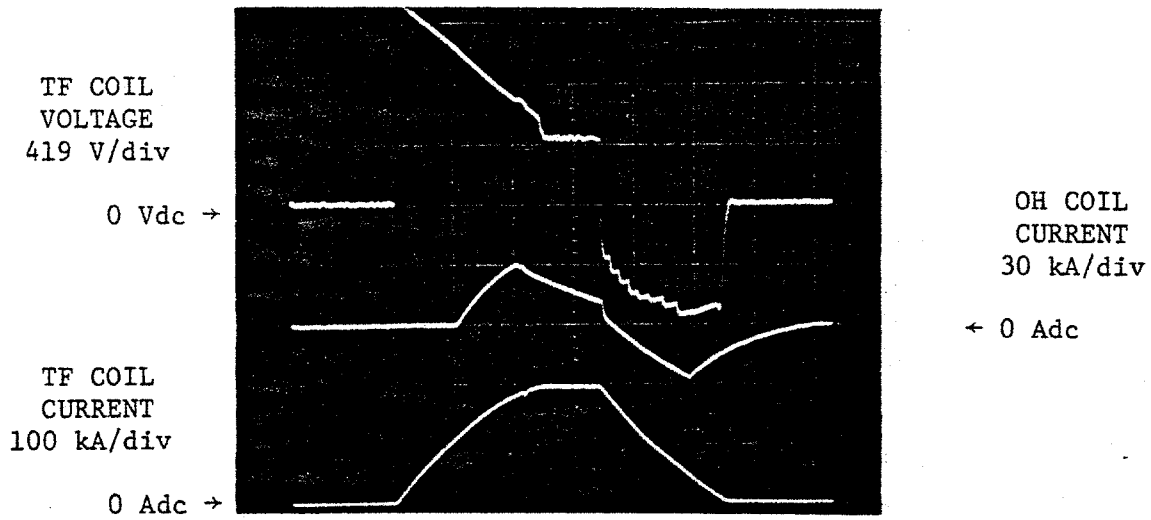

Figure 1-15: Oscillogram showing results from Alcator C power supply model tests; initial alternator voltage = 16.6 kV

15% initial alternator overvoltage. Under this condition, we predict the actual Alcator C pre-flat-top TF coil voltage to be 540 Vdc. This contrasts sharply with the original system design, which specified that the pre-flat-top voltage be 750 Vdc prior to a 200 kA flat-top current level.

The mechanisms responsible for the sub-specification voltage level are described in chapter 4, where the relative contribution of each mechanism is determined.

The Alcator C OH supply was found to be easily capable of generating the prescribed OH coil current profile. It was found that the disconnect and reconnect phases of OH operation did not create unusual bus disturbances.

CHAPTER II

PHYSICAL SCALE MODEL OF DOUBLET III POWER SUPPLY SYSTEM

In this chapter, the physical scale model of the General Atomic Doublet III power supply is described, and experimental results are presented. First, the actual Doublet III power supply is briefly described, along with the function it is expected to perform. Next, the physical scale model is introduced. Due to the similarities between the Doublet III and Alcator C power supplies, many of the parts of the Alcator model are utilized in the Doublet model, although component values are modified to suit the new Doublet III scale factors. Finally, actual measurements from the model, in the form of oscillograms, are presented, from which the expected performance of the real Doublet III power supply is directly inferred.

2.1 System to be modeled

The structure of the Doublet III machine is similar to that of the Alcator C machine, and again the operations of the confinement (TF) and ohmic heating (OH) supplies are modeled. In this case, however, the designed peak power consumptions of the TF and OH coils are nearly equivalent, whereas a 8 to 1 TF to OH peak power ratio was used in

Alcator C. Unfortunately, as a result of the transformer turns ratios selected in the Doublet III system, alternator overcurrents exceeding 70% are possible if the two Doublet III power supplies operate as designed. Therefore, General Atomic has decided to run only half of the OH supply in conjunction with the full TF supply, on order to reduce the peak alternator armature current. Consequently, this configuration (full TF/half OH) is modeled in the following simulations.

A major difference between the Doublet III and Alcator C systems is that Doublet III alternator excitation is supplied by a high speed exciter/regulator which is connected for closed-loop regulation of the alternator terminal voltage. Although the Alcator C experiments can be run effectively using only constant field voltage excitation, the longer Doublet III experimental interval would allow rotor flux decay and consequent alternator ouptut voltage loss if no field forcing had been implemented.

General Atomic discovered during tests of a similar but smaller Doublet II system that unusual and alarming transients of the alternator terminal voltage resulted from system operation. An important motivation for the present scale model study was to identify the mechanisms responsible for the alternator voltage transients and to predict the transients that might be expected during the operation of the new Doublet III system.

The Doublet III system is designed to return the energy remaining in the TF coil to the alternator after the experiment. However, during initial testing and low level operation of the system, a free-wheeling diode (FWD) is to be connected across the TF load. Although a FWD does not allow for inversion of the coil current at the end of an experiment, it does afford some measure of protection in case of rectifier or dc bus failure. If the load current is interrupted at any time during the TF current pulse by rectifier or dc bus failure, the FWD will "pick up" and circulate the TF coil current, allowing it to decay at the natural L/R time constant of the coil. It was desired to know what effect, if any, the FWD might have on system operation, particularly with regard to power supply control strategies and the previously mentioned alternator voltage transients.

The interconnections of the major parts of the Doublet III TF and OH supplies are shown in figure 2-1. The specified time-functions of the TF and OH coil currents are shown in figures 2-2 and 2-3. The sequence of TF supply operations which gives rise to the current profile of figure 2-2 is explained:

> Phase 1: <u>TF current ramp-up period</u>. During this period, the TF supply rectifier set is operated without intentional phaseback. The TF supply output voltage jumps from a pre-phase 1 value of 0 Vdc to a value in the

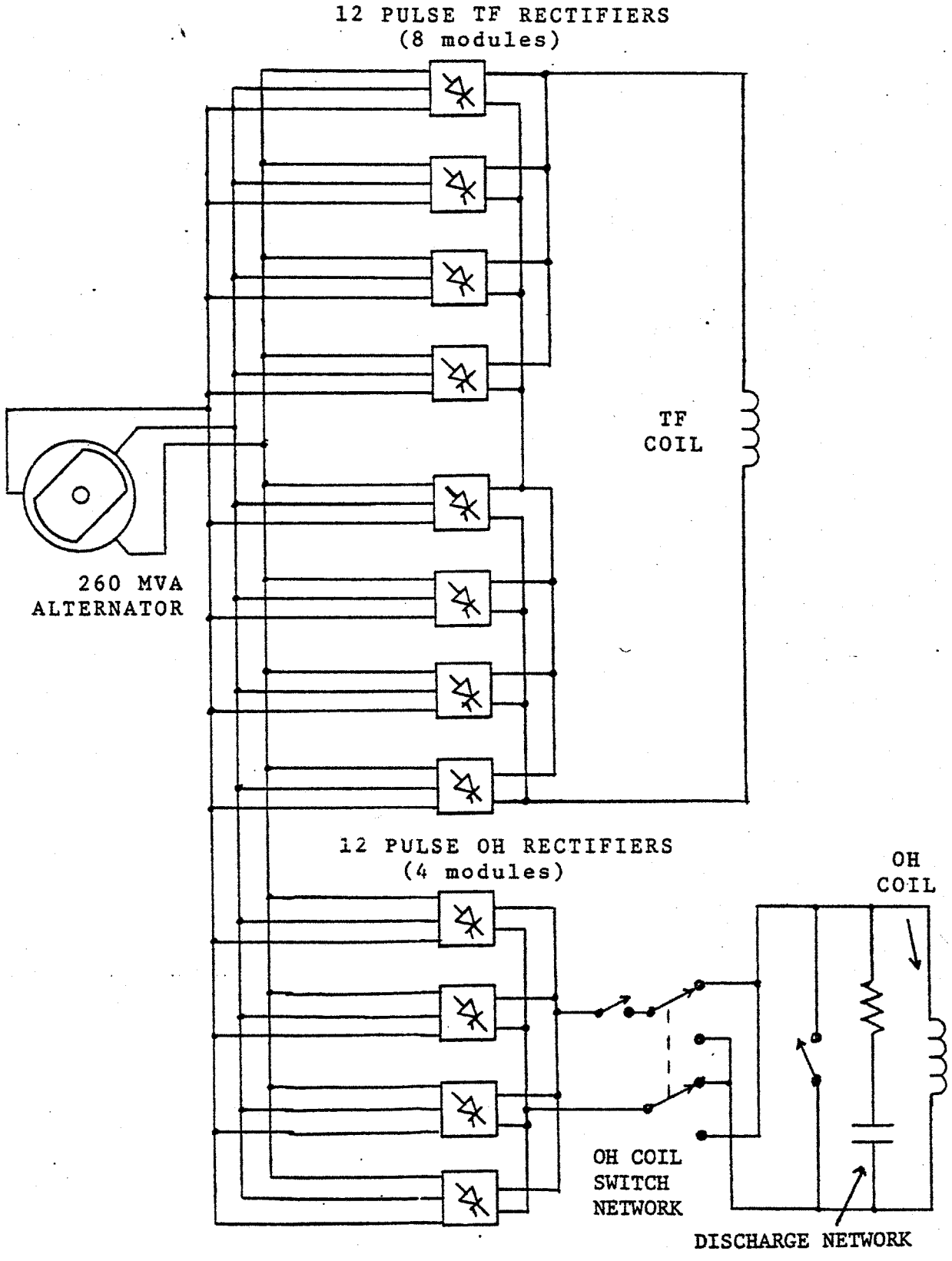

Figure 2-1: Interconnections of Doublet III power supply

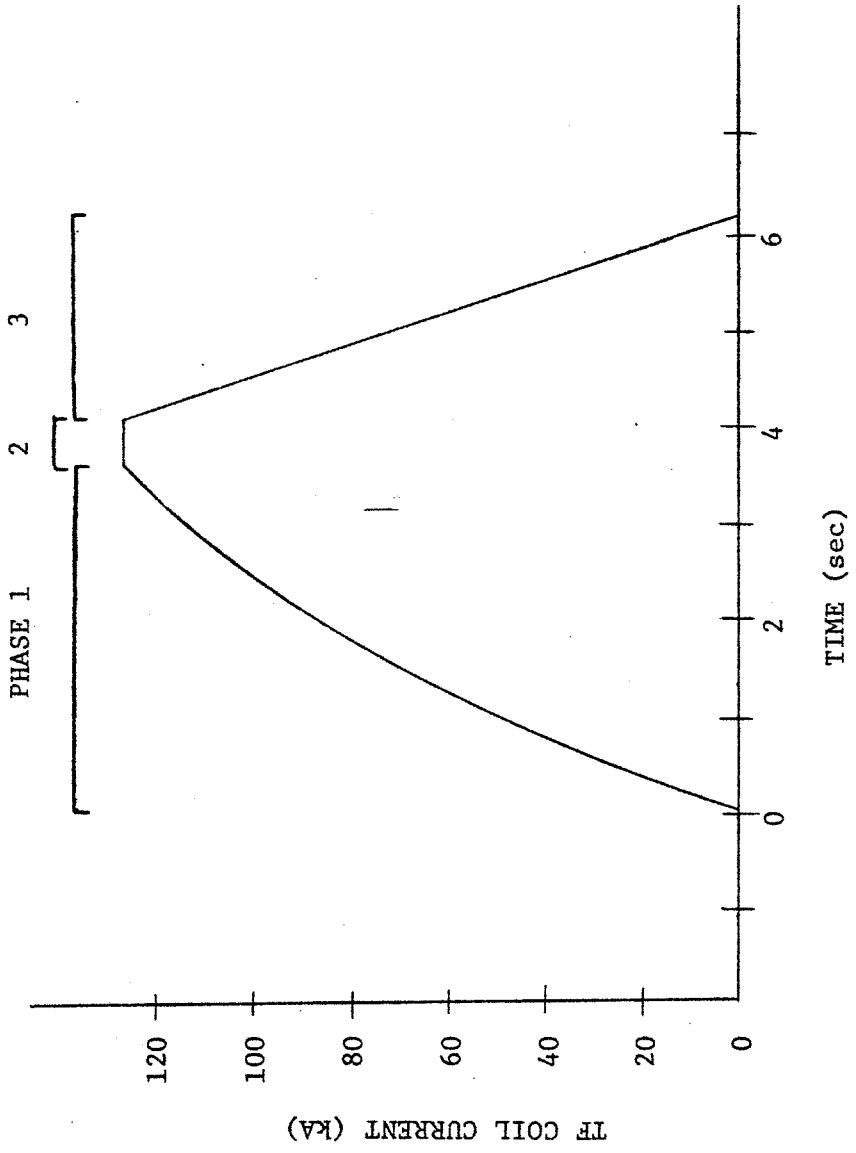

Figure 2-2: Doublet III TF coil current profile

neighborhood of 1500 Vdc. As phase 1 continues, the current in the inductive load rises, being accompanied by a steady decrease of the supply output voltage. The supply output voltage falls due primarily to the voltage lost to the commutation reactance.

Phase 2: TF current flat-top period. When the TF coil current reaches the preset value of 126 kA the TF supply is phased back to the regulation mode. As in the Alcator C experiments, the duration of the flat-top period is .5 seconds.

Phase 3: TF coil inversion period. When the flat-top period has ended, the rectifier set is phased back to delay angles of greater than 90 degrees in order to invert the coil current and return the remaining stored magnetic TF coil energy to the alternator. If a FWD is placed across the load, then the coil current will abruptly cease to flow through the rectifier set upon rectifier phaseback, and no energy is returned to the alternator. In this case the coil current decays with the natural L/R time constant.

The sequence of OH supply operations which gives rise to the current profile of figure 2-3 is explained:

Phase 1: OH coil ramp-up period. During this period the OH supply is connected across the OH coil and operated as a simple rectifier. As in the TF case, the inductive OH coil current rises, being accompanied by falling supply output voltage.

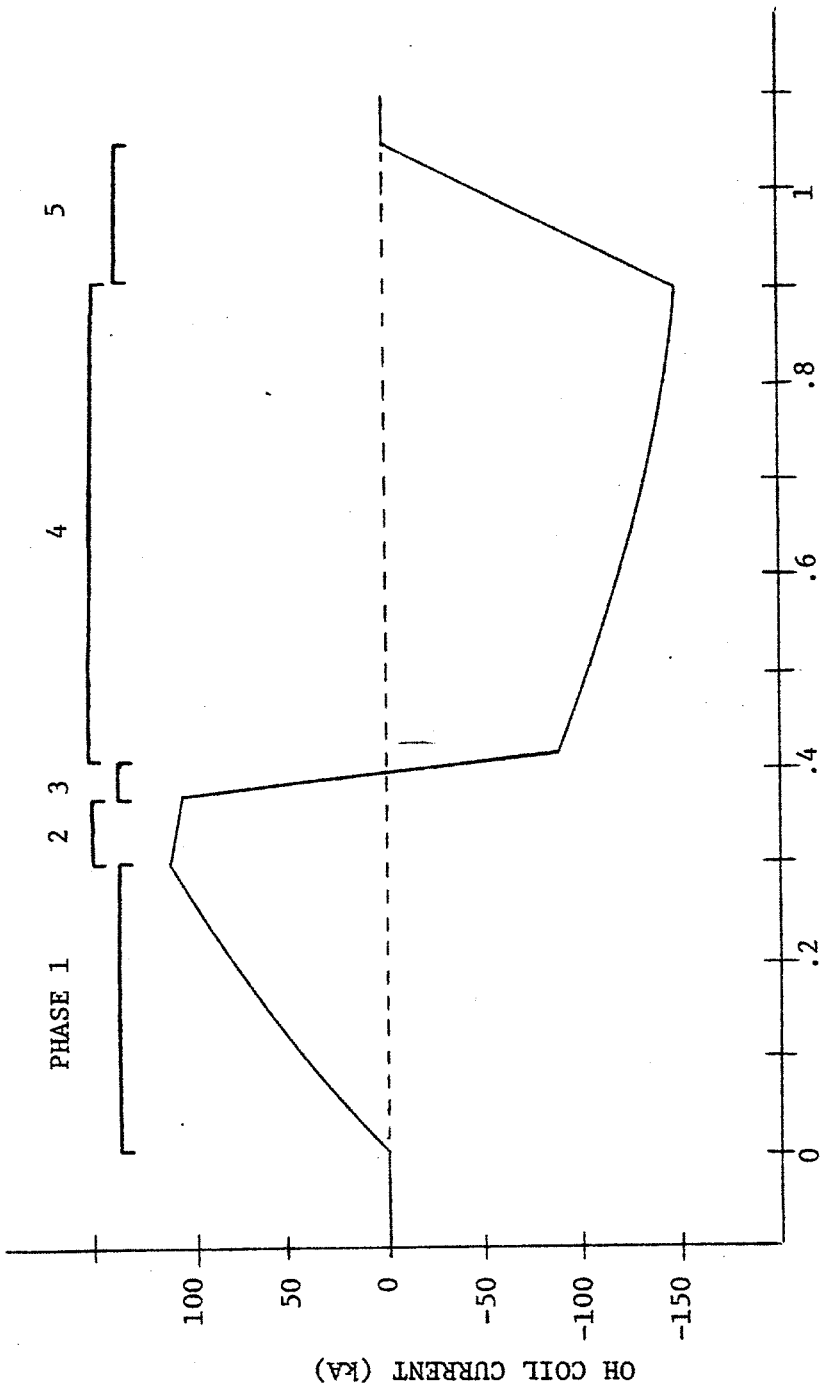

Figure 2-3: Doublet III OH coil current profile

Phase 2: OH coil crowbar period. When the OH coil current reaches 110 kA, the supply is rapidly phased back and shorted with a crowbar switch. This results in supply misfire, causing the coil current to circulate in the OH coil/crowbar switch loop. When the OH supply current is known to be zero, the supply is disconnected using a second switch. The output polarity of the supply is now changed using a DPDT reversing switch, in preparation for the 4th phase.

Phase 3: OH coil discharge period. When the OH supply is safely disconnected, OH discharge is initiated. A capacitor/resistor combination is connected in parallel with the crowbar switch; when the switch is opened, signalling the beginning of the discharge period, the entire coil current of nearly 110 kA is forced through the R-C branch resulting in a damped oscillation with a natural frequency of around 3.5 Hz. The OH coil current falls rapidly, reversing direction as the capacitor begins to return energy.

Phase 4: Second OH coil ramp-up period. When the OH coil current reaches a value of -85 kA, the OH supply is reconnected and phased on. The polarity of the supply is reversed from that of the first phase due to the reversal switching which took place during phase 2; therefore, the current ramps in the opposite direction. Timing of the entire OH supply cycle is adjusted so that this second OH coil ramp-up period begins and ends with the TF flat-top period.

Phase 5: OH coil inversion period. At the end of the second OH ramp-up period, the OH supply is inverted to return the remaining OH coil magnetic energy to the alternator.

As in the case of the Alcator C system the first step towards the construction of a physical scale model is to represent the modeled system by a one-line impedance diagram. This is accomplished in figure 2-4. Next the impedances are scaled, and the scaled values are then used in the construction of the physical scale model.

2.2 Physical scale model scale factors

The model scale factor selection is accomplished using the principles and constraints outlined in chapter 1. The selected scale factors for the Doublet III model are listed in table 2. along with the actual and model values of the system parameters.

2.3 Physical scale model construction

The physical scale model of the Doublet III power supply system can be broken down into six subassemblies, which are:

(1) Model alternator
(2) Model TF supply
(3) Model TF supply load
(4) Model OH supply
(5) Model OH supply load
(6) Model alternator exciter/regulator

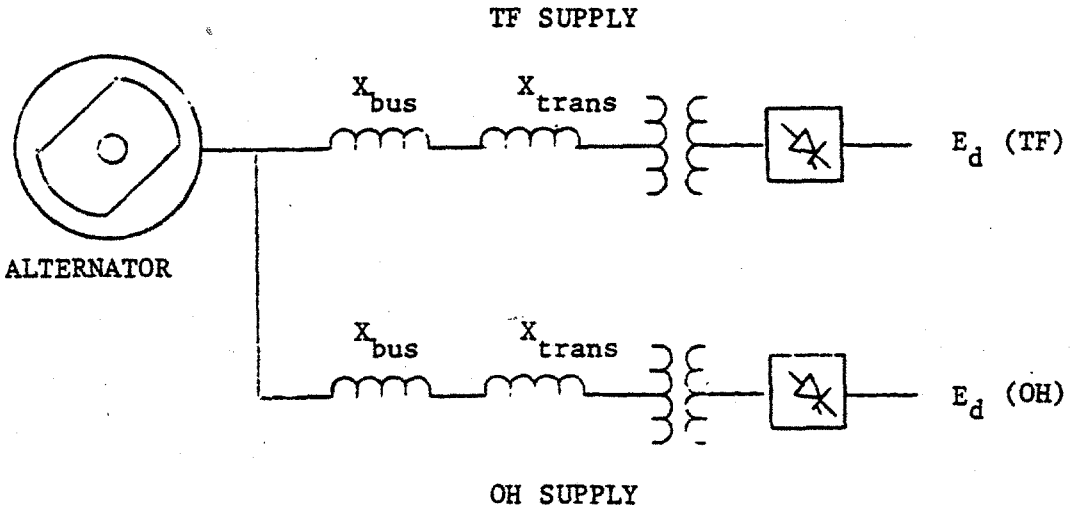

Figure 2-4: One line impedance diagram of Doublet III power supply

TABLE II

PARAMETERS OF DOUBLET III POWER SUPPLY SYSTEM MODEL

MODEL SCALE FACTORS:

POWER	1 MODEL WATT	CORRESPONDS TO	755,813 ACTUAL WATTS
VOLTAGE	1 MODEL VOLT	CORRESPONDS TO	97.2 ACTUAL VOLTS
CURRENT	1 MODEL AMP	CORRESPONDS TO	7826 ACTUAL AMPS
TIME	1 MODEL SEC	CORRESPONDS TO	1 ACTUAL SEC

ALTERNATOR PARAMETERS:

PARAMETER	ACTUAL VALUE	MODEL VALUE	COMMENT
X_d	2.22 pu	2.22 pu	synchronous reactance
X_d'	.33 pu	.33 pu	transient reactance
X_d''	.232 pu	.232 pu	subtransient reactance
T_{do}'	6.0 s	6.0 s	open circuit field
T_d'	1.0 s	1.0 s	short circuit field
H	5.215 s	5.2 s	inertia constant
V_{base}	13.8 kV	142 V	
I_{base}	10878 A	1.39 A	
P_{base}	260 MVA	—344 VA	
f_{base}	60 hz	60 hz	

TF SUPPLY PARAMETERS:

Coil L	30.57 mH	327 H	
Coil R	4.185 mΩ	44.5 Ω	
X_{trans}	.2815 pu	.28 pu	pu on alternator base
Turns Ratio	23.03:1	1:1	
$X_{ac\ bus}$	.021 pu	.02 pu	pu on alternator base

OH SUPPLY PARAMETERS:

Coil L	1.55 mH	47 H	
Coil R	1.1 mΩ	33 Ω	
X_{trans}	.437 pu	.44 pu	pu on alternator base
Turns Ratio	19.43:1	1:1	
$C_{discharge}$	1.36 F	45 μF	
$X_{ac\ bus}$	.059 pu	.06 pu	pu on alternator base

The interconnection of the subassemblies is illustrated in the model system diagram of figure 2-5. Detailed circuit descriptions are given in Appendix B. The following subsections are meant to supplement the Alcator C model descriptions of section 1.3 by outlining the changes which are required in order to adapt the Alcator C model to perform to Doublet III specifications.

2.3.1 Model alternator

The model alternator is adjusted to the new Doublet III parameters using the procedures of section 1.3.1. The Doublet III model alternator is excited by the model exciter/regulator which is described in section 2.3.6.

2.3.2 Model TF supply

The actual Doublet III supplies are twelve pulse rectifiers, whereas six pulse rectifiers are used in this simulation. The discussions of six and twelve pulse rectifiers in Appendix A show that the regulation characteristics (which describe how the dc rectifier output voltage will vary with load) of these two types of rectifiers are identical until the rectifier load exceeds a certain value. Unfortunately, calculations reveal that the Doublet III TF and OH supplies exceed this value during times of peak output current. This implies that the model TF and OH six pulse rectifiers will not give the proper output voltage

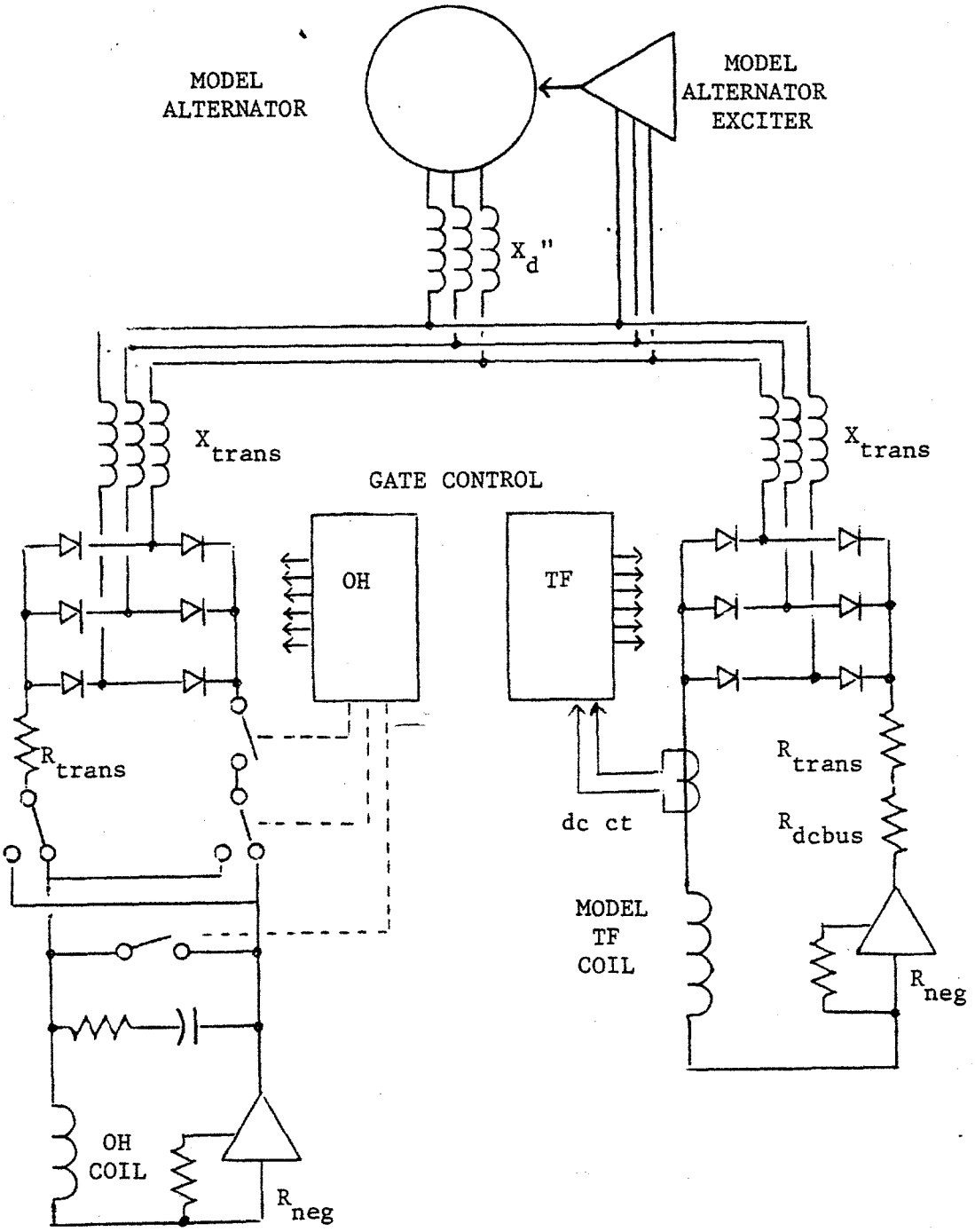

Figure 2-5: Doublet III scale model system diagram

during the critical times near the TF flat-top period. Also, supply input power factors will be in error due to the six pulse modeling of the twelve pulse system. Due to the fact that the rectifiers operate only slightly outside the regions where six pulse modelling is appropriate, it is possible to compensate, to a first order, for these errors by increasing the model commutation reactance.

Due to the nature of six and twelve pulse rectifier regulation characteristics, a twelve pulse rectifier operated with a certain commutation reactance can have regulation and input power factor characteristics very close to those of a six pulse rectifier which has slightly higher commutation reactance. The amount which the six pulse rectifier commutation reactance must be raised to achieve a twelve pulse emulation depends on the load current at which the minimum simulation error is desired.

In this study, we desire that the modeling be accurate during the critical TF coil flat-top period. Adding 15% to the actual pu values of the TF and OH supply commutation reactances significantly reduces six pulse regulation and power factor errors during TF flat-top.

2.3.3 Model TF supply load

The model TF supply load used in section 1.3.3 was adjusted to the appropriate Doublet III value. Again, the use of a series connected negative resistor was required.

2.3.4 Model OH supply

During Doublet III OH supply operation the output of the supply must be reversed using a special switch. The Alcator C simulation made use of just such a switch (see section 1.3.4). Consequently, no modification was necessary in order to include this feature.

In the actual Doublet III system a series R-C circuit replaces the resistor used in the Alcator C OH coil switching network. The appropriate scaled R-C values were therefore installed in the model for this simulation.

2.3.5 Model OH supply load

The model OH supply load was appropriately adjusted and used, as before, in combination with a series connected negative resistor.

2.3.6 Model alternator exciter/regulator

The model alternator has a high power exciter available. It was necessary to measure the alternator terminal voltage, compare it to some set point level, and supply an appropriate error signal to the exciter in order to complete the regulator loop.

In this study, the actions of the regulator are of particular importance. Therefore it is critical that the model regulator and the actual regulator are both attempting to regulate the same measure of the alternator terminal

voltage (RMS, peak, etc.). To be sure of this, the design of the alternator voltage sensing input stage of the model regulator was copied directly from the schematic of the actual G.E. exciter.

The error amplifier utilized uses a special compensation (anti-hunting) network in order to maximize regulator speed while maintaining stability.

2.4 Scale model limitations

The scale model of the Doublet III power supply contains some compromises which may affect the accuracy of the simulation results. These limitations are discussed below. The limitations mentioned here are meant to supplement the additional limitations which are described in section 1.4.

Some error is incurred due to the six pulse modeling of twelve pulse rectifiers. In the Alcator C simulation the effects of rectifier regulation contribute importantly toward the findings of the scale model study, finding which are related to the serious loss of the TF coil forcing voltage. Fortunately, as we will show, the findings of the Doublet III scale model study are not heavily dependent on the accuracy of rectifier regulation modeling. Clearly, actual scale model twelve pulse rectifiers would be appropriate in this application; however construction of same was prohibited by considerations of cost and complexity.

The actual Doublet III alternator exciter has special protective features which, if tripped, will prevent the exciter from regulating the alternator voltage. None of these features were modeled in the scale model system. However, these features should not be triggered during the relatively brief Doublet III experiment, since they operate via time delay relays.

2.5 Scale model tests of Doublet III power supply

The simulation results from the Doublet III physical scale model are presented in the oscillograms of figures 2-6 through 2-15. The vertical scales represent actual Doublet III values of the variables, and were computed using model scale factors. Load voltage measurements were made with a 60 Hz two-pole low pass filter to remove ripple. The alternator frequency at the start of the experiment was 81 Hz in each case. Measurements of alternator voltage transients were taken from the output of the exciter/ regulator sensing circuit, and correspond to filtered versions of the rectified alternator output. The initial alternator voltage was 1 pu (corresponding to 13.8 kV) for all tests.

Figure 2-6: This figure shows the TF voltage and current profiles for the case when the OH supply is not operating. The 126 kA flat-top level is easily attained and the dc output voltage droop is less than 15% during the current

ramp. The ramp-up time is significantly shorter than the time specified in figure 2-2.

Figure 2-7: This figure shows the OH voltage and current profiles for the case when the TF supply is not operating. The prescribed OH coil current profile is generated (compare with figure 2-3). Note the 2.8 kV OH coil voltage pulse which occurs during the OH coil discharge period.

Figure 2-8: This figure shows the alternator terminal voltage transient which results from TF supply operation. In this case a FWD was connected across the TF coil, resulting in the slow decay of the TF coil current after flat-top. The upper curve can be thought of as the "envelope" of the ac alternator terminal voltage. Note the terminal voltage drop at the onset of flat-top, and the overhshoot which occurs at the end of flat-top. The OH supply was not operating during this test.

Figure 2-9: This figure shows the alternator terminal voltage transient which results from OH supply operation. In this case the TF supply was not operating. Note the overshoot which occurs at OH supply disconnection. Also, smaller transients result from the other times when the OH supply changes the magnitude or power factor of the alternator load.

Figure 2-10: This figure shows the frequency change which accompanies TF supply operation. The minimum frequency, which occurs at the end of flat-top, is 67.5 Hz. The OH

supply was not operated during this test. The rise of the frequency of the alternator which occurs after the TF current profile has ended is due to the action of the motor which is used to bring the alternator up to speed between experiments. Due to the windage losses of the model machine, which could not be scaled, it was necessary to use an oversized motor to perform this function.

Figure 2-11: This figure shows the frequency change which results when both the TF and OH supplies are operated. The minimum frequency, which occurs at the end of TF flat-top, is 65 Hz. This corresponds to a loss of 36% of the original kinetic energy of the alternator. At the end of the experiment, the frequency is up to 76 Hz. Subtracting the estimated error due to the oversize motor, the overall alternator kinetic rotational energy loss at the end of the experiment is 15%.

Figure 2-12: This figure shows the alternator voltage transient which results from the simultaneous operations of the TF and OH supplies. Note that this transient is nearly the sum of the transients that were produced by the individual supplies (figures 2-8 and 2-9). The transient resulting from TF phaseback at the end of flat-top is smaller in this case, when compared to figure 2-8, which is attributable to the fact that the FWD was not used in this (figure 2-12) experiment.

Figure 2-13: This figure shows the alternator transient which results when OH supply disconnect is synchronized with the beginning of TF flat-top. Note that the overshoot which normally results from OH disconnect is cancelled by the voltage drop resulting from the start of TF flat-top.

Figure 2-14: This figure shows the alternator transient which results when both the TF and OH supplies are operated, and the TF supply misfires during inversion due to inadequate margin angle. Note the unusual ripple present on the rectified alternator voltage, which results from attempted TF supply commutation. Also, note the large transient which accompanies the beginning of the misfire.

Figure 2-15: This figure shows the large transient which results when TF inversion phaseback (with FWD) is synchronized with OH disconnection. In this case an overshoot of 20% is observed. When the timing of these two events is exactly right, overshoots of over 25% have been observed. In this recording, the duration of the flat-top period was set to zero. Note that the OH coil current was inadvertently inverted in this figure as compared to the other oscillograms of this section.

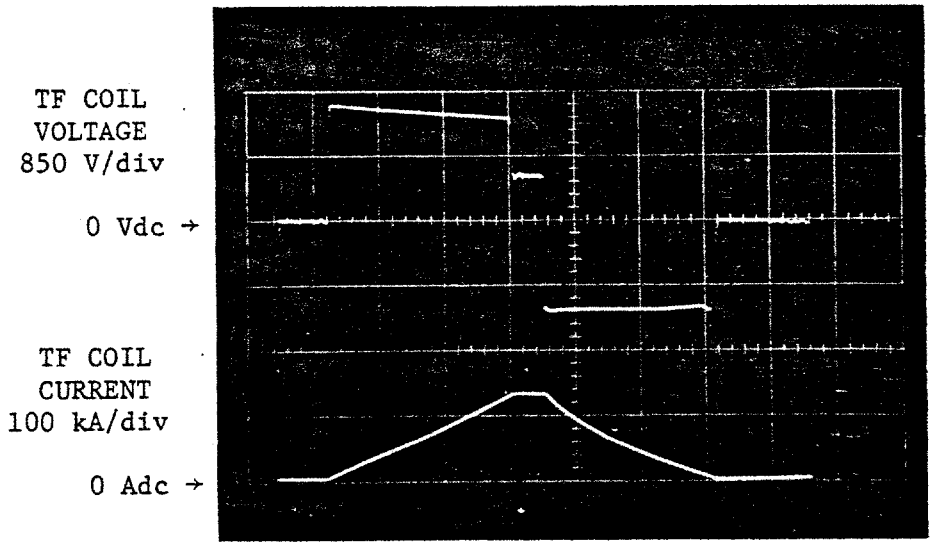

Figure 2-6: Oscillogram showing results from Doublet III power supply model tests

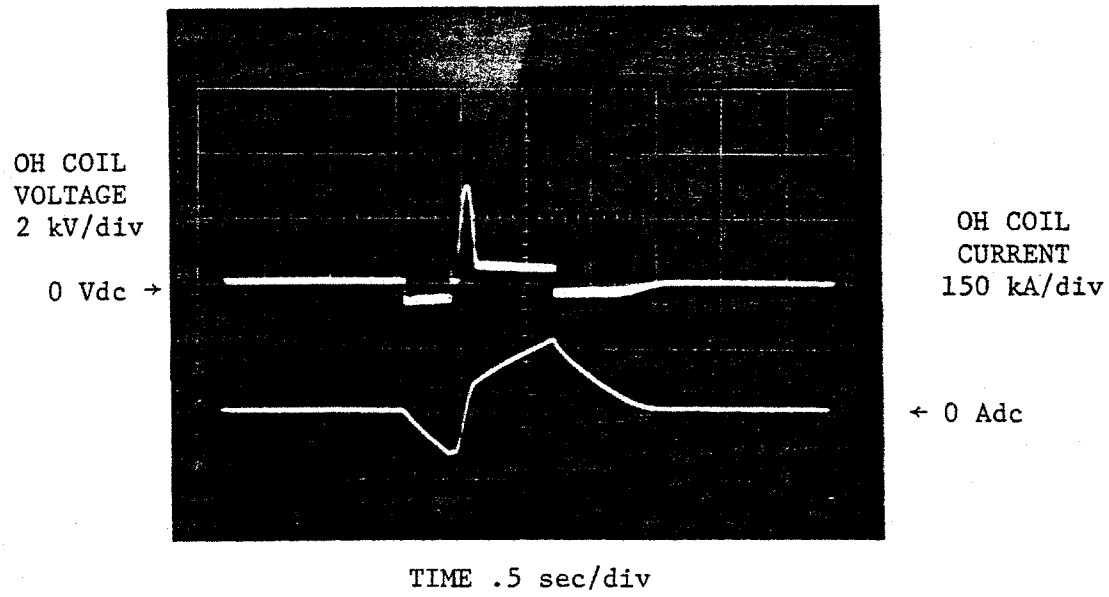

Figure 2-7: Oscillogram showing results from Doublet III power supply model tests

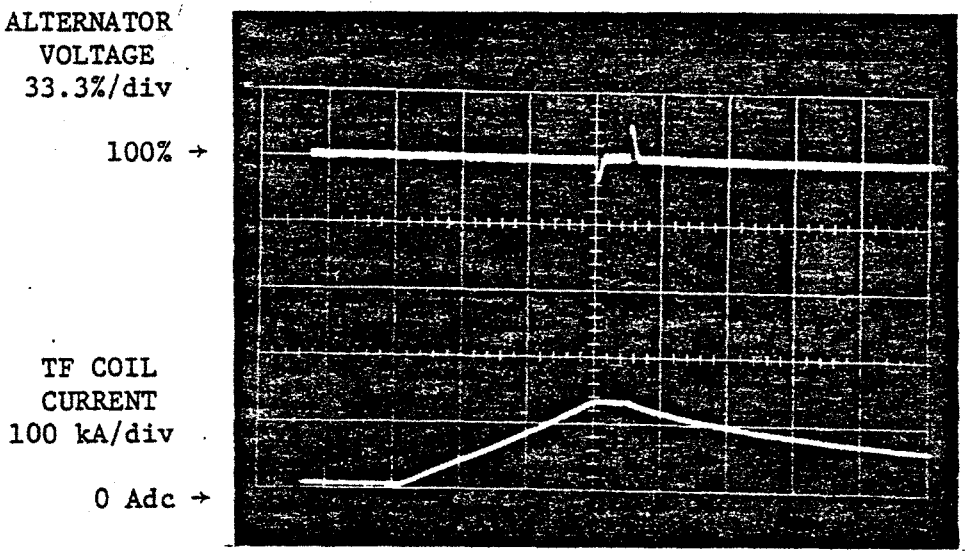

Figure 2-8: Oscillogram showing results from Doublet III power supply model tests

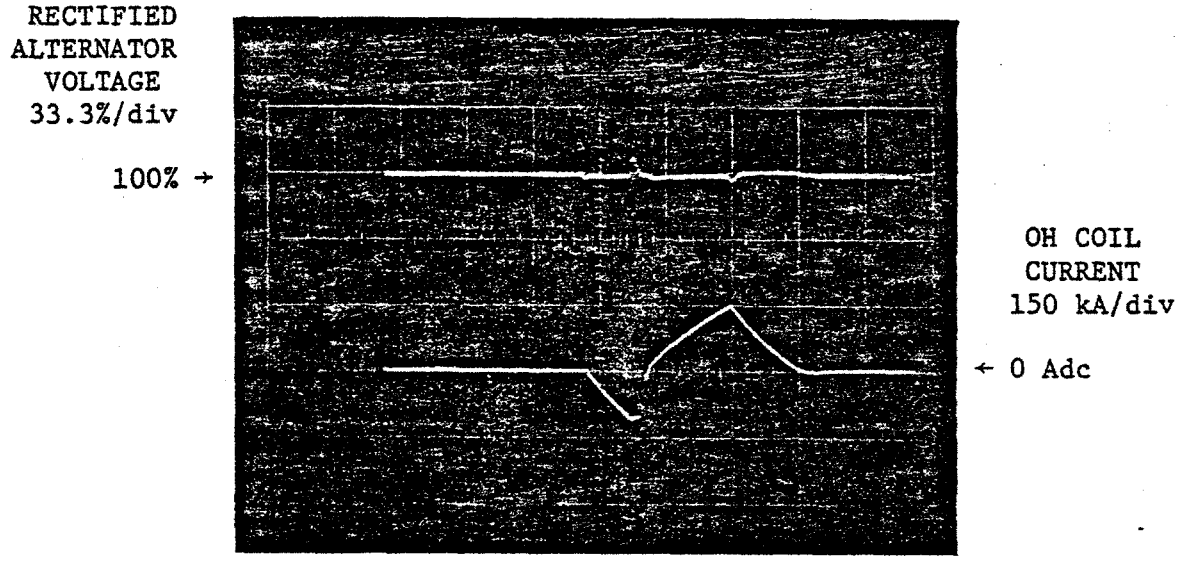

Figure 2-9: Oscillogram showing results from Doublet III power supply model tests

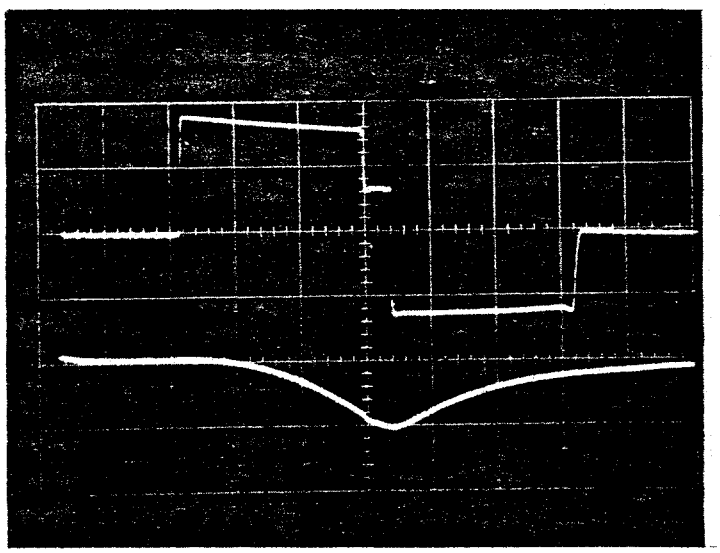

Figure 2-10: Oscillogram showing results from Doublet III power supply model tests

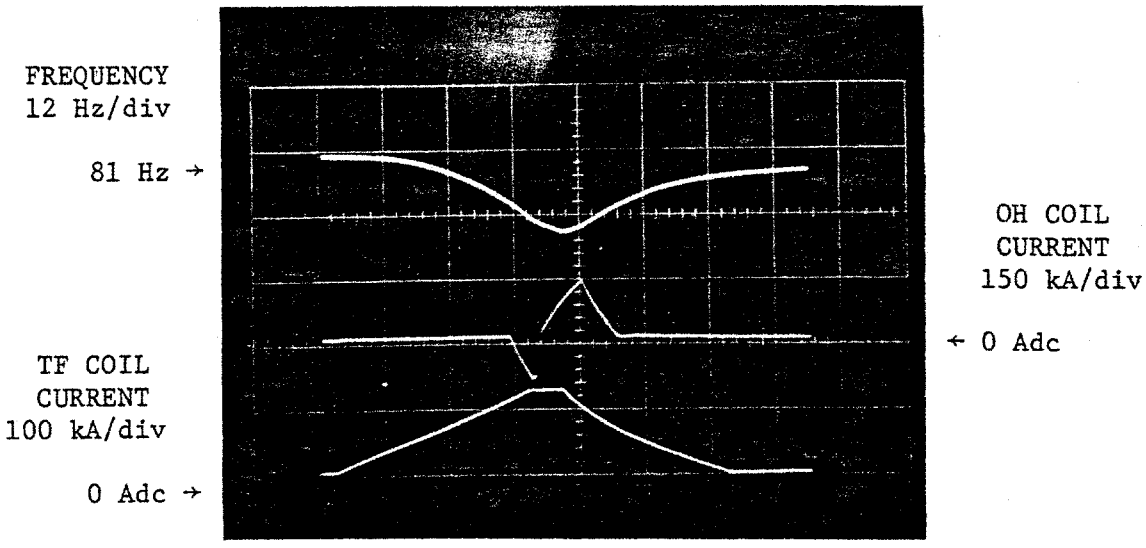

Figure 2-11: Oscillogram showing results from Doublet III power supply model tests

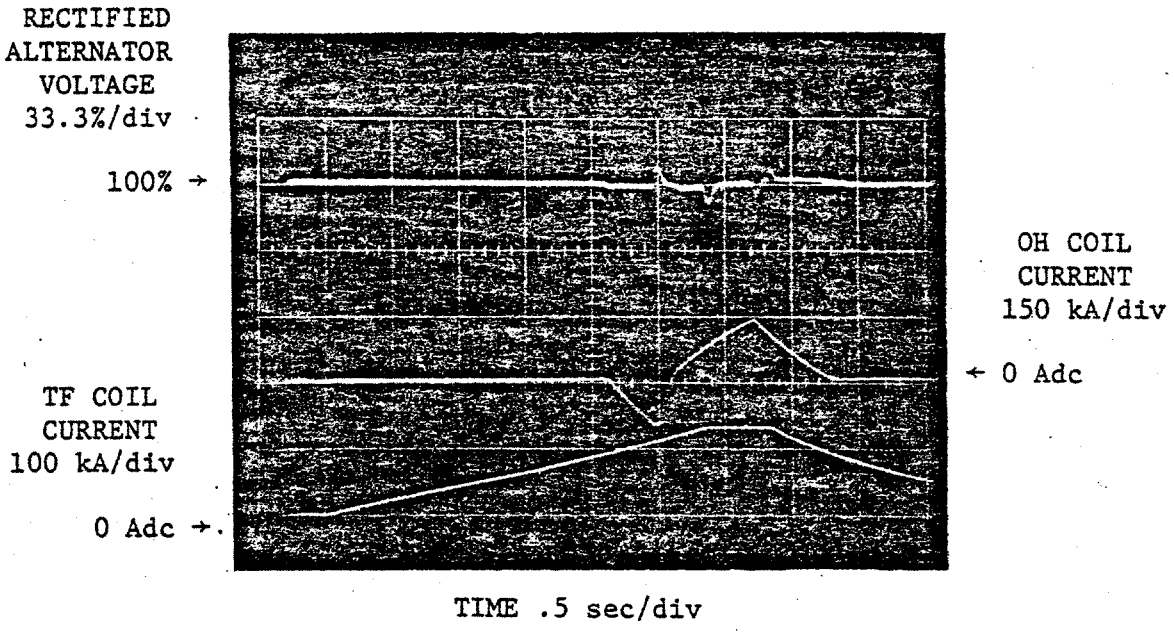

Figure 2-12: Oscillogram showing results from Doublet III power supply model tests

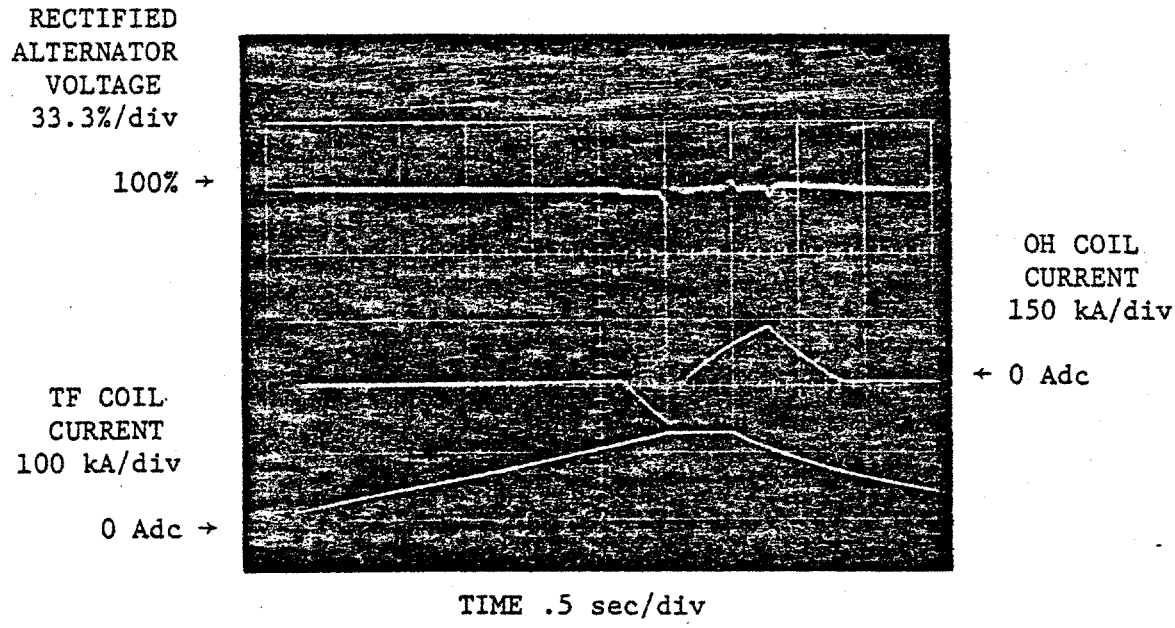

Figure 2-13: Oscillogram showing results from Doublet III power supply model tests

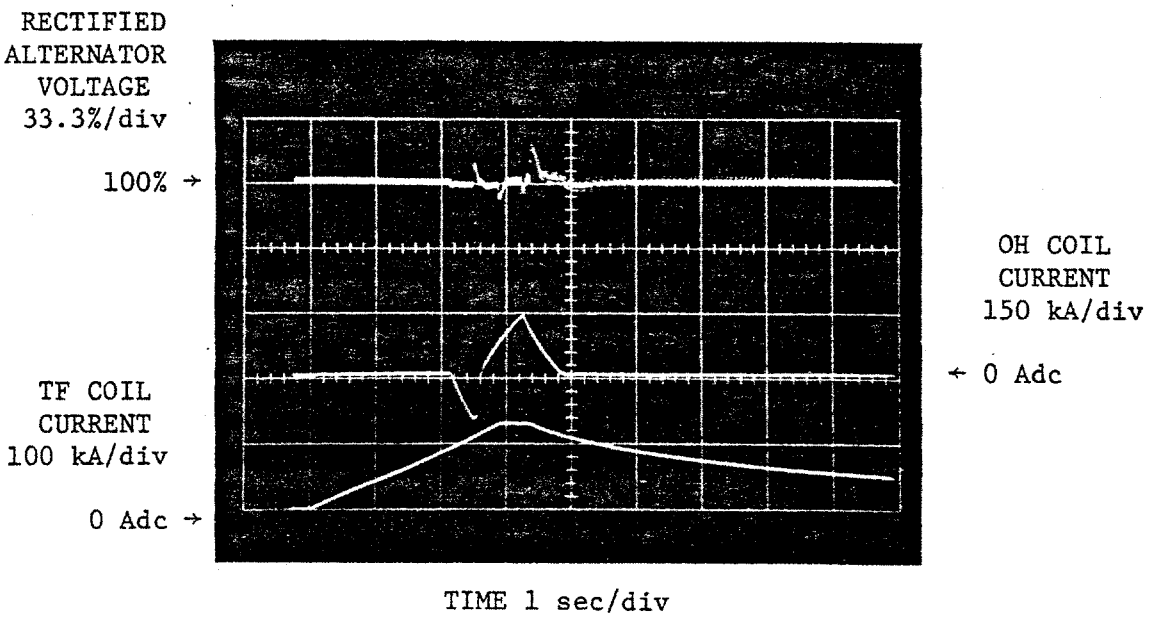

Figure 2-14: Oscillogram showing results from Doublet III power supply model tests

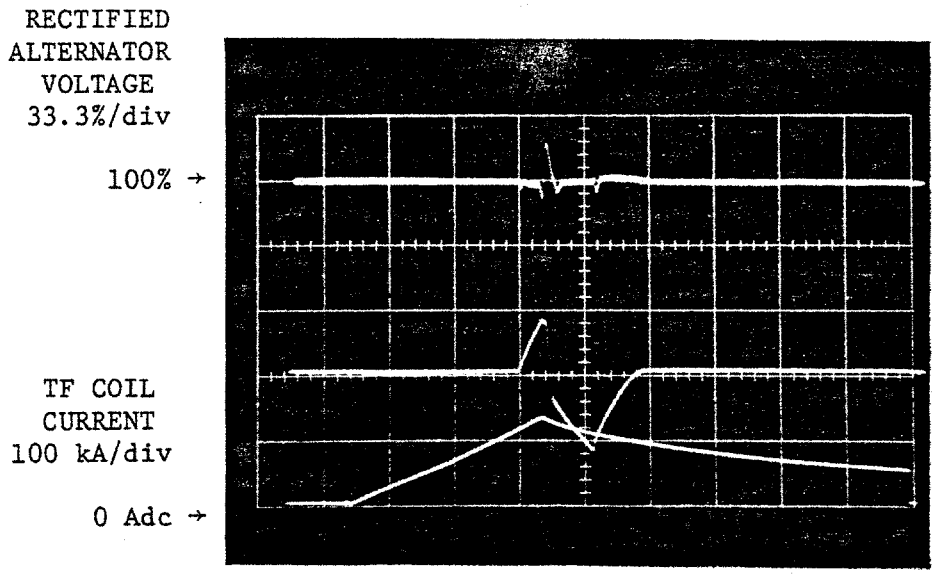

CHAPTER III

COMPUTER MODEL OF
ALCATOR C POWER SUPPLY SYSTEM

In this chapter, a computer model of the Alcator C power supply for the TF coil ramp-up period is introduced. The algorithms used are evolved from mathematical models of the constituent segments of the power supply. The results of the computer simulation are directly compared to those of the physical scale model and the correspondence is used to justify the algorithm selection.

A significant advantage of a computer simulation is the ease of parameter adjustment. However, for the purposes of this study, the value of the program lies in its ability to simulate physically impossible supply conditions, in order to gain a better understanding of the system. Particularly, internal alternator voltages are easily measured or manipulated in a computer model, whereas in the real world they cannot even be accessed. Clearly, the measurement and/or manipulation of normally inaccessible variables permits concrete statements to be made about the relationship between said variables and the system response. In this way, it is possible to quantify the relative contributions of the various mechanisms which together define the overall system performance.

In the following sections, the computer program implementation is first outlined; next, the computer results are compared to the results of the physical scale model. Finally, the computer program is used to test special cases of system operation.

A detailed description of the computer algorithm is contained in Appendix C.

3.1 Description of computer algorithm

The program used is dynamic, being driven by difference equations describing the TF coil and the alternator. The difference equations result from three state variables, which are due to the energies associated with:

(1) alternator flux
(2) magent (load) flux
(3) alternator angular velocity

The solution of the equations is accomplished in the direct numerical fashion, using small time-steps; unique algorithms (Appendix C) are utilized due to the non-linear nature of the equations.

The rapid switching actions of the thyristors in the TF power supply, which occur six times per ac cycle, are opposed by internal alternator reactance. Since the switching times are short compared to the subtransient time constant, the effective alternator reactance opposing the commutation is equal to the subtransient reactance X_d''. The

result is that the ac waveform at the alternator terminals contains substantial distortion. The calculated distortion is shown in figure 3-1, where the generator terminal line-to-line waveform is shown for a TF coil current of 190 kA, prior to flat-top. To account for the non-sinusoidal alternator waveform, the alternator can be represented by its internal (sinusoidal) voltage behind subtransient reactance (E_d'') in series with its subtransient reactance (X_d'') as shown in figure 3-2. This is a critical step which allows the system to be divided into two parts, the division taking place at the internal alternator voltage behind subtransient reactance. The subtransient reactance is incorporated into the model of the rectifier set where it contributes to the commutation reactance, and the internal alternator world of sinusoidal phasors ends at the voltage E_d''. The rectifier can now be mathematically described according to the principles of Appendix A, while the remainder of the alternator (above E_d'') is represented by a phasor diagram or d-q axis model.

The essential structure of the program is revealed in the flow chart of figure 3-3. At each time step N, the program computes the new values of the state variables based on the previous values. In this way, the expected time domain solution is directly approximated.

Referring to the flow chart, we can follow the expected course of a trial computer run. First, the program variables

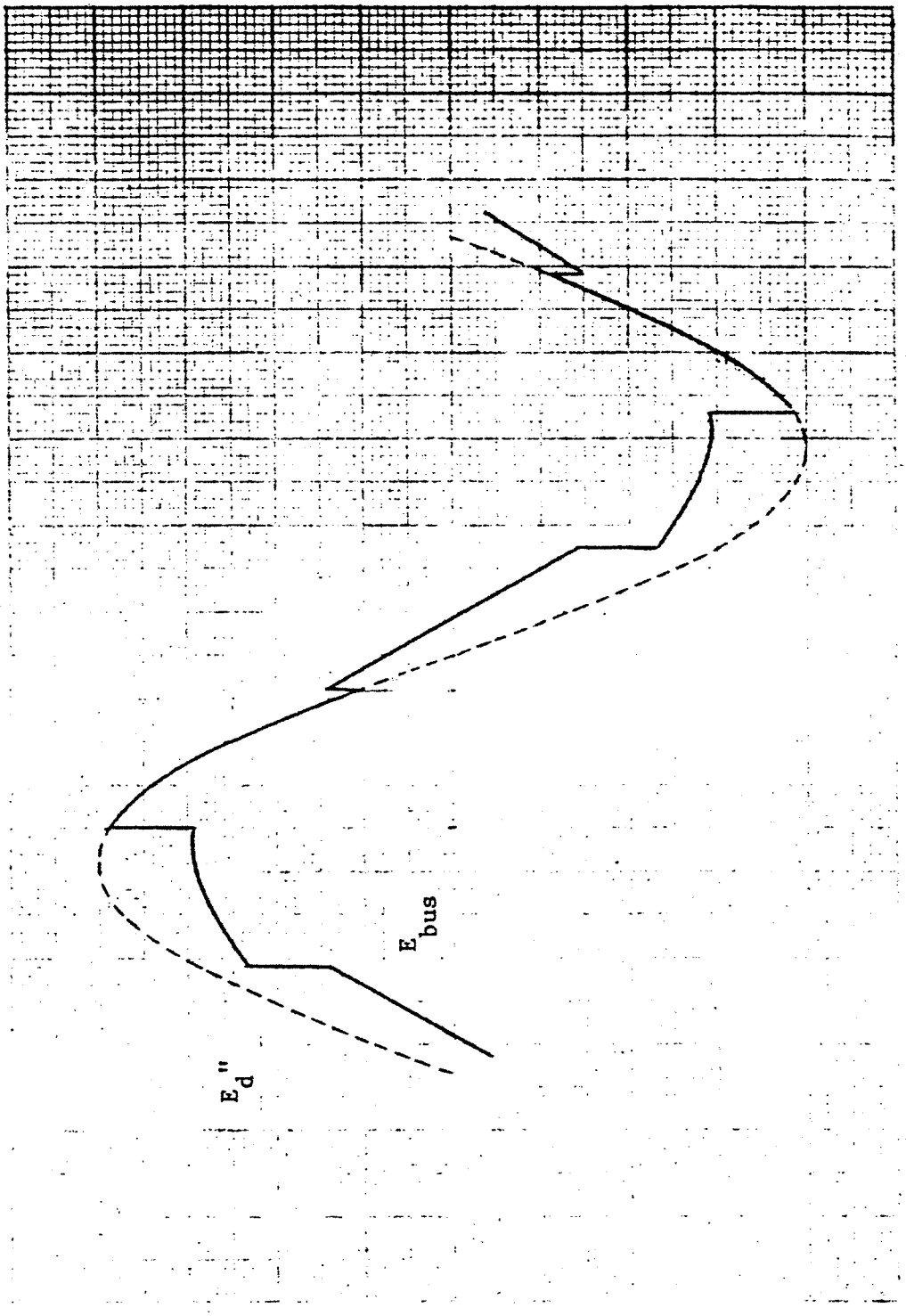

Figure 3-1: Alcator C alternator line to line waveform showing distortion prior to flat-top

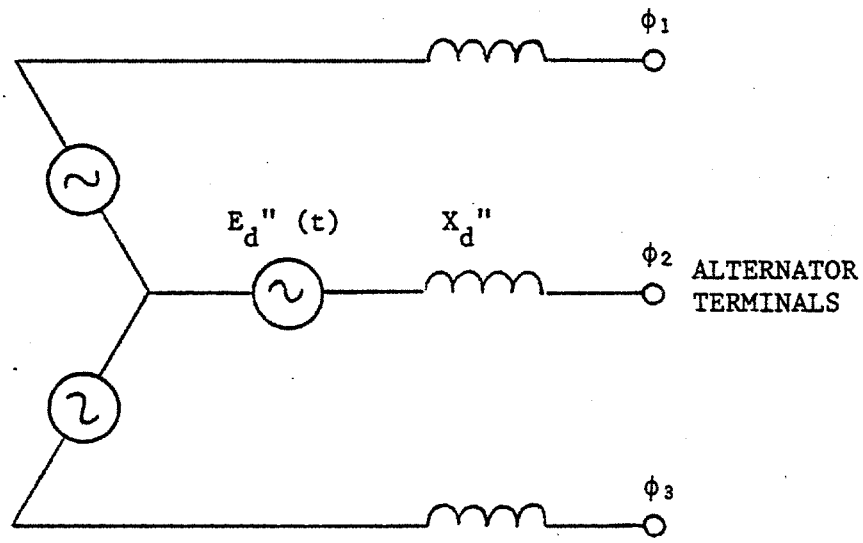

Figure 3-2: Representation of alternator for rectifier calculations

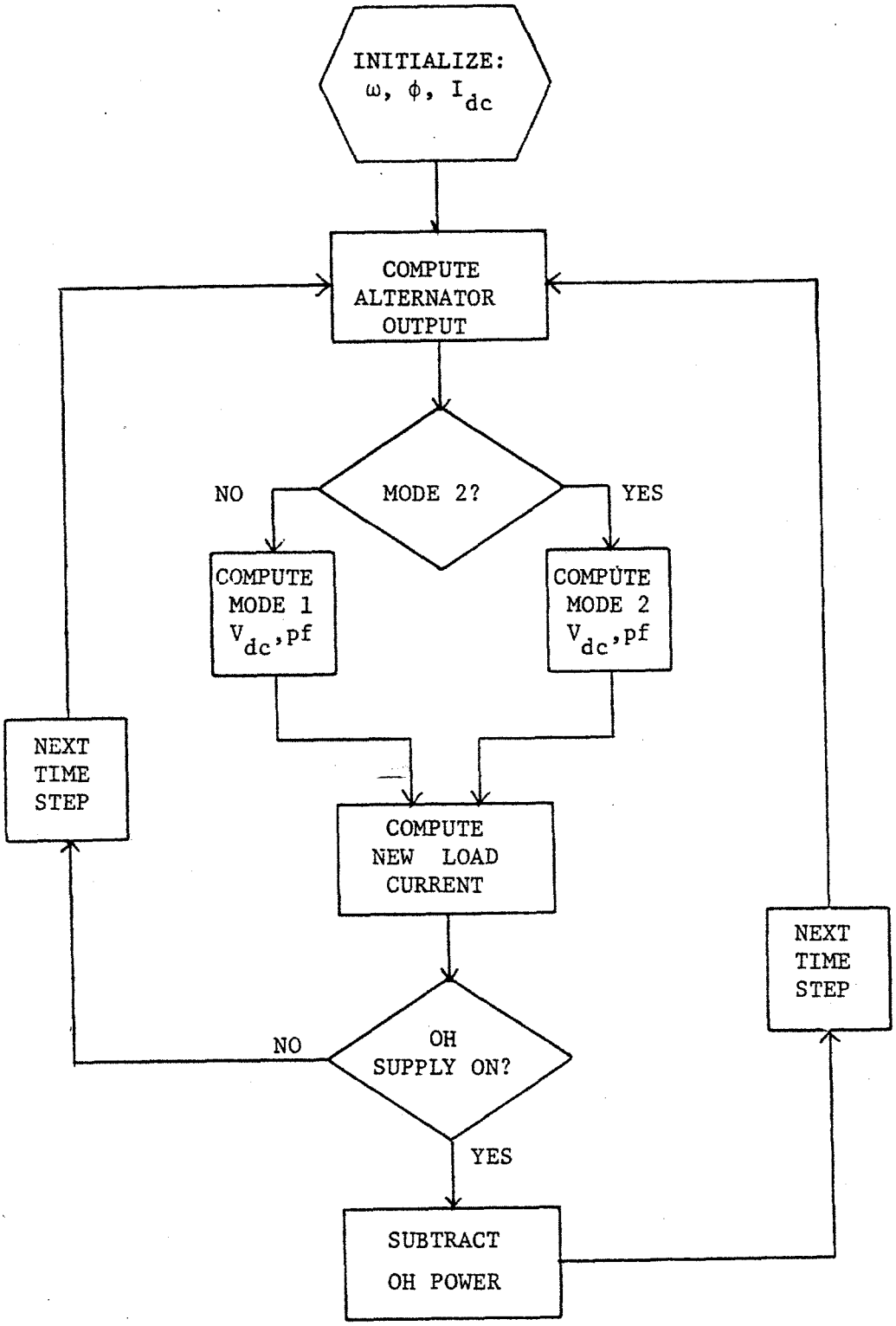

Figure 3-3: Flow chart for Alcator C computer simulation

are initialized, including the alternator and load conditions at t = 0. The recifier output voltage is now calculated based on the initial values of the state variables. This output voltage is used to determine the rate of change of the inductive load current, which is itself a state variable. Based on the rate of change of the load current at t = 0, the load current at the time t = ΔT is estimated. This new value of the load current is used to determine the rates of change of the two state variables associated with the alternator, namely speed and flux, which are, in turn, multiplied by the time step ΔT to yield updated alternator conditions. Eventually, after many time steps, the load current increases to a point where the TF rectifier will enter a new mode of operation, and a new set of equations must be used to describe this second operational mode. Mode switching is provided by the conditional in the center of the flow chart. Information concerning the various modes of rectifier operation can be found in Appendix A.

Another conditional is implemented to represent the operation of the OH power supply. Operation of the OH supply is started in this program at a predetermined level of the TF supply load current, the predetermined level being empirically selected to give good agreement with the specified timing (figures 1-2 and 1-3).

3.2 Verification of algorithm

To demonstrate the validity of the computer algorithm, we compare the computer results to those of the physical scale model for identical initial conditions. The result of this comparison is shown in figure 3-4. In the figure, the physical scale model results which were taken directly from figure 1-6 (dotted curve), are found to correspond closely to those of the computer simulation (solid curve).

3.3 Results of computer tests

In this section the results of the computer simulation of the Alcator C TF ramp-up period for the following three situations are presented:

(1) constant alternator flux (E''_d/ω = constant)
(2) infinite alternator inertia (ω = constant)
(3) alternator field forcing ($V_f \cdot \omega$ = constant)

The first situation is modeled to answer the question: "Does the alternator flux change significantly during the TF current ramp, and if so, what performance sacrifice is incurred by this flux change?"

The second situation is modeled to answer the question: "What is the effect of the decrease of alternator speed during the TF current ramp?"

The third situation is modeled to answer the question: "How much can the performance of the supply be improved by forcing the alternator field?" The field forcing strategy

chosen in this case is $V_f \cdot \omega$ = constant, which is the strongest field forcing that can be used with complete safety. This field forcing strategy is safe because if the alternator current is terminated at any time during the experiment by bus failure, supply misfire, or breaker action, the maximum voltage that the alternator terminals can experience is equal to the no-load voltage at the start of the experiment.

The results of the three simulations outlined above are shown in figures 3-5, 3-6, and 3-7. In each case, the simulation was run for four different values of initial alternator voltage. The significance of these results, and the answers to the questions put forward above, are given in the Interpretation of Results, chapter 4.

3.4 Limitations of computer modeling

In light of the advantages of the computer routine and the excellent correlation between computer and physical scale model results for the Alcator C TF ramp-up period, the implementation of computer routines to model the flat-top and inversion periods was considered. In addition, computer modeling of the Doublet III system was proposed. It was determined that none of these possibilities were practical, the reasons falling into two major groups:

(1) the difficulty of modeling the dynamics of exciter or rectifier regulators

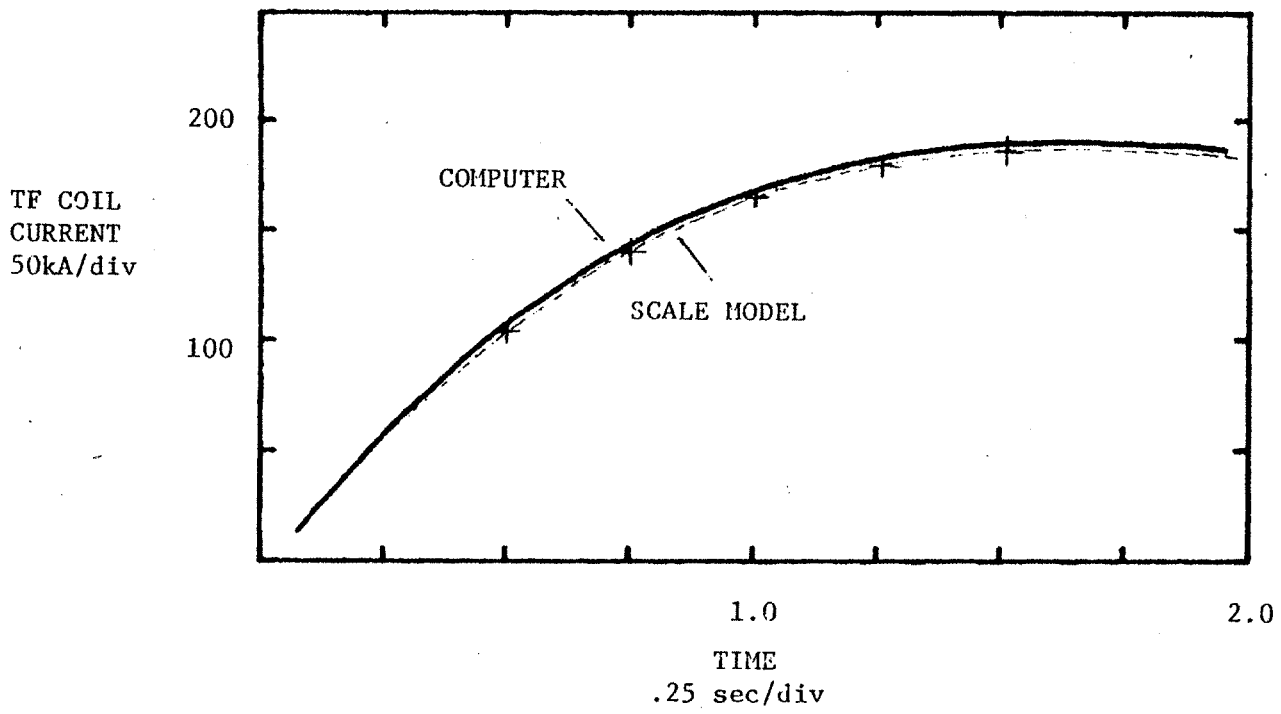

Figure 3-4: Comparison of TF coil current profile as predicted by scale model and computer simulations; alternator voltage at start of experiment = 14.6 kV

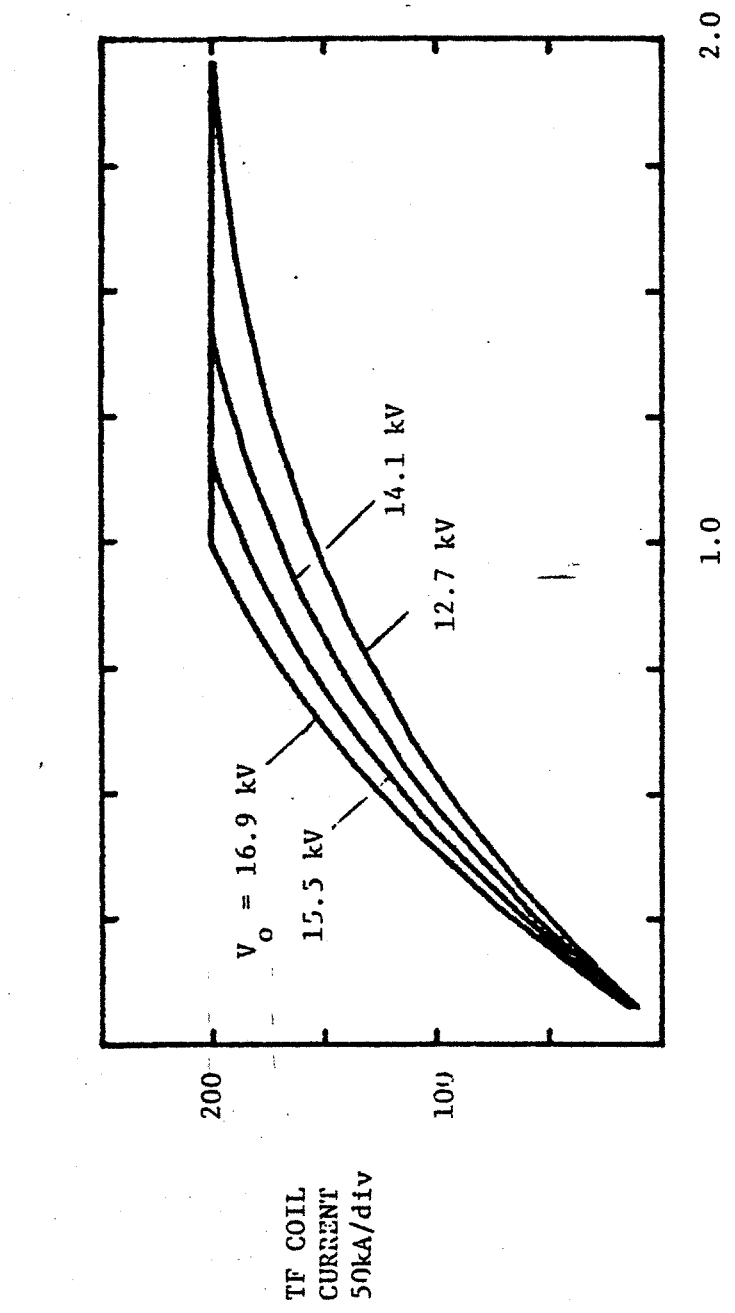

Figure 3-5: TF coil current profile for various values of starting alternator flux; case 1: E_d''/ω = constant

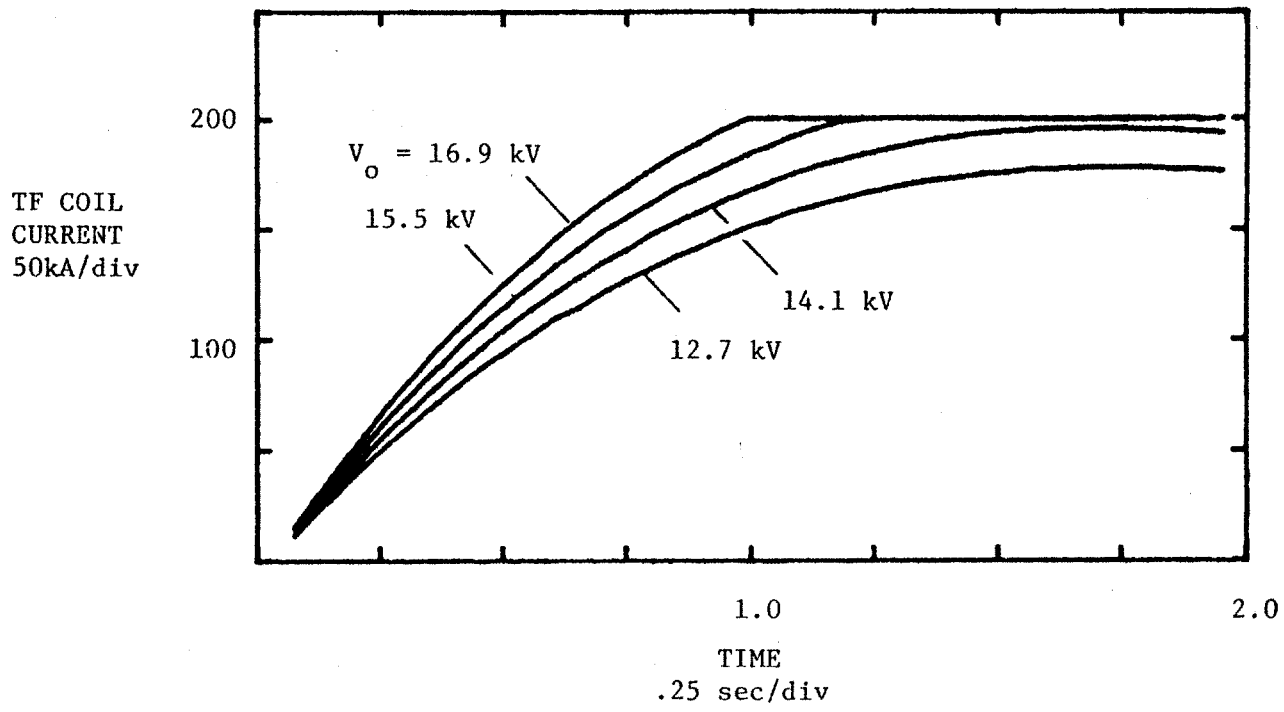

Figure 3-6: TF coil current profile for various values of starting alternator flux; case 2: infinite flywheel

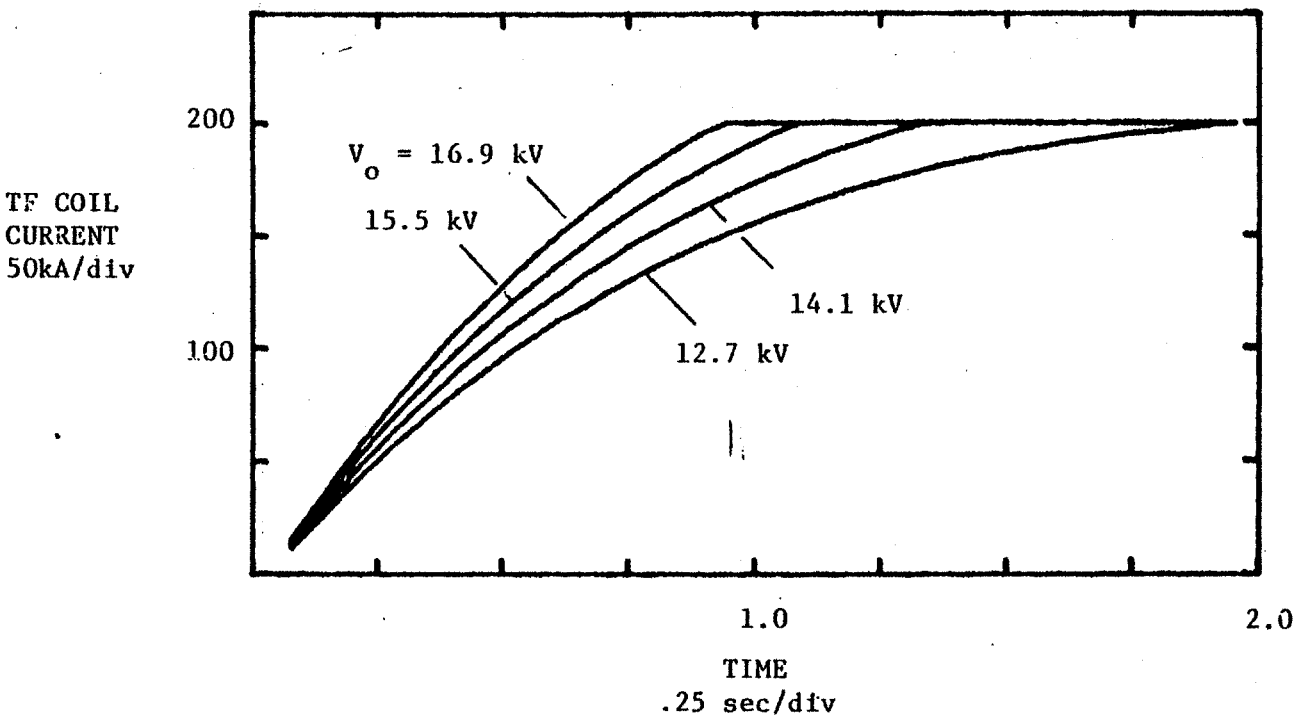

Figure 3-7: TF coil current profile for various values of starting alternator flux; case 3: field forcing

(2) the difficulty of determining the regulation characteristics of multiple supplies (TF and OH) driven by a single reactive source (alternator)

3.4.1 Computer modeling of regulator dynamics

In general, the computational complexity of a computer simulation is strongly dependent on two system parameters: (A) the number of state variables and (B) the time-constant spread. Although the number of state variables is small in the systems investigated here, the time constants associated with regulator dynamics approach a few hundred Hertz, while load time constants are measured in seconds. Consequently, the number of time steps required to reach a solution becomes very large. In this case, extra precautions must be taken to guarantee convergence of the solution; these precautions may include the use of complex predictor/corrector algorithms.

During the TF ramp-up period, the time constants associated with the load and alternator state variables which are used by the program are all in the neighborhood of 5 seconds (the TF supply regulator does not operate during the ramp-up period). This allows excellent accuracy using 50 millisecond time steps. With this size time step the program can be run in approximately 2 minutes using the minicomputer interpreter BASIC language. We expect a program which models regulator dynamics to require 2 to 3 times

more computer time per iteration, with a 2000 times higher iteration rate. This would require 8000 to 12000 minutes of time on the same computer. This limitation by itself is not particularly severe, until it is combined with the problems relating to multiple supplies, problems which are discussed in the next subsection.

3.4.2 Computer modeling of multiple supplies

In the Alcator C computer simulation of the TF coil ramp-up period, it was assumed that the operation of the OH supply would not significantly modify the mathematical input/output relations of the TF power supply. This assumption is permissable due to:

(A) the large difference in TF and OH supply power levels
(B) the low ratio of the shared reactance to the total TF supply commutation reactance (16%/40%)

In the Doublet III system, neither of these conditions is satisfied, since:

(1) the TF and OH supplies operate at similar power levels
(2) the ratio of shared to total commutation reactance for the TF supply is significant (30%/60%)

Due to the extraordinary difficulty in mathematically defining the multiplicity of operational modes of rectifier operation (in addition to the modes described in Appendix A)

which are the consequence of the supply interference, it was not considered feasible to model the Doublet III supply on the computer.

3.4.3 Summary of limitations

It was determined that computer modeling of the Alcator C and Doublet III power supplies was not expedient in the light of the advantages of the physical scale model, except in the simple case of the Alcator C TF ramp-up period, where computer modeling was found to be effective. For the types of systems investigated in this study, utilization of the special advantages of computer simulation can only be accomplished when:

(A) mathematical solutions of the multiple converter problem are found, and implemented on a very high speed computer using efficient algorithms

or

(B) generalized very high speed network analyzing programs are developed, allowing power converters to be represented at the component level.

CHAPTER IV

INTERPRETATION OF RESULTS

In this chapter, results of the Alcator C and Doublet III power supply simulations are examined. In the case of the Alcator C supply the mechanisms which result in the large decrease in the dc forcing voltage during the TF coil current ramp-up period are described. In the case of the Doublet III supply the mechanism responsible for alternator terminal voltage transients is explained.

4.1 Analysis of Alcator C TF supply output capability

This section contains an explanation of the mechanisms responsible for the severe Alcator C TF coil voltage decay which occurs during the TF current ramp-up period.

The results of the Alcator C simulations show that the TF supply design is not capable of generating the required TF coil current profile unless considerable alternator overvoltage is utilized. In section 1.1 it was noted that the dc TF coil voltage would fall during the current ramp due to:

(1) voltage lost to commutation reactance
(2) voltage lost to internal supply resistance
(3) voltage lost due to decay of alternator speed
(4) voltage lost due to decay of alternator flux

It would be expedient to establish a measure of TF supply performance degradation, and then attribute some percentage of this degradation to each of the four factors, such that the total contribution sums to 100%. Unfortunately, this is not possible since these factors are not independent but instead possess both synergistic and antagonistic interrelations. Rather than explicitly defining these complex relationships, the remainder of this section describes the benefits to the system performance that can be accrued by the reduction of each of the four factors. Also, the practicalities of the modifications which would be required to achieve these reductions are mentioned.

4.1.1 Output capability lost to commutation reactance

For a given value of the load current, the dc output voltage of the TF supply which is lost due to the commutation reactance can be determined from the curves in Appendix A. Using the curves, we find that if the commutation reactance were zero, then we would expect an increase of approximately 30% in the available dc supply output voltage prior to flat-top, which would allow the supply to meet the original specifications. The commutation reactance consists of three parts:

(1) alternator subtransient reactance (.125 pu)
(2) ac bus reactance (.05 pu)
(3) transformer reactance (.28 pu)

The only one of these reactances that can be changed is the transformer reactance, which is 60% of the total commutation reactance. The transformer reactance can be decreased by parallel connection of multiple units; each time the number of transformers is doubled, transformer reactance is halved. Therefore, the total commutation reactance can be reduced 30% by doubling the number of rectifier transformers. This very expensive modification would give an approximate pre-flat-top dc voltage increase of 10%.

4.1.2 Output capability lost to power supply resistance

The dc output capability lost to the internal TF power supply resistance can be directly estimated using Ohm's law. If the supply resistance (dominated by transformer resistance) were eliminated, then we would expect an 8% increase in the available pre-flat-top voltage. As in the case of the commutation reactance, this loss can be reduced, in this case to 4%, through paralleling of additional transformers.

4.1.3 Output capability lost due to alternator speed decrease

The Alcator C alternator speed decreases during the TF pulse; the alternator output voltage must fall at least as rapidly. This is true because the alternator output voltage is dependent on the product of the rotor flux and the rotational speed. This situation is complicated somewhat by the

decay of the values of the alternator and rectifier commutation reactances which must accompany the frequency decrease.

The extent to which the rotor speed decrease influences the performance of the power supply can be determined from figure 3-6 of the computer simulation results. In figure 3-6 the effects of the decay of the rotor speed are removed by connecting the alternator to a flywheel of infinite inertia. Comparing these curves to the physical scale model results shows that a small improvement of the system performance is achieved. This improvement amounts to approximately 10 kA of additional attainable flat-top current or a 5% increase in the available pre-flat-top dc coil voltage. Doubling the alternator inertia by adding a finite flywheel would allow about half of this gain to be realized; therefore this is probably not a cost-effective way to improve the performance of the system.

4.1.4 Output capability lost due to alternator flux decrease

Due to the finite subtransient and transient time-constants, the alternator air-gap flux will decay during the TF current pulse due to the presence of the armature reaction flux. Any alternator output voltage loss in this case is more severe than a comparable loss due to rotor speed decay, since no decrease in system reactances accompany this (flux decay related) loss. The extent to which the air gap flux decay influences the performance of the

power supply can be determined from figure 3-5 of the computer simulation results. In figure 3-5, the ratio of the voltage behind subtransient reactance (E''_d) to the rotor speed has been maintained artificially constant during the TF coil current ramp. This implies that the air-gap flux is also constant.

Comparison to the physical scale model results shows a marked improvement in power supply capability; indeed, in this case the power supply meets the original design specifications.

In the real Alcator C power supply, the value of the alternator air-gap flux can only be indirectly controlled via the alternator field terminals. By forcing the field with high voltage it is possible to attempt to maintain air-gap flux during the experiment. As explained in section 3.3, the strongest field forcing scheme which is recommended is one which attempts to hold constant the product of the internal alternator voltage E_f and the rotational speed. Such field forcing gives rise to the TF coil current profiles of figure 3-7. Coincidentally, the results of the field forcing simulation are nearly identical to the results of the constant air-gap flux simulation. We conclude that field forcing can be used to hold the air-gap flux approximately constant.

In order to determine the practicality of such a field forcing system, it is necessary to determine the field

excitation required to hold constant the product of E_f and the rotor speed. Since E_f is due to the flux associated with the field current, the required time-function of the alternator field voltage can be determined if the time-varying impedance looking into the field terminals is known. This impedance is approximately that of a simple L-R circuit, where R is the dc field resistance, and L is a time varying function given by the product of R and the loaded field time constant (see alternator description in Appendix C). Using this information, the field excitation required to generate the curves of figure 3-7 was determined. This excitation is shown in figure 4-1. In generating these curves, the saturation characteristic of the alternator was neglected; unfortunately, the extent to which these curves are modified by saturation is unknown. Consequently, additional work is required before the exact required field excitation can be determined. Nevertheless, we conclude that the benefits of field forcing are large, and the ease and flexibility of installation of a high speed exciter make field forcing the preferred, cost-effective method to improve the performance of the Alcator C power supply.

4.2 Analysis of Doublet III alternator transients

The results of the Doublet III physical scale model indicate that variations of the regulated alternator terminal voltage will arise from two principal causes:

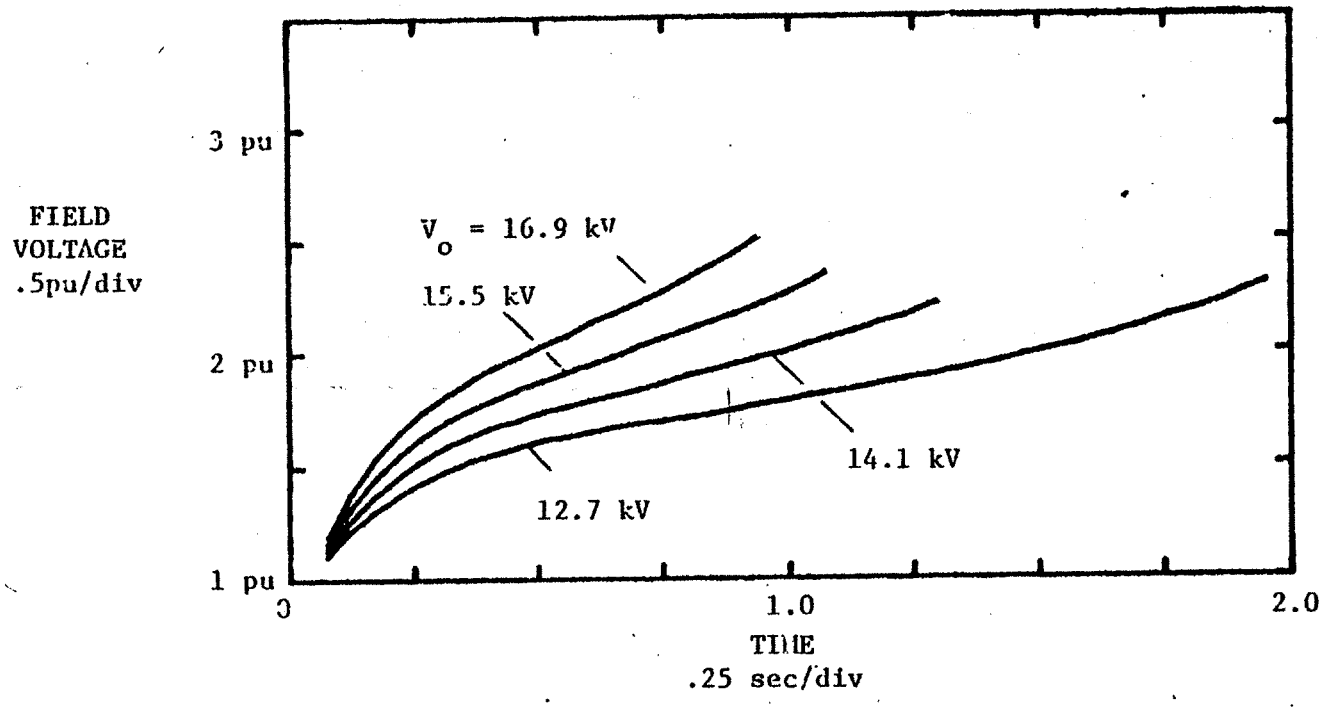

Figure 4-1: Alternator field voltage required to generate figure 3-7

(1) Rapid change (faster than 1-2 cycles) of the magnitude of the armature current due to supply disconnect, thyristor misfire, fault conditions, etc.

(2) Rapid change of the alternator power factor angle with constant armature current due to converter phase-back or phase-forward.

These variations can result in undervoltage as well as overvoltage conditions.

Many measures of the alternator terminal voltage are available, and it is important to understand their interrelation. Some useful measures include: the RMS voltage, the RMS of the fundamental component of the voltage, and the average of the rectified voltage. Percent variations of these measures of the alternator terminal voltage will track one another as long as the alternator waveform is sinusoidal. We expect that the largest possible overshoots will be sinusoidal, since they will occur as a result of the rapid termination of the armature current. Given that the alternator voltage waveform prior to the experiment is sinusoidal, we conclude that the recorded percent overshoot will be the same for each of the suggested measures of the terminal voltage.

In the physical scale model study of the Doublet III power supply, the results include records of the rectified alternator terminal voltage. This voltage is particularly significant because it is the measure of the terminal voltage which the exciter/regulator attempts to regulate. To

illustrate the nature of the process which gives rise to overshoot, and to predict the alternator terminal voltage profile for experimental situations which were not tested, it is useful to construct a simple phasor diagram representation of the alternator. Since any such representation must make use of the fundamental component of the alternator terminal voltage, it is necessary to describe a relationship between the magnitude of this quantity and the rectified terminal voltage.

The relation between the fundamental component of the alternator voltage and the rectified alternator voltage is very complex during the ramp-up and flat-top periods due to substantial bus distortion. The alternator terminal voltage waveform is a well defined function of the system reactances, the voltage behind subtransient reactance, the load current, and the rectifier phaseback angle. An example of this waveform is given in figure 4-2 for TF supply operation (OH supply off) with a coil current of 126 kA at the peak of the ramp-up period (prior to flat-top). The dotted curve represents the internal alternator voltage behind subtransient reactance, E_d''. The magnitude and phase of the fundamental component of the distored bus waveform can be calculated directly by Fourier analysis. Based on our calculations we find that the average rectified alternator voltage will differ from the magnitude of the fundamental component by less than 1.5% for operation of the TF supply

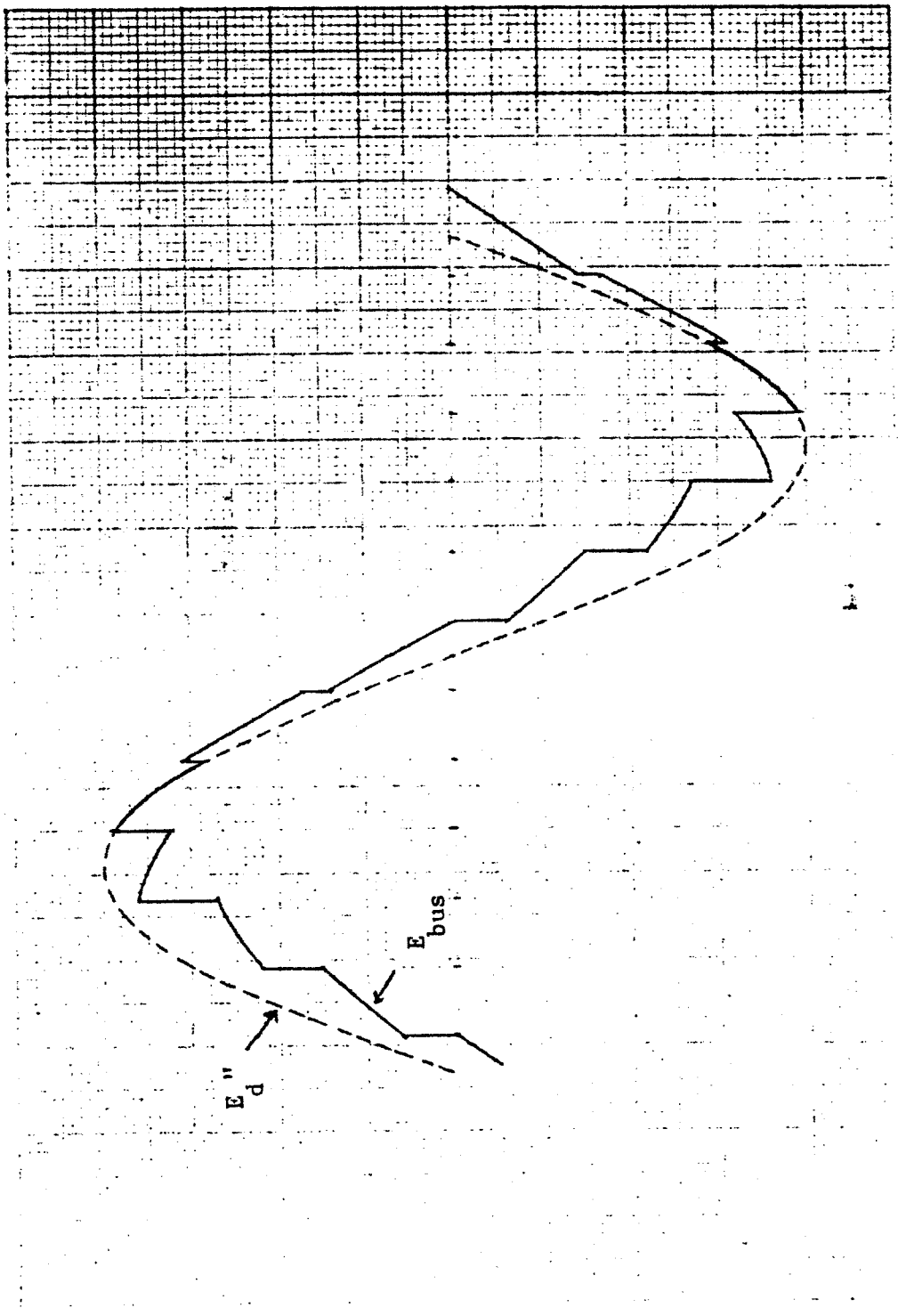

Figure 4-2: Doublet III alternator line to line waveform showing distortion prior to flat-top

(only) and less than 3% for operation of both the TF and OH supplies at the end of the ramp-up period (when both measures of the alternator voltage are normalized to the no-load values). This finding has the following implications:

(A) If the exciter/regulator is maintaining the rectified terminal voltage constant during the ramp-up period, then the fundamental component of the terminal voltage must also be very nearly constant.

(B) Conversely, if the fundamental component of the alternator is found, by experiment, to fall during the ramp-up period, then the regulator cannot be holding the rectified voltage constant.

(C) Any transient recorded on the rectified alternator voltage will accurately represent a transient of the fundamental component of the voltage, so long as alternator loading is balanced.

(D) The rectified alternator voltage can be used to represent the RMS terminal voltage (V_t) in the simplified phasor diagram for the calculation of overhsoots when normalized to the unloaded value of V_t.

Based on the results of the physical scale model study, we find that the regulator/exciter will hold the fundamental of the alternator terminal voltage constant within about 2% during the ramp-up periods of the TF and OH supplies (figure 2-12). The magnitude and duration of alternator voltage transients are controlled by the dynamics of the

exciter/regulator control loop; alternator voltage overshoot will occur as a consequence of armature current interrupt. Under this condition the terminal voltage will rise immediately to E_d'' and then approach E_d' with a time constant on the order of τ_{do}'' (τ_{do}'' is the subtransient time constant given in section 2.2 as .05 seconds). The exciter/regulator will attempt to restore the alternator voltage to the pre-interrupt value. Based on the results of this study and experience with the similar Doublet II exciter, the small signal exciter/regulator response time is estimated to be on the same order as τ_{do}''. Therefore the voltage E_d' will fall during overshoot as the terminal voltage approaches it. The peak terminal voltage overshoot will consequently be limited by the regulator to some intermediate level between the pre-interrupt values of E_d'' and E_d'. This increment from the regulated value will then be driven to zero within about 10 cycles by regulator action if exciter voltage limits are not reached.

The exciter forcing voltage limit effectively defines an incremental maximum rate of change of the alternator output voltage that the exciter/regulator feedback loop can create. The ability of the exciter to invert the field current is of particular importance. If the exciter cannot invert then the maximum rate at which the alternator output voltage can be restored to its pre-interrupt value is:

$$\frac{100\%}{\tau_{do}'} = \frac{16.6\%}{\text{sec}}$$

This implies that a small signal (linear) exciter loop model will hold only for overshoots of less than:

$$\frac{100\% \cdot \tau_{loop}}{\tau_{do}'} = .8\%$$

The ac input to the exciter is 480 Vac. Analysis of G.E. specifications indicates that the exciter is capable of nearly full inversion, and therefore of supplying -1250 Vdc to the generator field. The field voltage at flat-top will be approximately 200 Vdc; the maximum rate of change of the alternator voltage is therefore:

$$\left(1 + \frac{1250}{200}\right) \frac{100\%}{\tau_{do}'} = \frac{121\%}{\text{sec}}$$

Which implies that the exciter will not voltage-limit, and that a small signal exciter loop model is accurate, for overshoots less than:

$$\left(1 + \frac{1250}{200}\right) \frac{100\% \ \tau_{loop}}{t_{do}'} = 6.04\%$$

The use of τ_{do}' in the above discussion is valid when alternator loading is near zero during overshoot recovery, as it

is after flat-top for the case where the TF supply is used with a free wheeling diode (FWD). During loaded overshoot recovery τ_{do}' must be replaced by the loaded field time constant (see Appendix C). Taking the TF supply without a FWD as an example, we find that the loaded field time constant at the end of flat-top to be around 2-3 seconds, compared to the unloaded value of τ_{do}' which is 6 seconds. In this case the largest overshoot which will not cause the exciter to limit is around 15%.

If the exciter voltage limit is reached during overshoot recovery, then the recovery time will be larger than that predicted by the physical scale model (exciter voltage limits of the physical scale model were not reached during the Doublet III tests).

4.2.1 Use of the phasor diagram for overshoot estimation

In this section the use of the simplified phasor diagram as a tool for estimating generator transients is illustrated. Operation of the TF supply with FWD is used as an example (OH supply off). In figure 4-3 are shown the TF coil voltage and current profiles generated during normal system operation, indicating the times T_1 and T_2 which are referred to in the following analysis.

Immediately prior to T_1 the appropriate simplified phasor diagram representation of the alternator is shown in figure 4-4A. At time T_1 the converter is rapidly phased

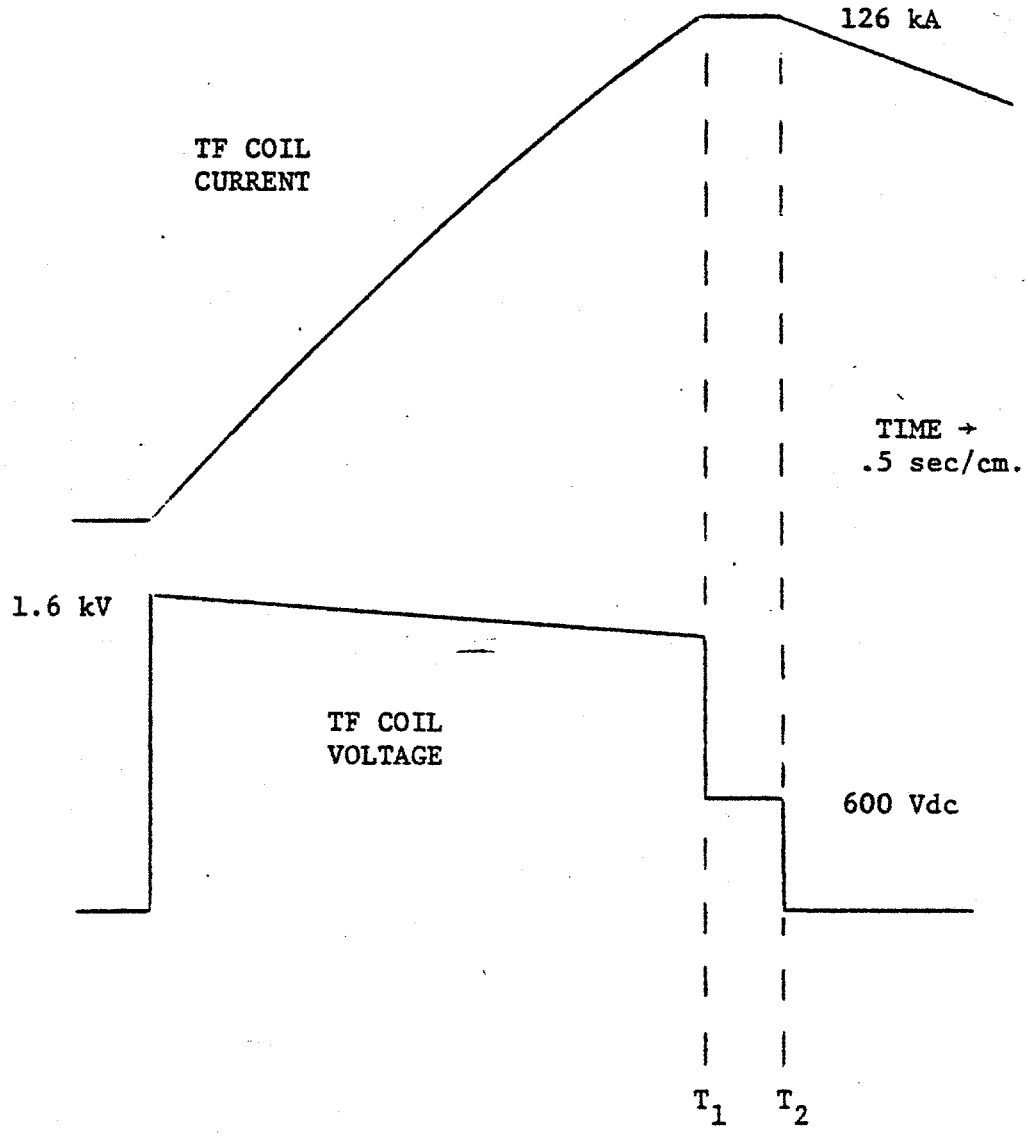

Figure 4-3: Doublet III TF coil voltage and current profiles indicating the critical times T_1 and T_2 for phasor diagram analysis

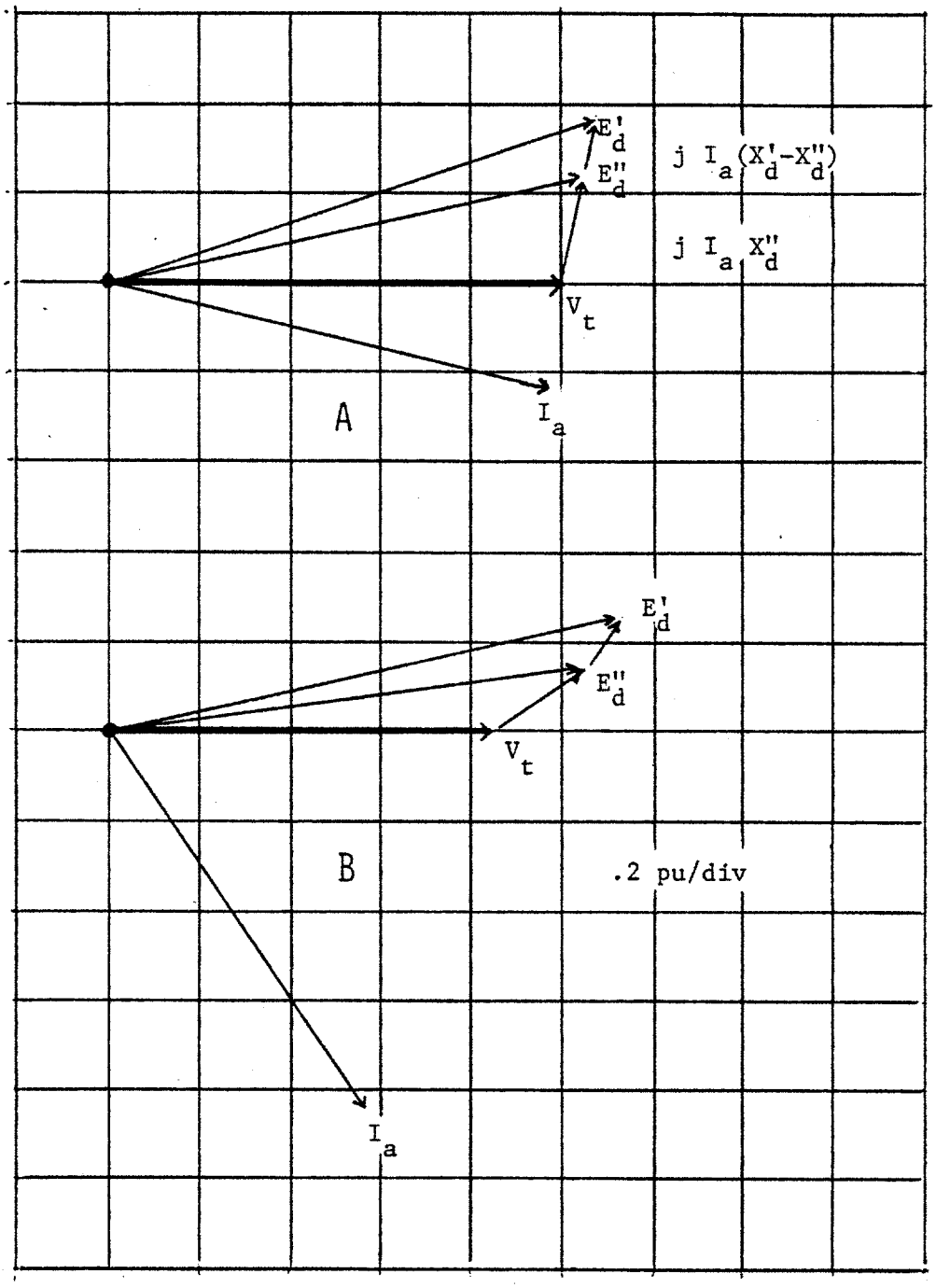

Figure 4-4: Phasor diagram sequence used for predicting alternator transient during TF coil current pulse (.2 pu / div)

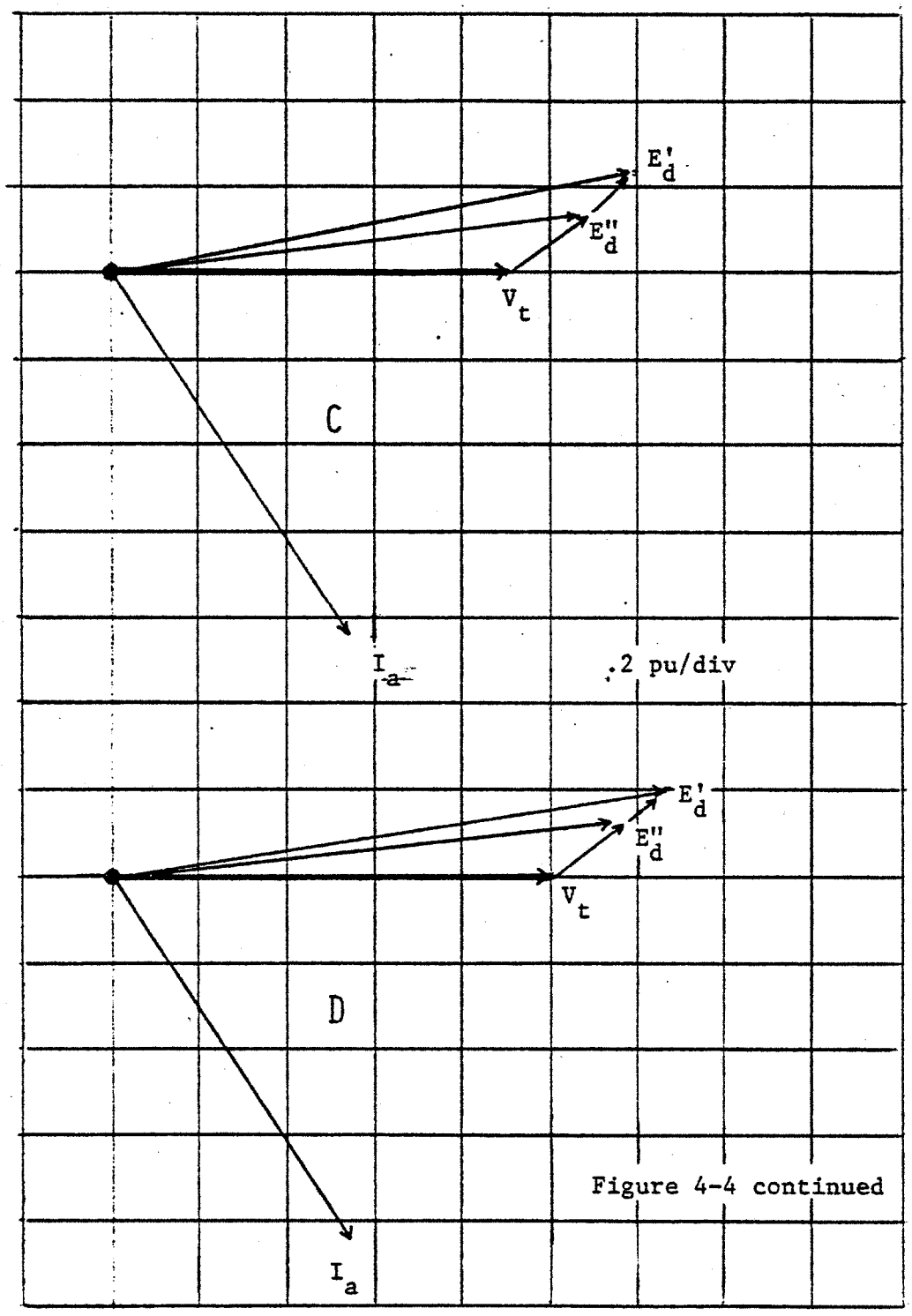

Figure 4-4 continued

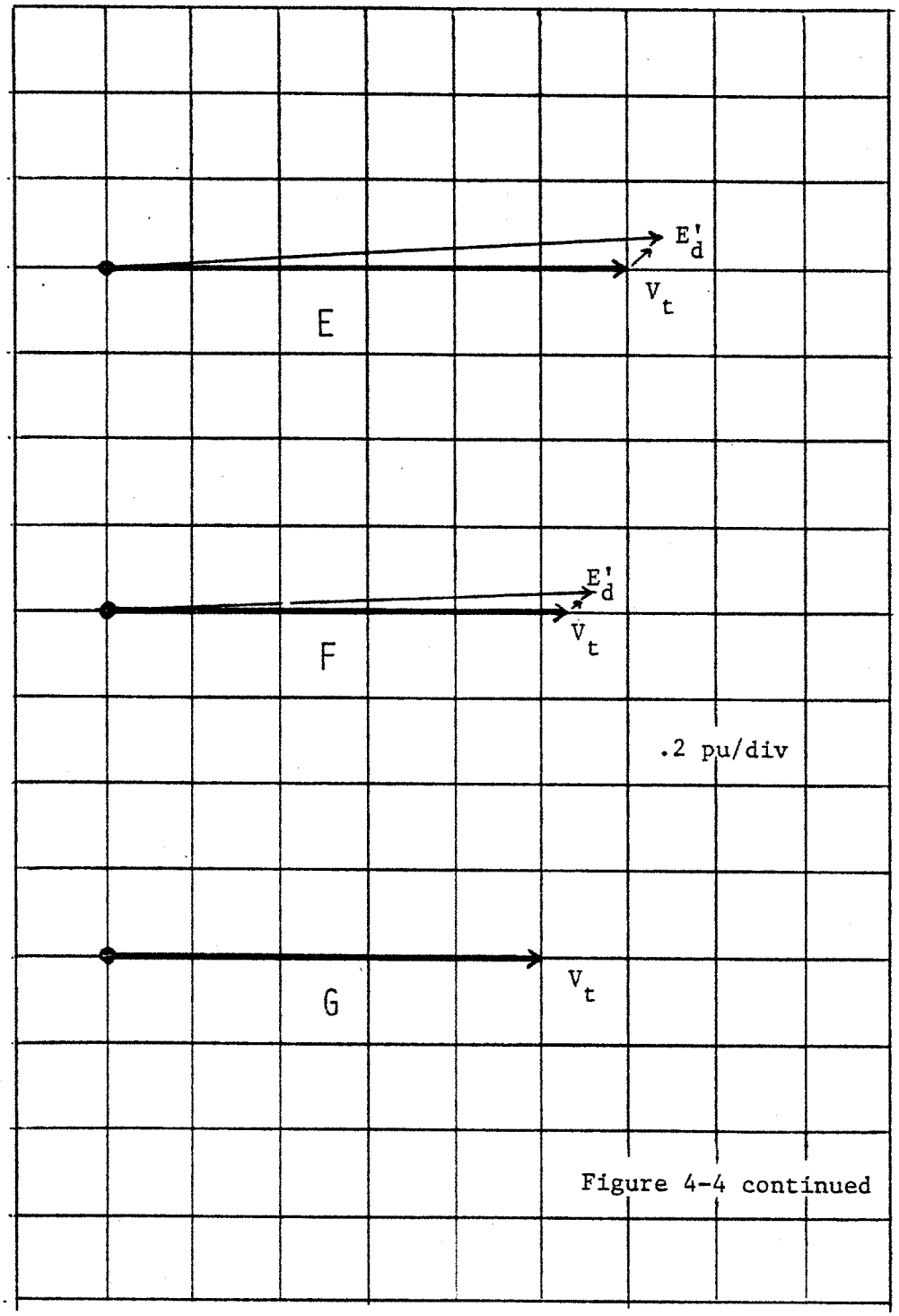

Figure 4-4 continued

back to flat-top. Since E_d'' and E_d' cannot change instantaneously, the phasor diagram of figure 4-4B will now apply. After about one subtransient time constant the combination of the natural alternator response and exciter/regulator action will give rise to the diagram of figure 4-4C. After about four time constants the system will stabilize according to figure 4-4D. This same diagram will represent the alternator immediately prior to the inversion command (although the machine voltages will fall slightly as the alternator frequency falls during flat-top). Following the inversion command at T_2, the load current is immediately transferred from the supply to the FWD and figure 4-4E is used. This diagram evolves into figures 4-4F and 4-4G after one and four T_d'' time constants, respectively. The magnitude of the alternator terminal voltage, V_t, taken from these diagrams, is plotted in figure 4-5 with the times T_1 and T_2 shown.

The alternator transient as predicted here corresponds closely with the result of the physical scale model test of figure 2-8, which demonstrates the validity of the phasor technique as applied to alternator transient prediction.

4.2.2 Alternator voltage transient prevention

The conditions which give rise to generator terminal voltage transients for normal system operation, as revealed by this study, are listed in their normal time sequence:

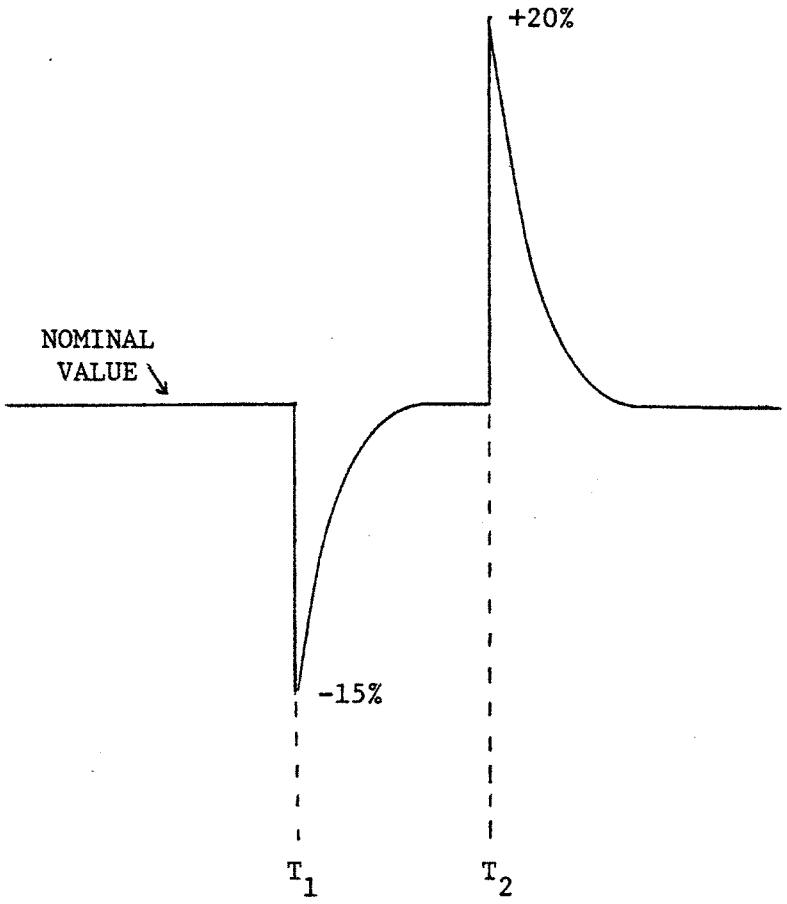

Figure 4-5: Alternator voltage transient as estimated using phasor diagrams

(A) transient undervoltage caused by TF supply phaseback to flat-top

(B) transient overvoltage caused by OH supply disconnect

(C) transient undervoltage caused by OH supply reconnect

(D) transient caused by OH supply phaseback to inversion (this was an undervoltage transient in the physical scale model tests, but the phasor diagram representation indicates that it can be an overshoot for certain values of pre- and post-phaseback angle)

(E) transient overvoltage caused by TF supply phaseback to inversion

The two important effects of these transient conditions are:

(1) overvoltage stress on alternator, rectifiers, etc.

(2) perturbations of the rectifier gate control circuits of all supplies connected to the alternator (at best this may cause only slight transients in supply outputs and at worst this may result in thyristor misfire and catastrophic failure)

It appears that the elimination of these transients would considerably enhance the reliability of the system and additionally may improve the experimental conditions. All transients caused by normal system operation are the result of rapid changes of the magnitude or angle of the armature current. Except for the reconnection of the OH supply during flat-top, all alternator terminal voltage transients

can be eliminated by decreasing the rates of change of their causative armature current magnitude/angle variations. In this way, the exciter/regulator may be given time to act, whereupon it will remove the overvoltage/undervoltage condition through regulator action. This solution is only made possible by the extraordinary speed of the G.E. exciter. The necessary modifications to the system are:

(A) Modify the TF supply control so that the phaseback to flat-top occurs over a period of about 100 msec. This will have the effect illustrated by the dashed line "A" in figure 4-6.

(B) Modify the TF supply control so that the phaseback to inversion occurs over about 200 msec. This will have no detrimental effect on the load current profile and will also work with an FWD.

(C) Modify the OH supply control so that the phaseback to disconnection is slowed to about 50-100 msec. Also install a FWD in series with the crowbar switch as shown in figure 4-7. The switch sequence would then be redefined as shown in figure 4-8. The crowbar switch would no longer be required to close with any voltage across it. The reason for adding the FWD is to allow the OH supply current to gradually transfer to the crowbar branch over the period of about 50-100 msec prior to supply disconnect.

(D) Modify the OH supply to slow the phaseback to inversion at the end of flat-top to about 100 msec.

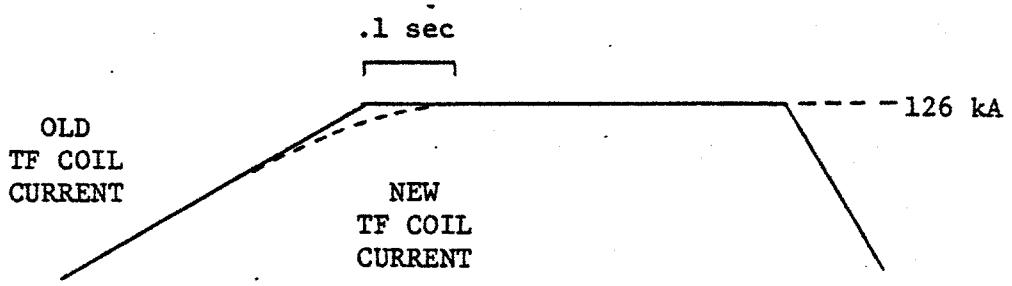

Figure 4-6: Effect of the modification which reduces the transient at the start of flat-top

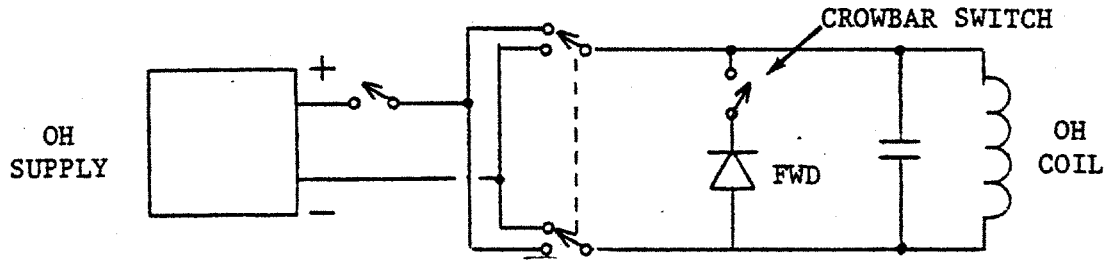

Figure 4-7: Location of FWD in OH coil switching network

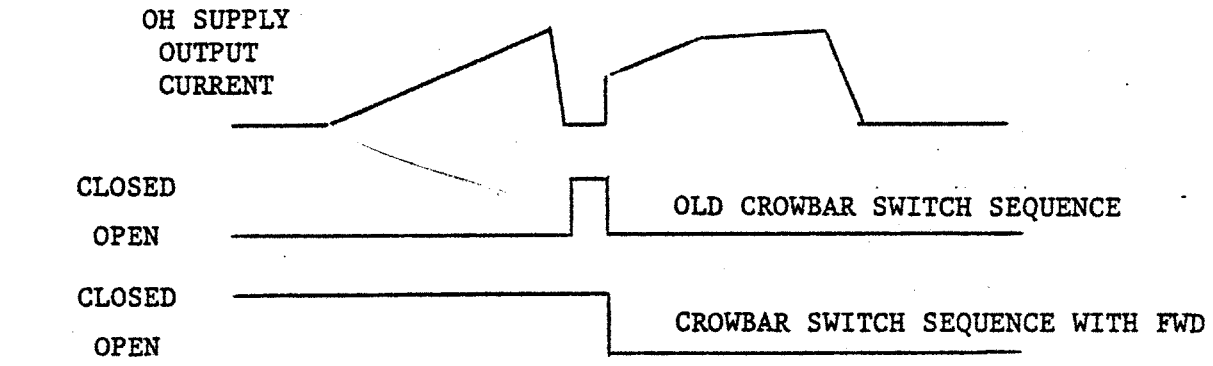

Figure 4-8: New OH supply crowbar switch sequence after installation of FWD

The times given in the modification descriptions are approximate and based on a small signal model of the exciter. If exciter voltage limits are reached, then these times must be extended slightly to prevent transients.

CHAPTER V

OPERATIONAL CONSIDERATIONS FOR REGULATED RECTIFIER SETS

Toroidal field supplies are, in general, required to produce constant output current during the experimental interval, which lasts for .1 to 2 seconds. In alternator driven rectifier set type supplies, the required constant current must be produced despite changes in the amplitude, waveshape, and frequency of the ac input to the controlled rectifier set and variations of the real and imaginary parts of the toroidal coil impedance due to heating and plasma generation.

Closed loop load current regulation schemes are employed in an attempt to regulate toroidal field coil current; in this chapter, the factors which influence the loop characteristics (and hence the transient response) of this type of current regulator are investigated, in order to ascertain the theoretical limits of effective regulation.

This chapter deals with a class of regulators of the form shown in the one-line diagram of figure 5-1. The main feedback control loop consists of an amplifier, rectifier, load, and adder as shown in figure 5-2. In order to analyze this feedback system using linear cir-

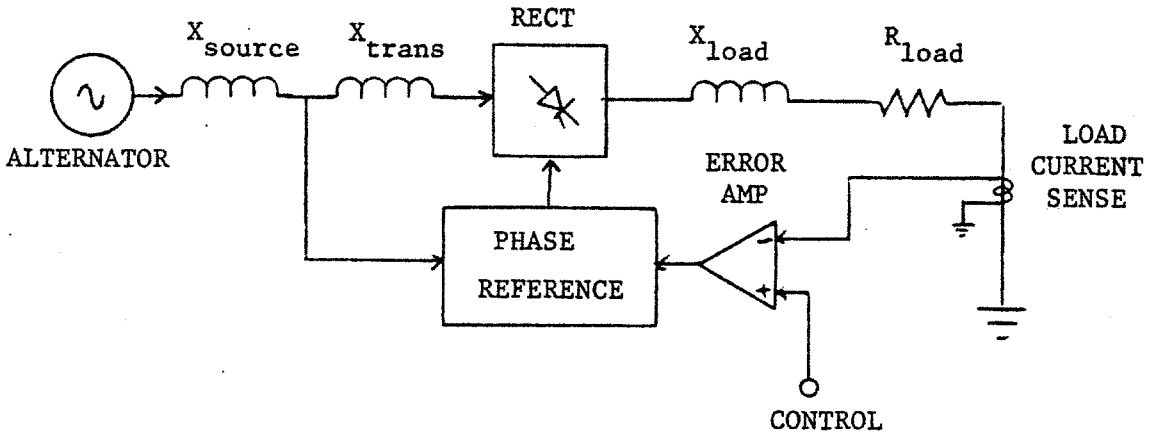

Figure 5-1: One-line diagram of regulated, alternator driven, rectifier set

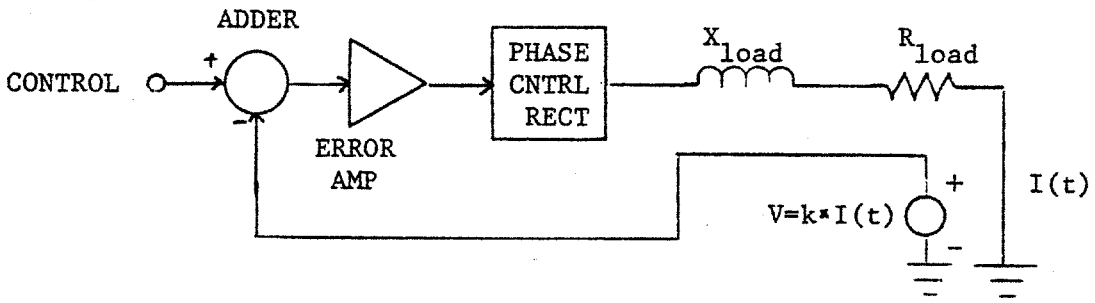

Figure 5-2: Main feedback control loop of regulated rectifier set

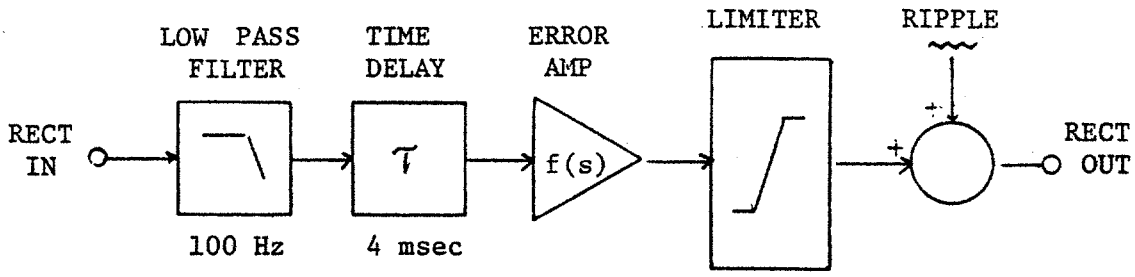

Figure 5-3: Describing function representation of rectifier control loop

cuit techniques, it is necessary to construct a describing-function representation of the rectifier set.

5.1 Regulator dynamics

The low level dc rectifier set phaseback control signal input is filtered to remove ripple and noise in the amplified error signal with a single pole at approximately 100 Hz. The filtered control voltage is then compared to a reference waveform to determine the rectifier firing angle. Due to the fact that the average dc rectifier output voltage is a cosine function of the rectifier firing angle, the reference waveform used is an arc-cosine function which is derived from the integral of the sinusoidal rectifier source voltage. The result is that the average dc rectifier output voltage is a linear function of the filtered low-level control voltage. The average dc no load output voltage of the rectifier set can be expressed as*:

$$V_{dc_{ave}} = \frac{k \times V_{control} \times E_d''}{\omega}$$

* A special circuit described in appendix B was implemented in the physical scale model to remove the ω dependence of this expression. This circuit was utilized in Doublet III simulations where the value of E_d'' was approximately independent of frequency due to exciter action. This circuit was not used in the Alcator C simulation since in this case constant field voltage excitation caused the ratio of E_d'' to ω to be approximately independent of frequency.

The instantaneous output voltage of the supply is pre-determined after the instant of a rectifier firing for a length of time given by:

$$t = 1/(f \times n)$$

where f is the input ac bus frequency and n is the pulse number of the rectifier set (six, twelve, etc.). As far as the control loop is concerned, the rectifier transfer characteristic includes an added ripple component and a delay with uniform probability distribution over the interval from zero to $1/(f \times n)$. In an unconditional stability analysis, the worst case value of the delay, which in this case is $1/(f \times n)$, must be assumed. In the Alcator C power supply system, $1/(f \times n)$ is equal to:

$$1/(f \times n) = 1/(40\text{hz} \times 6) = 4 \text{ msec}$$

The load current ripple resulting from the rectifier output voltage ripple component is less than .05% of full output; the value of this component is unaffected by feedback. A complete describing function representation of the rectifier set for low load current levels is diagrammed in figure 5-3.

For stability and well damped transient behavior, it is desireable that the open loop phase shift of the

load current negative feedback regulator loop be well under 180° for frequencies below the unity gain frequency so that adequate loop phase margin will exist despite the effective gain reduction which accompanies signals which excede the rectifier output swing capability. Therefore a 1/s open loop frequency response characteristic is selected for frequencies below the crossover (unity gain) frequency. This type of integral (1/s) feedback has the additional advantage that the static closed loop error is zero. To achieve the 1/s open loop characteristic the following transfer function is selected for the loop error amplifier:

$$f(s) = k_3 \times \frac{(1 + \tau s)}{s}$$

where τ is selected to cancel the excess pole resulting from the load time constant (L/R).

The open loop phase shift of the regulator is composed of three components, namely:

A) Phase shift due to 1/s characteristic.
B) Phase shift due to 100hz pole in rectifier set describing function.
C) Phase shift due to 4msec rectifier firing time delay

The phase characteristics of these three components are combined in order to plot the open loop phase margin at the crossover frequency as a function of frequency in

figure 5-4.

Fast transient response with overshoot less than 5% dictates a phase margin of around 60^{o}. The crossover frequency is therefore selected to be 15 Hz. This gives a gain margin of around 12 db. The open loop regulator gain function is shown in figure 5-5. The approximate closed loop response of the load current to a step command via the "set" input is shown in figure 5-6. Note the response uncertainty which results from the rectifier firing delay. The response to a step load disturbance, which might result from coil coupling in the fusion machine, is shown in figure 5-7. Note that attempts to minimize the response time by increasing the loop gain through the use of special loop compensation techniques will not compensate for the inherent rectifier delay. Therefore, the contribution of speed-improving compensations will be significant only in systems where the uncompensated closed-loop regulator response is long when compared with the rectifier delay. In any case, due to the stochastic nature of the rectifier delay it is unwise to allow it (rectifier delay) to dominate the transient response in systems where repeatability is essential, as it is in fusion experiments. If response speed is inadequate, then either the ac input frequency or the rectifier pulse number must be increased.

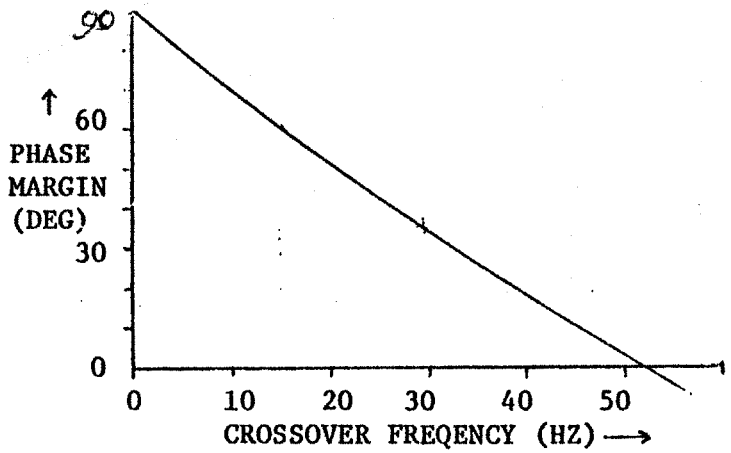

Figure 5-4: Regulator phase margin as a function of crossover frequency

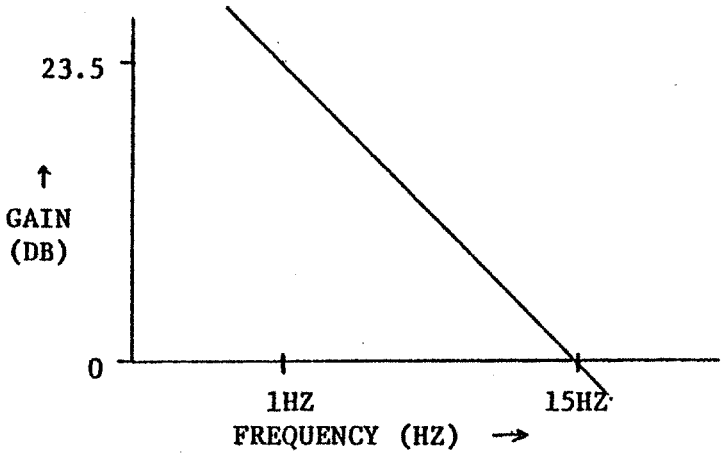

Figure 5-5: Regulator open loop gain as a function of frequency

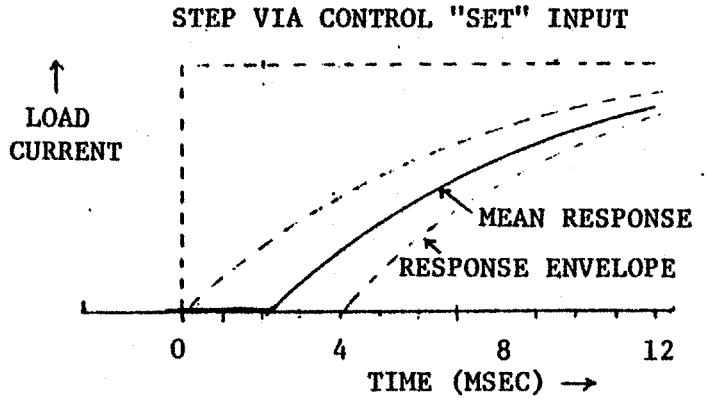

Figure 5-6: Regulated load current response to step via control "set" input

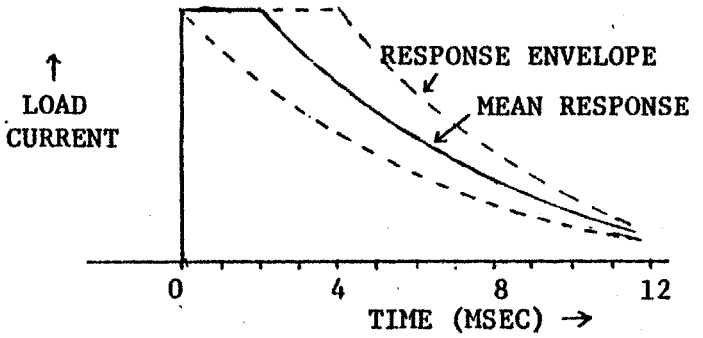

Figure 5-7: Regulated load current response to load disturbance

5.2 Loop Gain Variations at Extreme Phase Control Angles

It has been stated that the operation of the rectifier firing control requires low level sinusoidal reference waveforms derived from the sinusoidal rectifier source voltage. In Chapter 4 it was shown that the sinusoidal rectifier source voltage is the internal alternator voltage behind subtransient reactance E_d"; since this voltage is not accessable, the low level reference waveforms are instead derived from the alternator terminal voltage, which differs from E_d" by the voltage drop across the subtransient reactance X_d", a voltage which is equal to the product of j X_d" and the non-sinusoidal armature current $I_a(t)$.

For values of load current approaching 1 pu on the alternator base, the voltage drop across the subtransient reactance X_d" will approach 16% of the rated alternator voltage for the Alcator C system. Under this condition the magnitude and phase of the reference signals derived from the alternator terminals will differ appreciably from the theoretically required values derived from the sinusoidal source voltage. Due to the nature of the rectifier transfer characteristic, reference signal magnitude and phase errors will cause the rectifier set incremental gain ($\Delta V_{dc\ ave\ rect}/\Delta V_{control}$) to vary according to:

$$\text{gain} = k\ E_d" \frac{\text{slope optimal reference } (F_1)}{\text{slope actual reference } (F_2)}$$

where

$$F_2(\alpha) = M\, F_1(\alpha-\phi)$$

with M and ϕ related to the reference waveform parameters as in figure 5-8. Therefore the incremental gain is:

$$\text{gain} = \frac{\frac{\delta}{\delta\Theta}\cos\alpha}{\frac{\delta}{\delta\Theta} M\cos(\alpha-\phi)}\, k\, E_d'' = \frac{k\, E_d''}{M\,(\cos\alpha - \frac{\sin\phi}{\tan\alpha})}$$

The magnitude error (M) and the phase difference (ϕ) are determined from the phasor diagram of figure 5-9. The rectifier set gain expression is evaluated for the Alcator C alternator (X_d'' = .165 pu) with toroidal field coil flat top conditions, namely $E_d'' \cong .8$ pu $I_a \cong 1$ pu in figure 5-10 as a function of the phaseback angle α. From the figure note that large increases of open loop regulator gain will result from regulator operation at small phaseback angles for large values of load current. Consequently, regulator function or stability may be lost if the rectifier is forced to regulate at small phaseback angles. Designing with large loop gain margin at the crossover frequency is essential to accommodate this type of gain variation, with the consequence that the dynamic regulator performance will be compromised

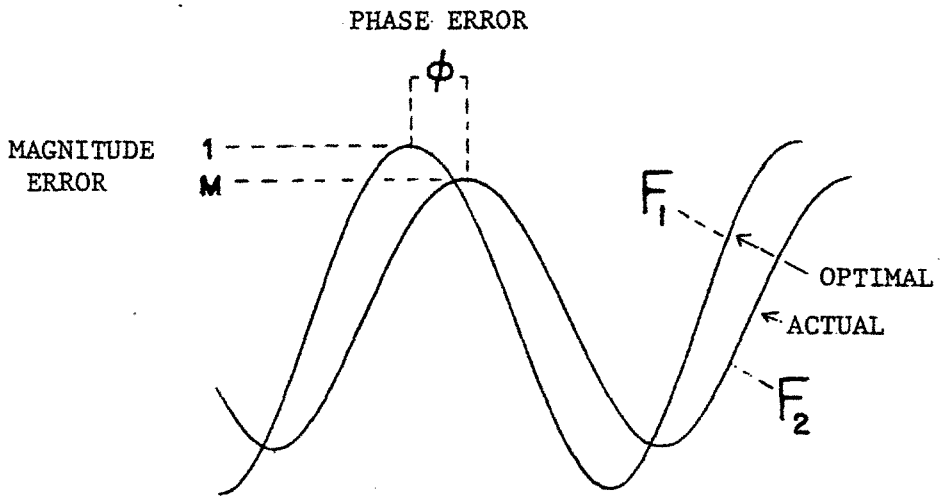

Figure 5-8: Relation between actual and optimal reference waveforms

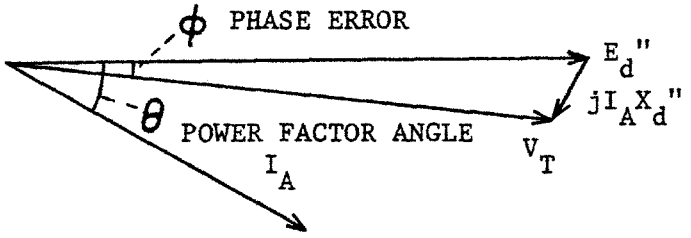

Figure 5-9: Phasor diagram for determination of reference waveform errors

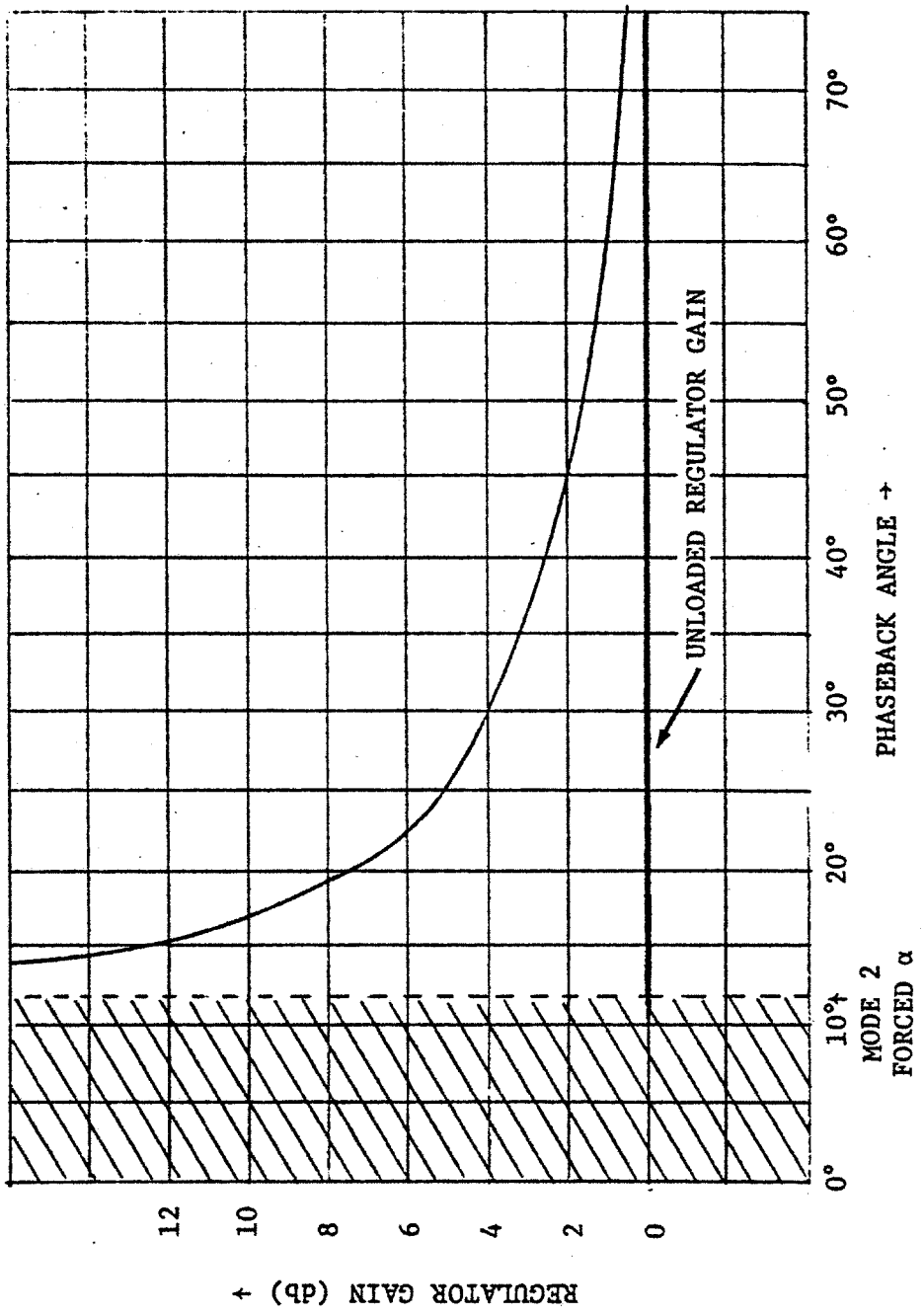

Figure 5-10: Normalized Alcator C TF supply open loop regulator gain at flat-top as a function of phaseback angle

by the accompanying decrease of the high frequency open loop gain. Phase control angle limits may be incorporated in the gate drive electronics to prevent the regulator from entering regions of excessive gain.

5.3 Rectification End-Stop Error

In addition to the load current regulator open loop gain changes which occur at small phaseback angles, there is a fundamental limit to the magnitude of the output voltage which occurs at $\alpha = 0$. In practical systems, an artificial limit is electronically established at around $\alpha = 5^{o}$, in order to guarantee that the fast rising edge of the gate pulses should not occur during times of negative anode-to-cathode SCR voltage, which would occur if $\alpha < 0$. Due to the cosine nature of the rectifier transfer characteristic as a function of α, the output capability sacrificed to the artificial 5^{o} phaseback ϕ is less than .5%. The phaseback angle α is measured with respect to the line-to-line voltage zero crossings of the sinusoidal rectifier source voltage behind the commutation reactance $E_d"$. Therefore, the proper approach to setting the artificial 5^{o} end-stop is to reconstruct the internal alternator voltage $E_d"$ from the alternator terminal voltage. The conventional approach is to derive the 5^{o} phase control end-stop from the fundamental component of the alternator terminal voltage waveform.

Unfortunately, the fundamental component of the alternator terminal waveform (V_t) is shifted in phase from the internal alternator voltage E_d" by an amount dependent on the load current. This phase shift is determined by the method described in the previous section. The composite artificial end stop limit is the sum of the electronic 5^o limit and the phase difference between E_d" and the fundamental of V_t. The tables in Appendix A can be used to determine the additional output voltage capability loss in this case.

5.4 Improved Reference Voltage Source

Rectifier power supply performance is degraded when the low level bus reference signals used by the SCR gate firing circuits do not accurately correspond to the sinusoidal rectifier source voltage in phase and magnitude. In particular, the previous sections have addressed issues of:

(A) Rectification end stop error due to reference phase error;

(B) Loop gain variations due to bus reference phase and magnitude error.

These undesirable effects would be eliminated if the internal alternator sinusoidal voltage behind subtransient reactance E_d" could be obtained as a reference signal source, instead of using the distorted rectifier terminal voltage.

In the course of this study, a circuit was designed which can reconstruct the sinusoidal voltage E_d" from the available alternator terminal-derived reference voltages. Since no circuitry of this type was used in the modelled power supply systems, it was not used in any of the described experiments. Nevertheless, the circuit principles are outlined here, since the elimination of the performance sacrifices due to the aforementioned undesirable effects may eventually be considered important for future designs.

Notches appear on the alternator terminal-derived reference waveforms due to voltage drop across the alternator subtransient reactance during commutation. These notches can be expressed as:

$$\underbrace{E_d"_A}_{\text{sine source}} = \underbrace{V_{bus\ A}}_{\text{ref. wave}} + \underbrace{k_{1A} \frac{\delta}{\delta t} I_A}_{\text{major term}} + \underbrace{k_{2A} \frac{\delta}{\delta t} I_B + k_{2A} \frac{\delta}{\delta t} I_C}_{\text{coupled terms}}$$

This expression shows that the addition of a weighted sum of the derivatives of the bus currents to the distorted reference waveform can generate a sinusoidal reference voltage which corresponds in magnitude and phase with E_d". The expression can be electronically realized so that actual notch-free reference waveforms can be produced. If each bus line is the single turn primary of a small current transformer, then the open circuit secondary voltage of each

transformer is proportional to the derivative of the primary current. These voltages can then be scaled and combined with the distorted reference waveforms using operational amplifier adder circuits. The values of the weighting constants are determined from the current transformer turns ratio, the current transformer magnetizing inductance, the inter-phase coupling coefficients of the alternator subtransient reactance, and the ratio of the subtransient reactance to the total commutation reactance. The major benefits of this type of scheme are:

(A) Slightly higher rectifier output voltage for high load current levels, due to elimination of rectification end stop error

(B) Improved regulator loop dynamics at phase-back angle extremes, due to correct reference phase and magnitude.

5.5 Multiple rectifier sets

It has been shown that serious regulator loop gain variations can result when rectifier firing reference signals do not correspond in magnitude or phase to the sinusoidal rectifier source voltage behind the commutation reactance. A solution to this problem has been proposed for the case of a single regulated supply operating from a reactive source. Unfortunately, the solution cannot be directly applied to the more general case of multiple rectifier sets driven from the same reactive source. In particular, the sinusoidal rectifier source voltage behind

commutation reactance is not the optimal reference waveform in multiple supply systems. When the control of one regulated rectifier set out of a group is considered, then the effects of other group members must be included in the rectifier source representation.

In a multiple rectifier set system where rectifiers share a common reactive source, each regulated rectifier set experiences two effects as a result of the firing angle or load changes which occur in adjacent units:

(1) The apparent rectifier source voltage behind the rectifier commutation reactance changes in magnitude and waveshape.

(2) The rectifier set transfer characteristic is modified, which changes the incremental open loop gain.

A regulated rectifier set responds to these disturbances by changing the rectifier firing angle to maintain the regulated output; the exact time response of the output of the disturbed regulator is determined by closed-loop regulator dynamics. Due to finite closed loop regulator gain and bandwidth, significant crosstalk will exist between rectifier set outputs; the degree of supply interaction will be strongly dependent on system loads.

A supply load disturbance resulting from operation of a neighboring supply can be prevented if the regulator-

controlled rectifier phaseback angle is modified by an appropriate "phaseback adjustment function". The phaseback adjustment function is related to control or load variables of the disturbing supply. In this way the closed loop dynamics of the disturbed regulated supply are bypassed, effectively increasing the ability of that supply to reject crosstalk interference. In addition, distortions of the transfer characteristic of the disturbed supply are cancelled if the phaseback adjustment function is properly selected.

If each regulated supply of a group receives appropriate phaseback adjustment functions from all other supplies in the group, then operation of the supplies can be considered orthogonal in the sense that changes in the operating conditions of any supply will not introduce effects on neighboring loads (note however that no phaseback adjustment is possible if the disturbed supply is in rectification or inversion phaseback limits). This result is independent of regulator open loop gains, and can therefore be extended to include rectifier sets which use open loop (programmed phaseback) control.

Real time synthesis of optimal phaseback adjustment functions is computationally difficult and is therefore only recommended when the ultimate in interference-free rectifier set control is required. In most cases the natural ability of a regulated supply to reject crosstalk interference will be adequate. The crosstalk rejection

ability of a regulated supply will decrease with increasing crosstalk frequency due to falling regulator open loop gain. In systems where high frequency crosstalk rejection is inadequate, crude bandlimited phaseback adjustment functions can be employed to advantage. In particular, if a supply is unable to adequately suppress the high frequency crosstalk which results from a step change in load or phaseback angle of an adjacent supply, then a high pass filtered step function of appropriate amplitude used as a phaseback adjustment function can reduce the high frequency load disturbance. Some power supplies investigated in this study have built-in provisions to accept phaseback adjustment functions. These provisions are called "feed-forward inputs".

5.5.1 Bandwidth limit of orthogonality

The bandwidth limit of orthogonality in an optimized orthogonal multiple rectifier set control system cannot exceed the frequency nxf, where n is the rectifier pulse number (six, twelve, etc.) and f is the ac source frequency. This limitation is due to the inherent rectifier firing delay. Note that there is always a large amount of unavoidable undesirable energy at and above the frequency nxf due to rectifier ripple.

5.5.2 Application for supplies using orthogonal control

The degradation that fusion experiments will suffer as a function of the magnitude and character of supply interference is not known at this time. Consequently, the quantitative effects of supply interference were not determined in this investigation. Nevertheless, the apparent desire to control plasma conditions with increasing precision will eventually dictate the use of centralized orthogonal control for multiple phase-controlled rectifier type magnetic field supplies driven from non-stiff sources.

5.6 Free-wheeling diode considerations

In power supply systems where the energy in the inductive rectifier load is substantial, arc-over and fire can result if the load current is interrupted by rectifier or dc bus failure. In such cases, protection of components and personnel can be improved through the use of a free-wheeling diode (FWD) electrically across and physically near the inductive rectifier load. A carefully designed spark-gap can replace the FWD when the inductive load energy is a few MJ or less.[4] A typical FWD connection is shown in figure 5-11.

The presence of an FWD across the rectifier load will have no effect on the supply operation as long as the rectifier set is operated without intentional phaseback. The FWD connection prevents the load from seeing the instantaneous

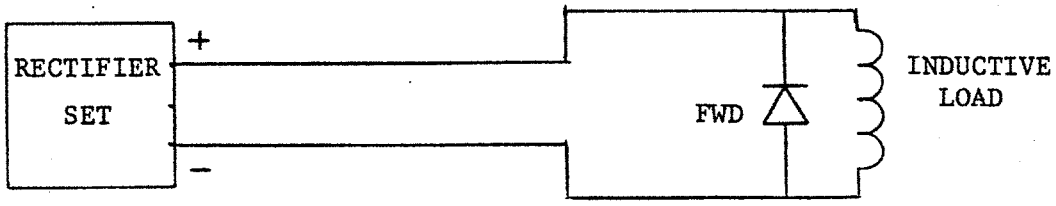

Figure 5-11: Diagram indicating location of FWD for system protedtion

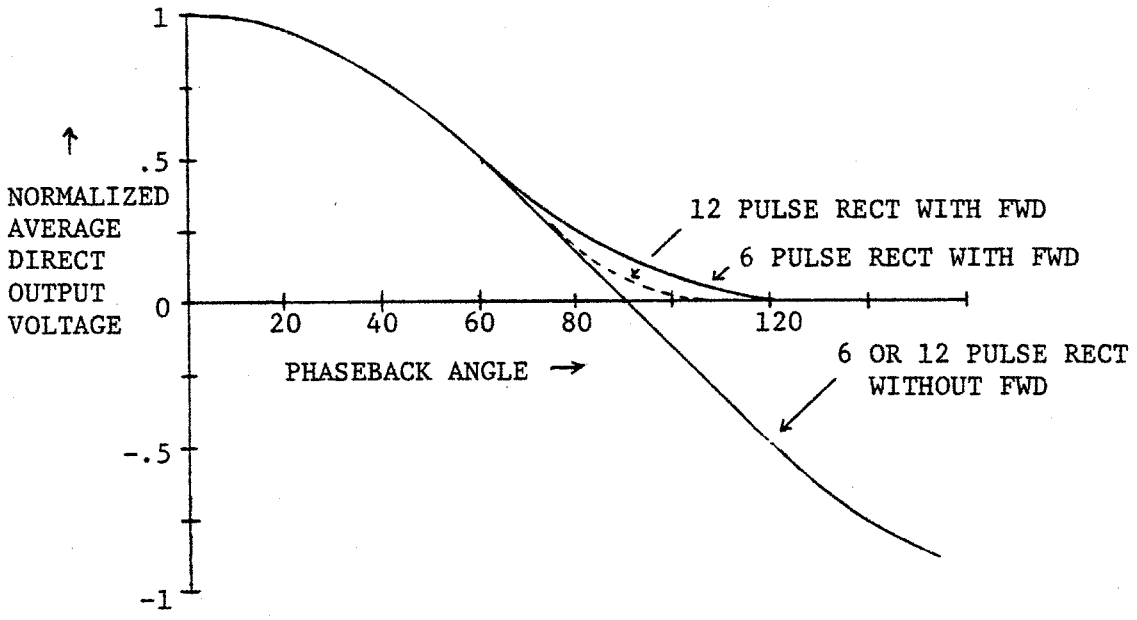

Figure 5-12: No-load transfer characteristic of rectifier set showing effect of FWD

negative rectifier voltage waveform peaks associated with phaseback; the return of energy for the dc load to the ac rectifier supply (inversion) is therefore prevented. Phaseback angles of greater than 120° will guarantee that the load is completely disconnected from the source, since it can be shown that the FWD clamp causes all rectifier bridge SCR's to be triggered under conditions of negative anode-to-cathode voltage (reverse bias). Under this condition inductive load current is forced to circulate through the FWD.

The cosine no-load transfer characteristic (E_d/α) of the standard 6 pulse rectifier is modified by the presence of the FWD as shown in figure 5-12; the figure implies that regulator open loop gain is decreased for phaseback angles greater than 60°.

Commutation between the rectifier set and the FWD occurs for phaseback angles between 60° and 120°; gate firing control design must be compatible with this mode of operation:

(1) The phase referencing circuits should not be disturbed by the additional ac bus distortion.
(2) Rectifiers must be supplied with <u>full 120° wide gate pulses</u>.

The second requirement is due to the fact that each of the six rectifier bridge legs is composed of a large number of parallel-connected SCR's. If this second requirement is not satisfied then the rectifier bridge may be damaged.

The conditions under which FWD operation may damage a rectifier bridge are examined:

> Consider the condition where the rectifier is operated at a phaseback angle between 60^{o} and 120^{o} at rated load. Assume that the load current path is as follows: Bus phase A→rectifier→load→rectifier→bus phase C. The next bridge commutation is from A phase to B phase. Due to the assumed phaseback angle the FWD will begin to conduct before the A to B commutation. Load current will attempt to transfer from the A and C phases to the FWD at a rate limited by the source commutation reactance. As the load current transfer to the FWD approaches completion, individual rectifiers in the bridge will begin to drop-out (cease condution) due to holding current limitations. Holding current drop-out of parallel-connected SCR's within a bridge leg will <u>not</u> be simultaneous. If the A to B commutation occurs when most C phase rectifiers have dropped-out, then the load current will begin to transfer back to the rectifier bridge and overload the C phase rectifiers which remain on. This situation can be prevented by using 120^{o} wide gate pulses in order to retrigger rectifiers which dropped out due to the holding current limit.

If an FWD system is chosen for safety reasons, then performance can be improved over the simple FWD connection by using a FWD-resistor series combination. The resistor might be selected to drop the rated supply voltage at the rated load current. The features of this system are:

(1) Rectifier or dc bus failures at the rated load current give rise to coil voltage within the rectifier set rating.
(2) A large part of the stored coil energy is dissipated in the resistor instead of the coil itself upon rectifier phaseback.
(3) Partial return of stored coil energy to the source is possible.
(4) Reduced ac bus distortion during FWD conduction.

CONCLUSIONS

The use of multi-megawatt variable frequency alternators to drive pulsed rectifier loads presents many unique system design problems. In this study, physical scale modelling has been used to evaluate two Tokamak power supply designs and to quantifiy the electrical interaction at the interface between the alternator source and the rectifier load.

Physical scale modelling is reccomended by its conceptual simplicity; the number of assumptions that must be made during physical scale model formulation is small when compared with the number required for numerical models and consequently the use of physical scale modelling offers an improved likelyhood of discovering any unanticipated modes of modelled system operation.

This investigation was instigated in order to address fundamental questions as to whether or not the selected power supply design parameters for the two fusion machines could, if implemented, be used to supply the required time functions of rectifier output voltage and current to the specified loads.

The physical scale models of the two power supply systems revealed unexpected performance shortcomings in both designs. Analysis of the scale model results

led to an understanding of the mechanisims responsible for the measured performance, and performance improving modifications were presented. The performance analysis revealed a number of fundamental principles which should be taken into account when attempting design or analysis of power supplies of this type. These principles are reviewed below:

1) The loaded rectifier output voltage must be calculated according to the formulas of Witzke et. al.[1,2], using the internal alternator ac voltage behind subtransient reactance as the sinusoidal rectifier source voltage. The alternator subtransient reactance must be included as a part of the commutation reactance.

2) The loaded alternator output voltage waveform is not sinusoidal, being equal to the difference between the sinusoidal voltage behind subtransient reactance and the product of the subtransient reactance and the derivitive of the non-sinusoidal armature current.

3) The air-gap flux of a pulse loaded alternator using constant field voltage excitation cannot be assumed to be constant if the load duration is a sizeable fraction of the loaded transient time constant of the alternator (as it is in the Alcator C system).

4) The output voltage of an alternator which is controlled by an output voltage regulating exciter can experience transients approaching 30% of the rated output voltage as a result of step changes of rectifier load or input power factor. These transients can be significantly reduced by proper

control system design.

5) In the Tokamak power supply designs which were investigated in this study there are two mechanisims through which individual power supplies can interfere with one another. The first mechanisim is due to magnetic coupling of the independently supplied coils within the fusion machine. The second mechanisim of inter-supply interference is a consequence of the relatively low stiffness of the ac alternator source when subjected to the large rectifier load, which allows the operation of one supply to change the input voltage of its neighbors. These two mechanisims allow the variations of load or firing angle of a supply to disturb the regulation of adjacent units.

6) If best Tokamak performance depends on controlling Tokamak coil currents with the highest possible accuracy within the largest possible bandwidth, then significant improvements in performance can be obtained through centrallized control of the various power supplies connected to the common alternator bus. Central control allows supplies to reject predictable inter-supply interference faster than individual supply dynamics would normally allow.

A considerable amount remains to be learned concerning the interactions of regulated power converters supplied from dedicated variable frequency alternators. A logical course of future investigation might address problems leading to general solutions for the phase controlled rectifier regulation characteristic when supplied from special classes of non-sinusoidal reactive sources. Solutions to this problem would allow the implementation

of centrallized orthoginal control strategies in order to improve the performance of multiple regulated rectifier sets supplied by a single non-stiff ac source.

APPENDIX A

EFFECTS OF COMMUTATION REACTANCE ON SIX AND TWELVE PULSE RECTIFIERS

The effect of ac source reactance on the six pulse bridge rectifier is to introduce commutation overlap, which reduces the average dc rectified output as a function of the load current. Three modes of rectifier operation are defined as rectifier load increases from no-load to short-circuit.

In the first mode of operation, as the load is increased from no-load, the commutation overlap angle increases from zero to 60°. As the load is incresed beyond this point, the overlap angle remains constant, and a start-of-conduction delay angle is introduced, even though the rectifiers are operated without intentional delay (phaseback). During this second mode the forced delay angle increases from zero to 30°. This forced delay angle remains constant at 30° during mode three, while the overlap angle increases from 60° to 120°.

Analytical expressions for the input-output relationships of six pulse rectifiers operated with zero intentional delay angle into inductive loads are found in the classic paper by Witzke et. al. ; the relationships from the paper are plotted in figure A-1.

In figure A-1 the average dc load voltage, normalized to the no-load value, is shown as a function of $X_c I_{dc}/E_s$

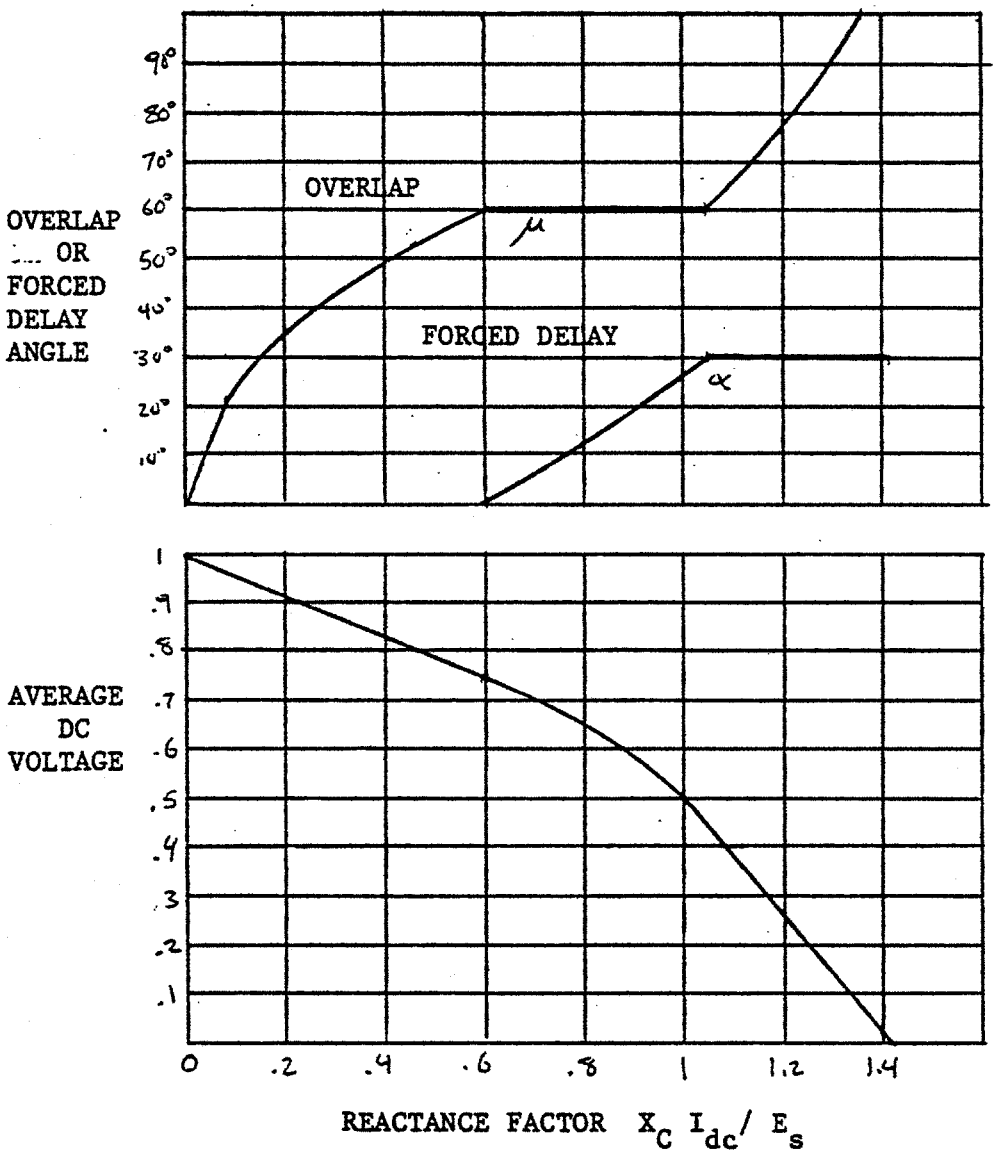

Figure A-1: Regulation characteristics of six-pulse rectifiers
Upper graph: Overlap and forced delay angles as a function of reactance factor. Lower graph: normalized dc output voltage as a function of reactance factor (from reference #1)

which is termed the "reactance factor", where X_c is the ac rectifier source reactance in ohms, I_{dc} is the commutated dc load current, and E_s is the sinusoidal line-to neutral voltage behind the source reactance. In the upper half of figure A-1 the overlap and forced delay angles are shown as a function of the reactance factor.

Two six pulse rectifiers connected in the twelve pulse rectifier configuration do not operate independently if any fraction of the commutation reactance is shared between them. If the two supplies share some fraction of the source reactance, then five modes of operation are defined as the rectifier load increases from no-load to short circuit. The ratio of the shared reactance to the total reactance, K, is used in conjunction with the reactance factor (as defined for the six pulse case) to determine the input-output characteristics of the twelve pulse circuit. As in the six pulse case, the modes of operation correspond to particular limits of overlap angle and forced delay angle. The twelve pulse relationships are plotted in figure A-2.

In power supplies of the type investigated in this study, rectifier load current is regulated and inverted by the use of intentional rectifier firing delay (phaseback). The curves of figures A-1 and A-2 can only be used when the intentional phaseback is zero. The curves can be expanded to include the effect of phaseback as ahown in figure A-3 for the six pulse case. The normalized output voltage is shown as a function of the reactance factor and the intentional p haseback angle.

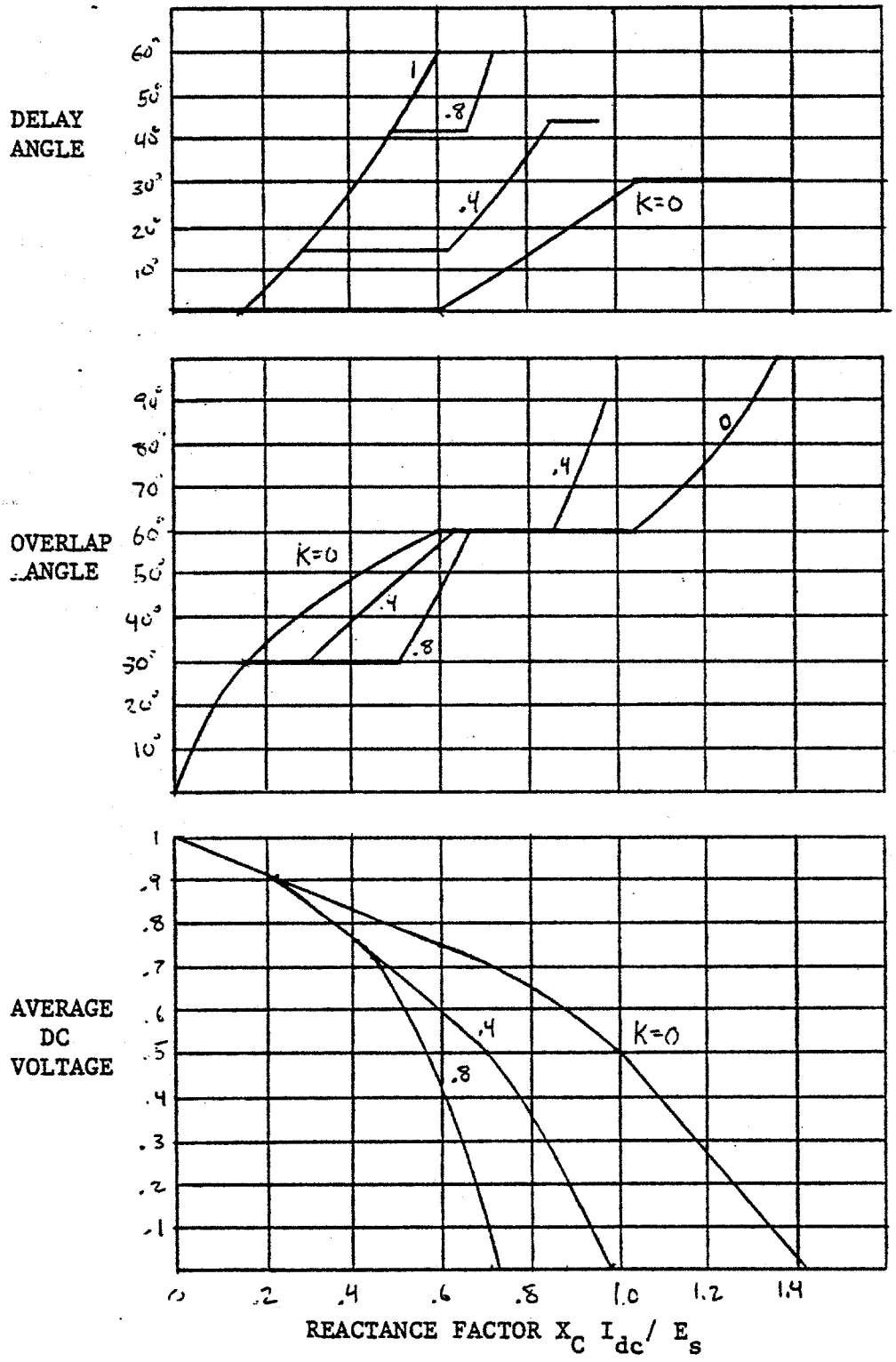

Figure A-2: Regulation characteristics of twelve-pulse rectifiers as a function of reactance factor. for various values of K. Upper graph: Overlap angle. Middle graph: delay angle. Lower graph: Normalized dc output voltage. (from reference #2)

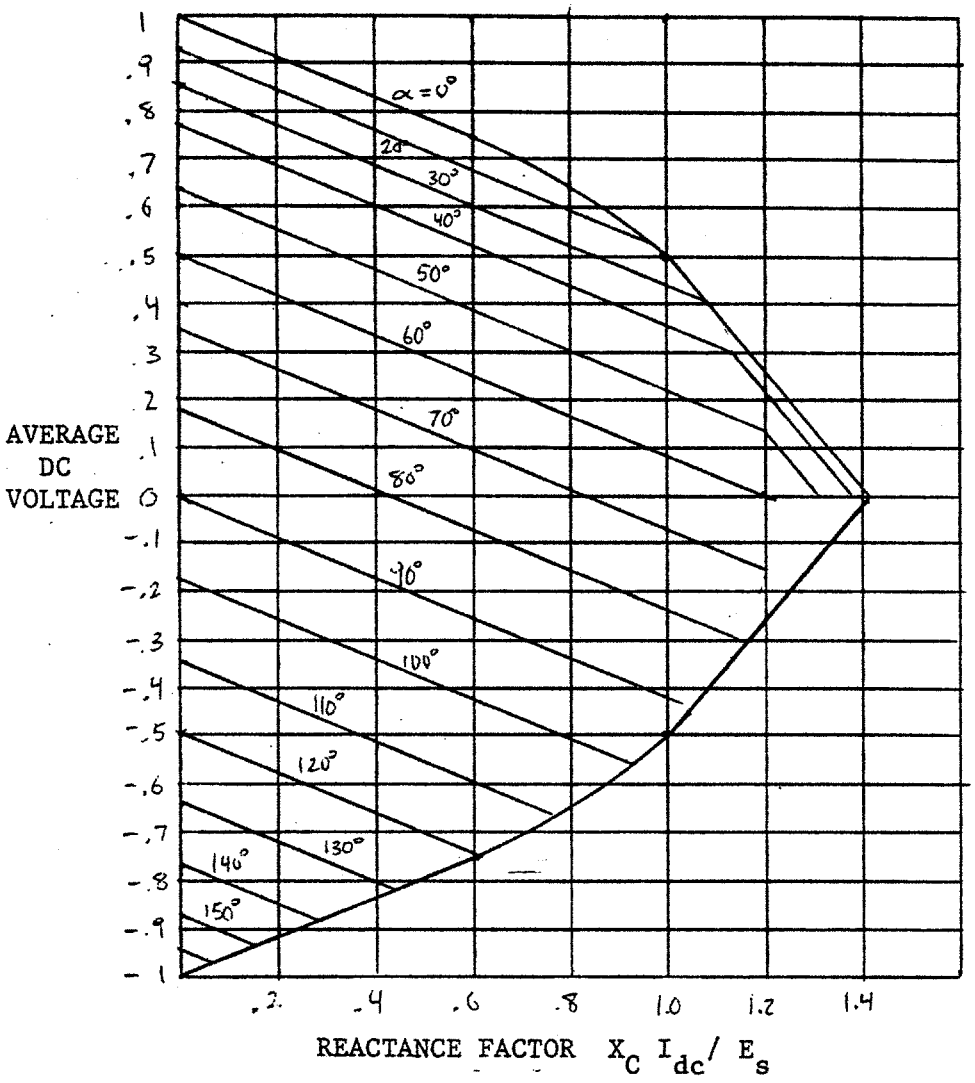

Figure A-3: Regulation characteristics of a six-pulse rectifier as a function of reactance factor for various values of rectifier phaseback

APPENDIX B

SCALE MODEL POWER SUPPLY
DETAILED CIRCUIT DESCRIPTIONS

This appendix contains circuit descriptions of the subsystems forming the physical scale model power supply. Subsystem divisions are according to the diagram of figure B-1; the principles of operation of each block are detailed in the following sections.

Figure B-2: Reference signal generator

The function of the reference signal generator is to provide attenuated, ground referenced line-to-line bus waveforms at the 15 V p-p level, which are ultimately used by the gate firing systems to properly time the thyristor gate pulses.

Referring to the schematic, the bus waveforms are applied to the primary of the delta-wye transformer. The neutral tap of the wye connected secondary is grounded, and the secondary terminal voltages referenced to ground are consequently A-B, B-C, and C-A. The transformer output A-B is coupled through an attenuator to the diode protected inverter A1. The low impedance output of A1 is the 15 V p-p B-A output. This signal is inverted by A2 to form the low impendance A-B output. Transformer outputs B-C and C-A are

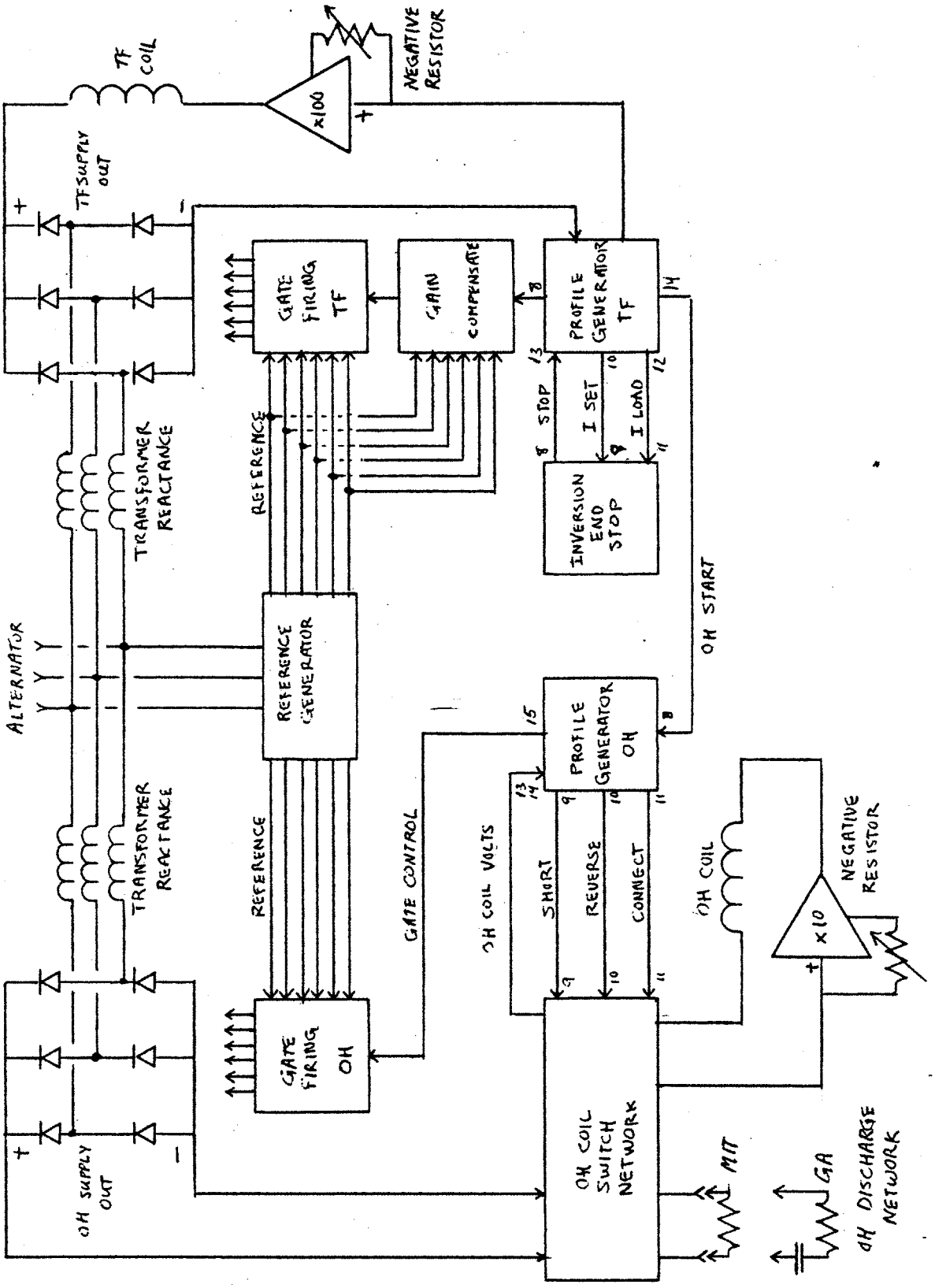

Figure B-1: Diagram showing subsystem divisions of scale model power supply system

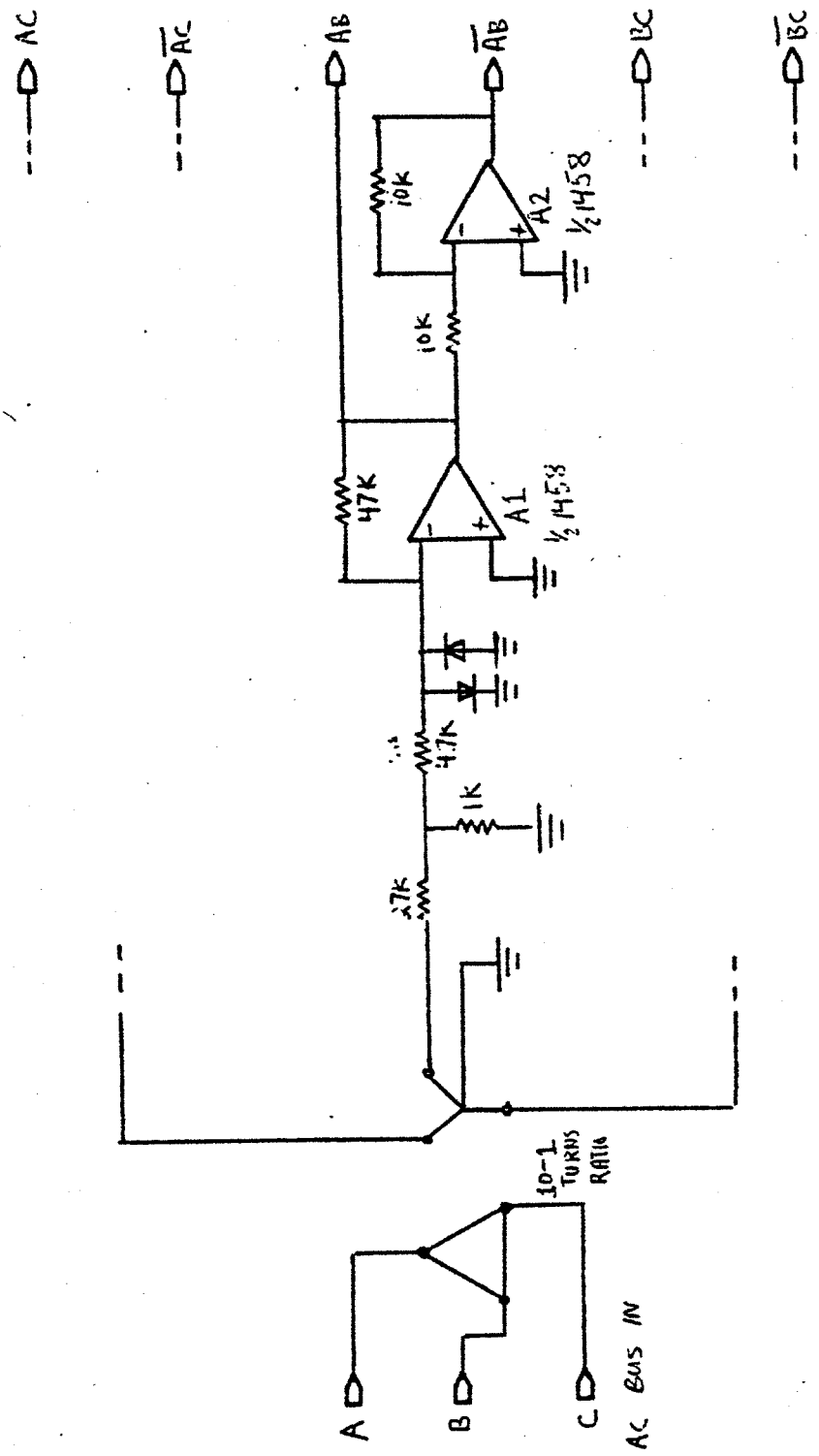

Figure B-2: Schematic of reference signal generator (1/3 of complete circuit)

processed in an identical manner to form the reference outputs B-C, C-B, C-A, and A-C.

Figure B-3: TF supply profile generator

The TF supply profile generator is the source of timing signals which begin the TF coil ramp-up and inversion periods. The "master/slave" switch selects the source of the sequence initiation signal. In the "master" position the initiation signal is supplied by the "start" switch, which is de-bounced by cross-coupled nand gates. The "slave" position allows for external triggering. The selected initiation signal triggers the monostable delay DL1 and provides a timing signal to the OH supply profile generator via connector pin 14.

The output of delay DL1 is used to provide temporary lock-out of DL2 triggering, and to set flip-flop FF1. When FF1 is set, the analog switch Q1 is closed via level shifter A1, causing the output at output-pin 9 to rise from zero to the value present at pin 10, which is set by the "level" control. Manual control of Q1 is provided for test purposes by the "regulate only" switch.

Due to the closing of analog switch Q1, the load current regulator, described in the next section, will force the rectifier load current to rise until it reaches a value (the flat-top level) which is determined by the output voltage at pin 9. When the flat-top load current level is reached, the main TF rectifier bridge is phased- back to

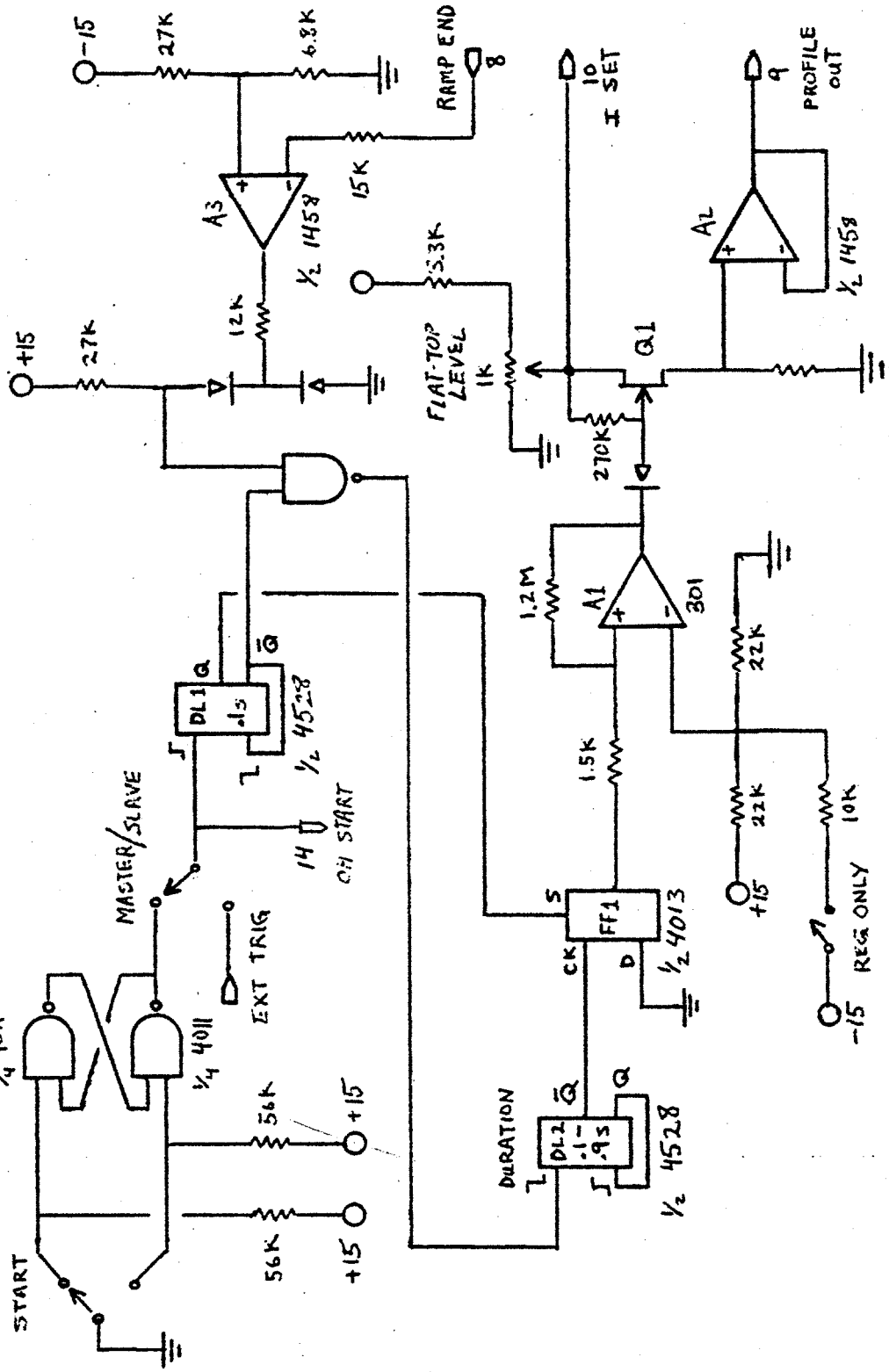

Figure B-3: Schematic of TF supply profile generator

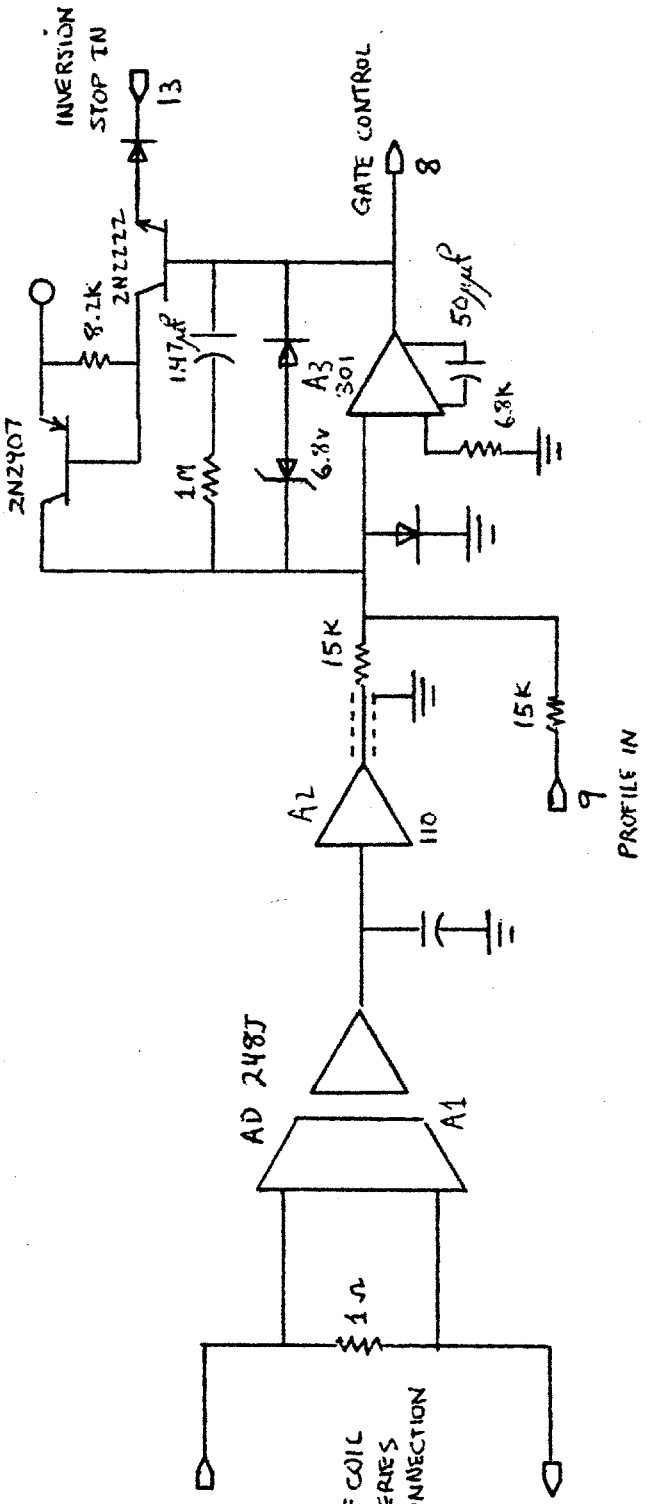

Figure B-4: Schematic of TF current regulator

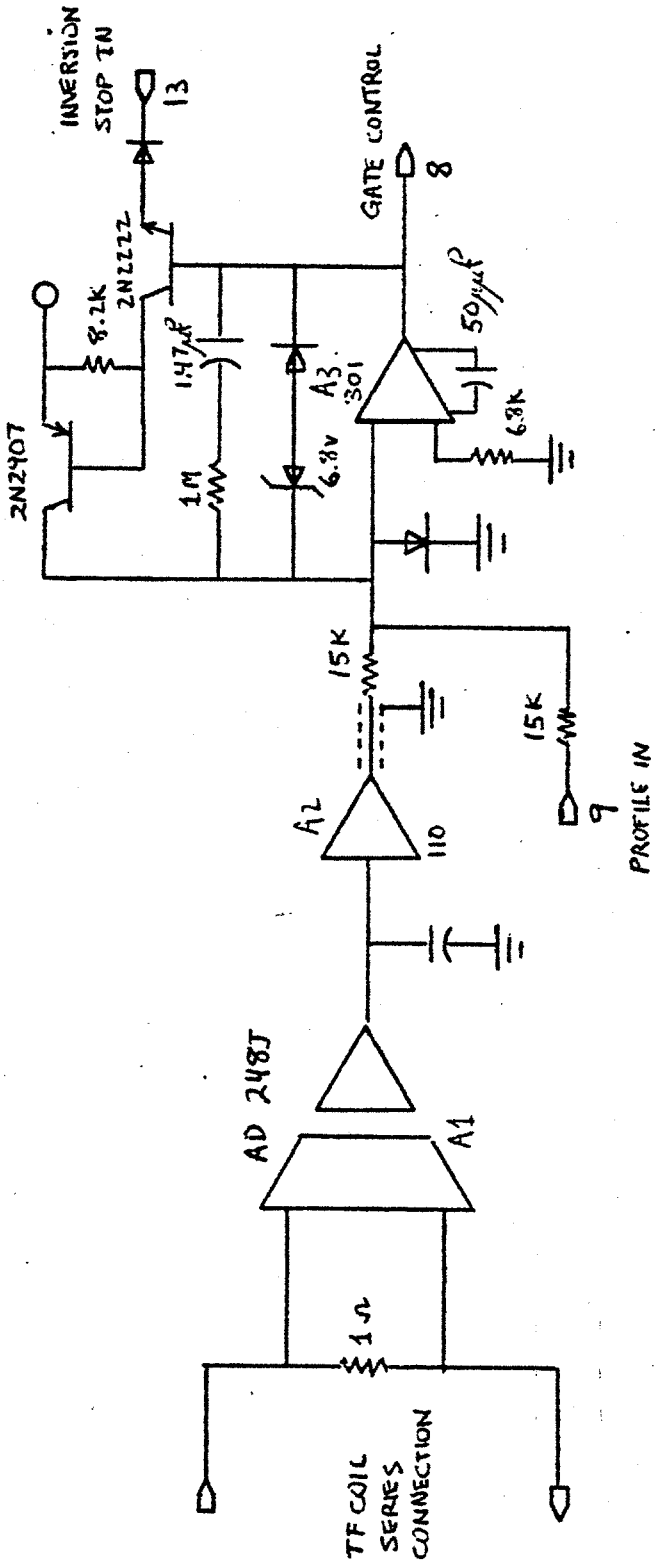

Figure B-4: Schematic of TF current regulator

maximum rectifier output voltage for the duration of the ramp-up period.

When the model confinement coil current rises to the flat-top level, the amplifier A3 will return to the linear mode of operation, and will control the main bridge firing angle via J8 in order to drive to zero the sum of the voltages at J9 and the output of A2.

A conventional 1/s (single pole) open loop characteristic is used to give well damped dynamic response and zero steady state regulator error. Amplifier A3 is therefore connected as an integrator. The resistor in series with the integrating capacitor, which adds a zero to the transfer function, is selected to cancel the excess pole generated by the rectifier load L/R time constant.

Figure B-5: Inversion end stop limit circuit

The inversion end-stop can be made an arbitrary single-valued function of the load current by adjustment of the nine inversion end-stop controls. The load current is inverted by A2 and compared to the set-point level buffered by A1. A voltage divider chain establishes eight voltage levels corresponding to the percentages of the set-point level from 0%-100% by increments of 12.5%. The end-stop control level is auctioneered to the lowest control wiper setting through the "diode or" system composed of R13 and D1-9. As the current in the load falls, comparators corresponding to successively lower percentages of the set-point current go "high", allowing the end stop control to rise to

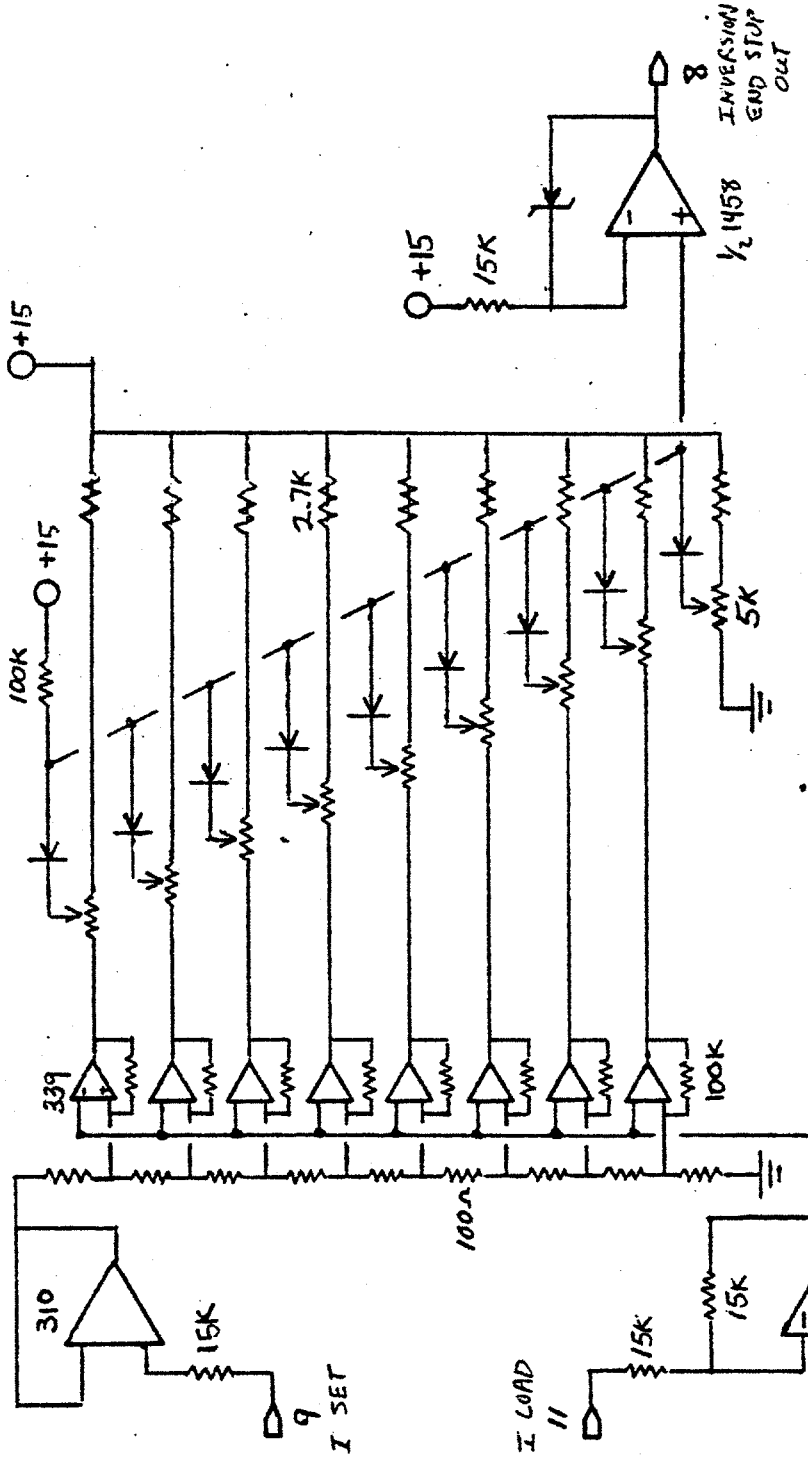

Figure B-5: Schematic of inversion end stop limit circuit

the value determined by the remaining "low" comparators. The final inversion limit is set by R21, and acts when the load current falls to less than 12.5% of the set-point value. A3 acts as an output level shifter. The output goes to a gate control signal clamp located in the profile generator circuit.

Figure B-6: TF regulator loop gain compensator circuit

This circuit compensates for regulator loop gain changes which result from variations of the main ac bus frequency. These gain changes are due to the nature of the gate firing circuit transfer characteristic.

The six reference waveforms from the reference signal generator circuit are integrated, rectified, and filtered. The resulting dc voltage, which is inversely proportional to reference frequency, is level shifted up to compensate for rectifier drop. This voltage is then multiplied by the regulator output voltage. The output of the multiplier drives the proprietary cosine-intercept type gate controller manufactured by Robicon Corporation of Pittsburg, Pa.

Figure B-7: OH profile generator

The OH profile generator is the source of timing signals which control the OH supply rectifier phaseback angle and the relay switches in the OH coil switching network.

A rising edge at input pin 8 indicates the start of the TF coil current ramp to begin the OH sequence. This signal triggers the "start delay" DL1 and sets FF1. The

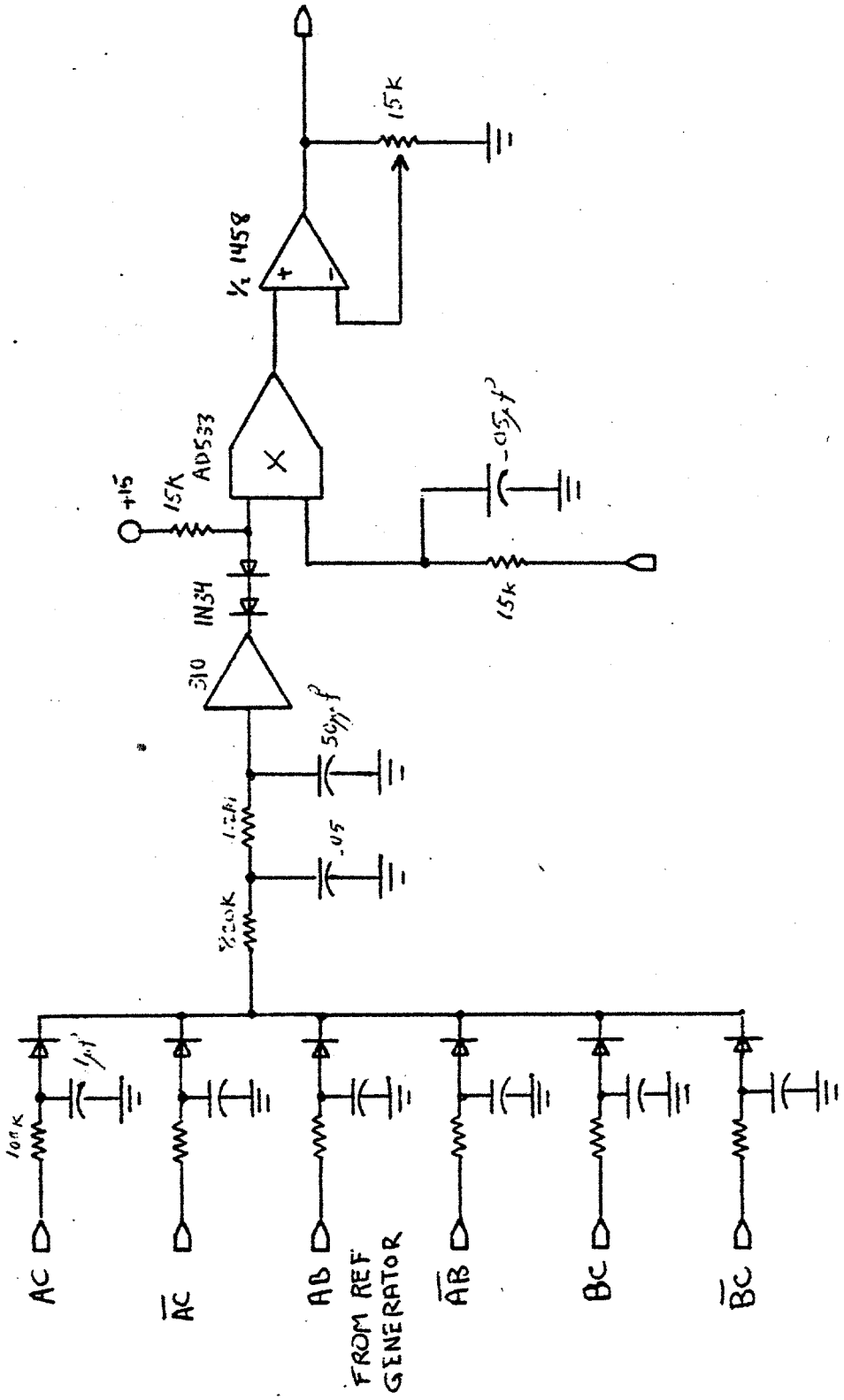

Figure B-6: Schematic of TF regulator loop gain compensation circuit

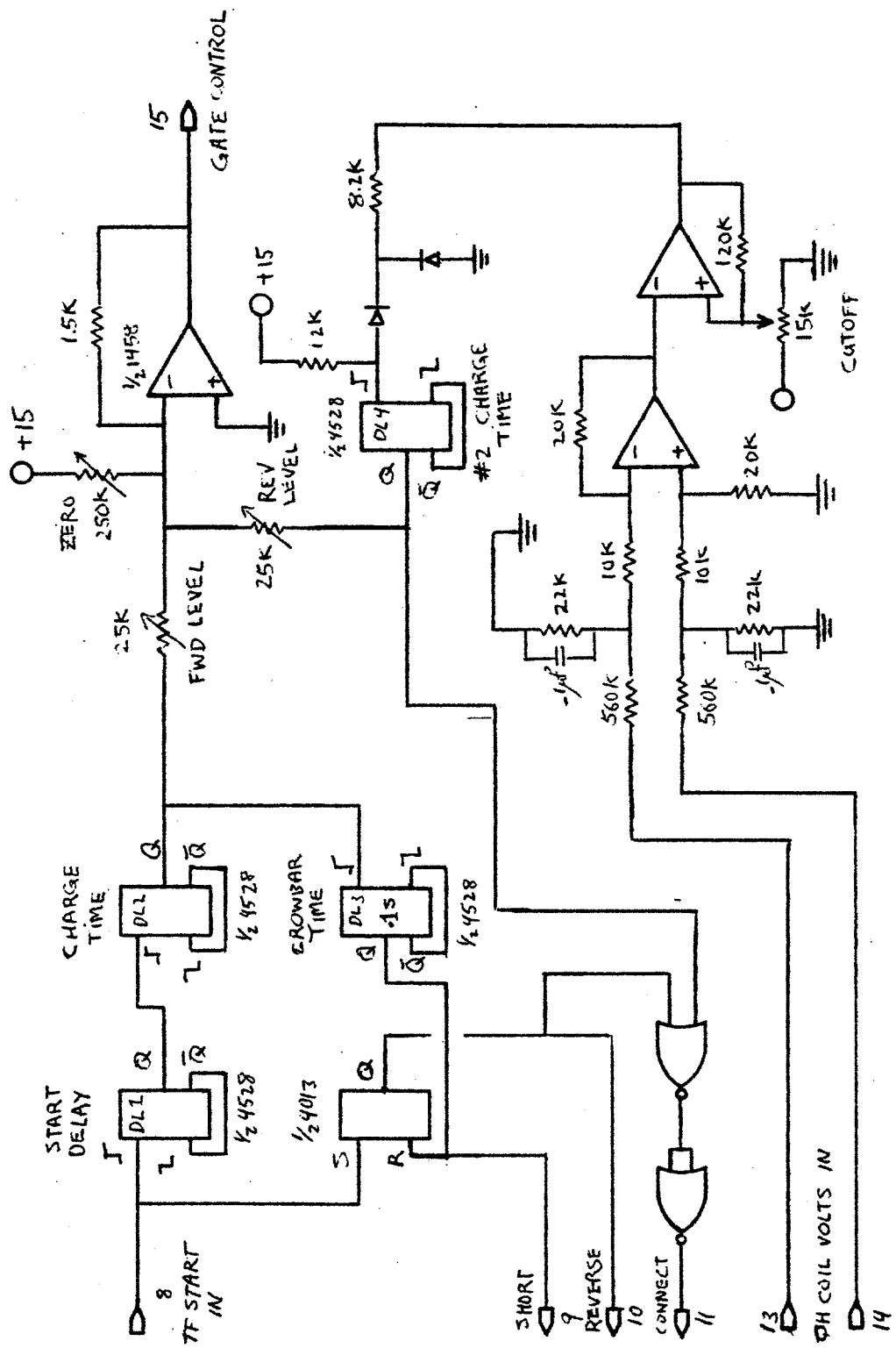

Figure B-7: Schematic of OH profile generator

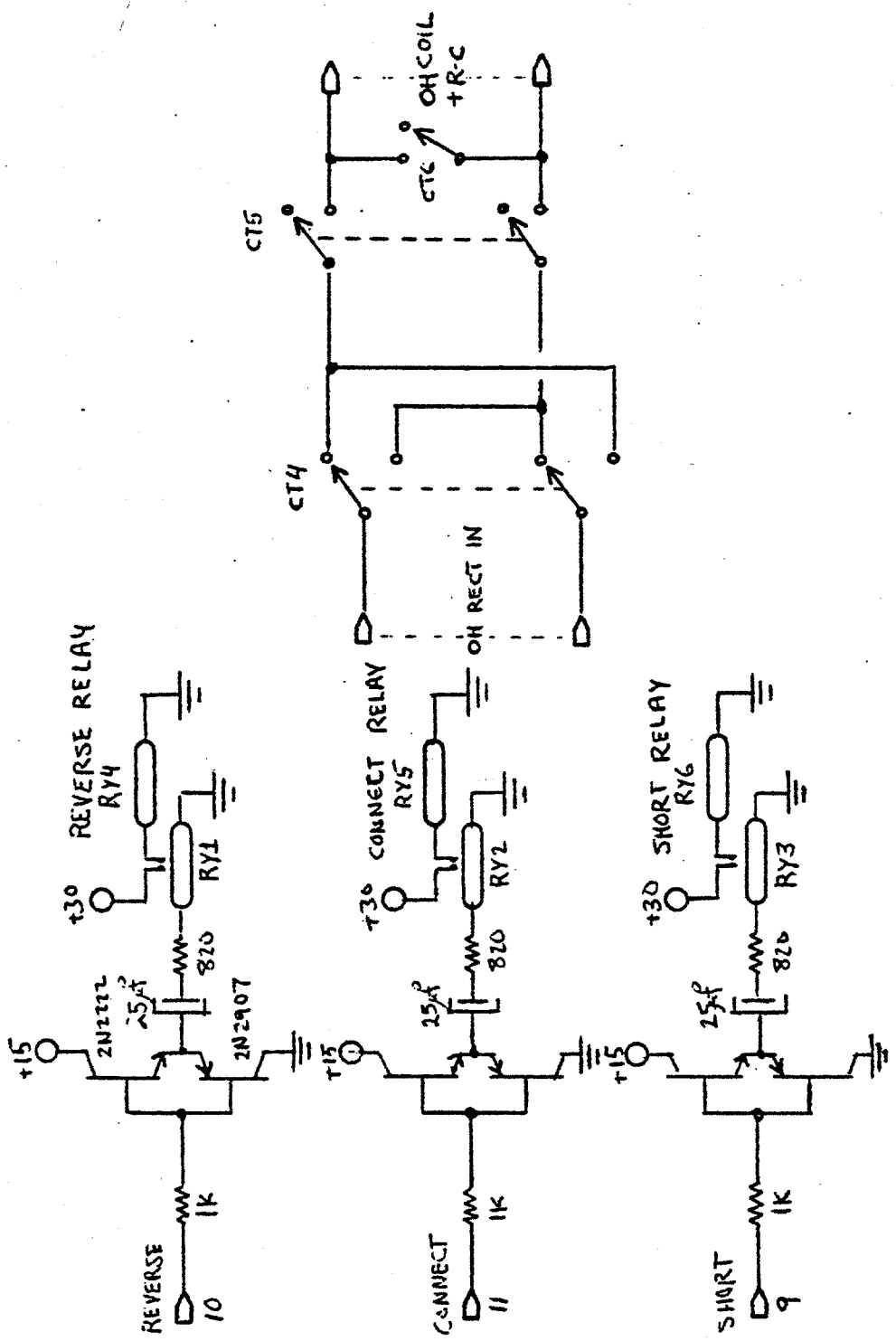

Figure B-7 continued

flip-flop FF1 drives output pins 10 and 11 high, commanding the OH coil switching network to connect the output of the OH supply to the OH coil. At this time the gate control output voltage is zero, which forces a rectifier set output voltage of zero. After a time which is adjustable from 0 to 6 seconds the output of the start delay DL1 will fall, triggering the charge time delay DL2. The output of DL2 will be high during the OH coil charging period, driving the gate control output negative to a level set by the FWD LEVEL control. The negative output at pin 15 forces the OH rectifier set phaseback angle to advance, causing the rectified output voltage to rise and begin charging the OH coil.

At the end of the OH coil charging period the output of DL2 falls, returning the rectifier set output voltage to zero via pin 15. The falling output of DL2 also shorts the OH coil with a relay switch for .1 second via DL3 and pin 9. At the beginning of this .1 second interval the rising edge of the DL3 output resets FF1, simultaneously disconnecting and reversing the polarity of the OH supply output via output pins 10 and 11. The supply is thereby prepared for the second OH coil charging interval.

At the end of the .1 second time period the output of DL3 falls, opening the OH coil shorting relay. At this time the charged OH coil is connected only to the high impedance OH coil discharge network, which conducts the entire OH coil current to develop a very high OH coil voltage and consequently high $\delta i/\delta t$.

When the OH coil voltage decays to within the OH supply output voltage range, comparator A2 changes state, reconnecting the OH supply via DL4 and output pin 11 for the second OH charging interval. The OH supply output voltage during the second charging interval is determined by the REV LEVEL control.

Figure B-8: Alternator voltage regulator

An alternator voltage regulator is required for simulation of the Doublet III system. The alternator voltage is supplied to the regulator circuit from three wye connected step-down transformers. The phase voltages are rectified and filtered using time constants taken from the schematic of the actual Doublet III exciter/regulator. The integral of the difference between the detected alternator voltage and a preset voltage is amplified by A2 and supplied to the voltage-controlled alternator exciter via the circuit output.

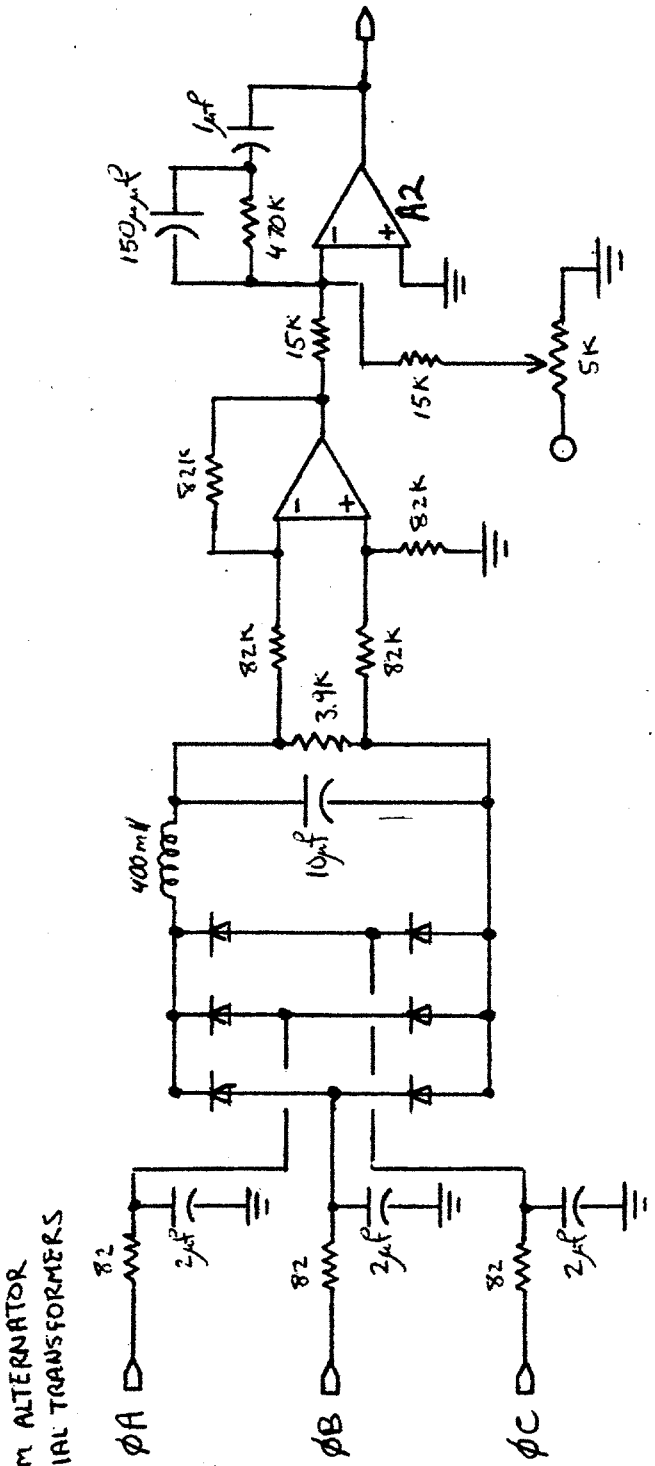

Figure B-8: Schematic of alternator voltage regulator

APPENDIX C

COMPUTER PROGRAM

DETAILED DESCRIPTION

The computer routine which was used in Chapter III to model the Alcator C TF power supply during the ramp-up period is described in this appendix. The program was run on an IMSAI 8080 minicomputer system using the BASIC programming language. The program itself is listed in table C-1. The program description that follows is divided into three parts which correspond to the numerical models of the alternator, the TF rectifier set, and the TF supply load.

Part 1: Computer model of Alternator

The alternator model is initialized by specifying the rotational speed (program line 120) and flux (line 130) of the alternator at the beginning of the experiment. A FOR loop (line 25) commands the program to run for four values (.9, 1, 1.1, and 1.2 pu) of starting flux consecutively. At each time interval ΔT, the alternator computer model accepts as inputs the most recent estimates of A) the armature current and B) the angle between the fundamental component of the armature current (I_a) and the sinusoidal voltage behind subtransient reactance (E_d"). The alternator model outputs are A) the value of E_d" and B) the value of the alternator electrical frequency (ω).

The value of the output variable E_d" is determined at each time step from a simplified phasor diagram. The vector

addition which is required in order to determine E_d" may be performed once the value of the alternator reactance, minus the subtransient reactance, is determined.

We expect that the alternator reactance above E_d", as seen by a small step increment in armature current, will start at the value X_d' and then rise to X_d with time constant T'_{dx}(loaded). Consequently, the response of the reactance to a time function of armature current, $I_a(t)$, is given by:

$$X = \omega(pu)\left[X_d' + (X_d - X_d') \int_{-\infty}^{t} u_{-1}(x) e^{-x/T_{dx}'} I_a(t-x)\,\delta x \right]$$

The variable T_{dx}' is the loaded field time constant and its value is approximately given by the formula [11]:

$$T_{dx}' = \frac{X_1 X_2 + X_e(X_1+X_2) + X_e^2 + R_e^2}{X_1^2 + 2X_1X_e + X_e^2 + R_e^2} \times T_{do}'$$

where $X_1 = X_d - X_d$", $X_2 = X_d' - X_d$", $R_e = \cos\theta / I_a$, and $X_e = \sin\theta / I_a$ with θ equal to the angle between E_d" and I_a

Unfortunately, the fact that the time constant T_{dx}' is a function of $I_a(t)$ causes the convolution in the reactance equation to be non-linear; therefore, the non-standard algorithims described below are used to perform the convolution.

On the nth time step, the convolution routine operates on the array variables ΔI_{ak}, $\Delta X(n-1)_k$, and the variables $I_a(n-1)$ and $\omega(n-1)$. The required value of X(n) is a routine output, along with the auxillary array variable $\Delta X(n)_k$

which is a required input for the n+1th routine. The array variable ΔI_{ak} is defined for k=0 to n and is given by:

$$\Delta I_{ak} = I_{ak} - I_{a(k-1)}$$

The array variable $\Delta X(n)_k$ is also defined for k=0 to n and is given by:

$$\Delta X(n)_k = \Delta X(n-1)_k + (X_d - X_d" - \Delta X(n-1)_k)\Delta t/T_{dx}'$$

where T_{dx}' is calculated using $I_a(n-1)$ as the armature current. The above expression is realized in program line 520.

The value of X(n) is determined at each time step to complete the discreet time convolution:

$$X(n) = \omega(n-1)\times\left[X_d' - X_d" + \left[\left(\sum_{k=0}^{n} \Delta X(n-1)_k \, \Delta I_{ak}\right)/I_a(n-1)\right]\right]$$

The voltage drop across X(n) is computed by multiplying X(n) times I_a. The above expression, including the multiplication by I_a, is accomplished in program lines 500 to 550. The phasor addition required to determine $E_d"$ is now performed in line 610.

The electrical frequency, ω, of the alternator is adjusted by the program at each time step, in order to model the change in rotational energy which must accompany electrical power transfer through the armature terminals. Conservation of energy dictates that:

$$\frac{\delta\omega}{\delta t} = E_d" \, I_a[\arccos(\text{power factor})]/J$$

The discreet time equivalent of this expression is used in program steps 450 and 460 to solve for the alternator electrical frequency. Notice that program steps 390 to 410 account for the presence of the OH supply to a first order by adding the OH load to the armature current.

In summary, the computer model has been shown to generate the required alternator output variables at each time step, namely $E_d"(n)$ and $\omega(n)$. These variables are required by the rectifier set model, which is described in the next section.

Part 2: Computer model of TF supply rectifier set

This coumputer routine is required to represent the TF supply six pulse rectifier set during the TF coil current ramp-up period, when the rectifiers are operated without intentional phaseback. For six pulse rectifiers with source reactance, the average dc rectified output voltage can be determined from the equations from reference[1], which are implemented in program steps 230 through 360. A description of the effects of source reactance on six pulse rectifiers can be found in Appendix A.

The routine inputs are the commutation reactance, the alternator frequency, the magnitude of the internal alternator voltage $E_d"$, and the load current I_{dc}. The routine outputs the values of the average rectified dc output voltage and the rectifier input power factor. The described routine is called upon during each time interval ΔT, and makes use of the latest computed values of the input variables to determine the current values of the output variables. The

routine contains no difference equations or memory terms and consequently does not require initialization.

First, the program computes the commutation overlap angle (line 240). If this angle is less than 60 degrees, then the rectifier is in mode one operation, and the overlap angle is used to determine the mode one output voltage (line 340) and power factor (line 360). If the overlap angle is greater than 60 degrees, then the rectifier is in mode two operation, and the delay angle is computed (line 310) and is then used to determine the mode two output voltage (line 290) and power factor (line 320). The power factor output from this routine is used by the previously described alternator model, while the value of the average dc rectifier output voltage is used by the load model, which is described in the next section.

Part 3: Computer model of TF supply load

During a program time step the rectifier load is modelled as a simple series L-R circuit. The current increment occuring a time step is given by:

$$\Delta I_{dc} = (V_{dc} - I_{dc}R)\Delta T/L$$

where

$$V_{dc} = V_{rect} - I_{dc}(R_{bus}+R_{transformer})$$

This expression is realized in program line 370.

TABLE C-1

LISTING OF COMPUTER PROGRAM

```
10 X1=1.41    'SYNC REACTANCE
20 DIM DI(40),XX(40),ZD(40)
25 FOR BJ=0 TO 3
30 X2=.265'TRANS REACTANCE
40 X3=.12'SUBTRANS REACTANCE
50 XT=.27'TRANSFORMER X
60 XB=.05'BUS X
70 T1=7'TDO'
80 T2=1.09
90 T3=T1
100 R3=3E-04   'RTRANS
110 R2=1E-04   'RBUS DC
120 W=.98
130 V1=.9+(BJ*.1)
131 I=0
132 N=0
133 FOR QK=0 TO 40
134 XX(QK)=0
135 NEXT
140 RL=2.2E-03   'LOAD R
150 LL=4.5E-03 'LOAD L
160 M1=530   'ROTATIONAL INERTIA
170 H=16'TRANSFORMER TURNS RATIO
180 J=(W^2)*M1'ROTATIONAL ENERGY
190 V=V1*W*14400    'LINE LINE VOLTAGE
200 T=.05'TIME INCREMENT
205 GOTO 220
210 PRINT USING "\        \";"TIME";"FREQ";"CURR";"VDC";"PF";"ED'"
220 X4=X2-X3     ' X LOADED
230 X=(XT+XB+X3)*.922*W   'XC IN OHMS
240 C=1-(2^.5)*X*I/V'COSINE OF OVERLAP ANGLE
250 IF C<.5 GOTO 270
260 GOTO 340
270 C=.5'MODE 2
280 S=(2^.5)*I*X/V'MODE 2
290 E=3*(1.5^.5)*V*((1.0001-S^2)^.5)/3.1416'MODE 2 OUTPUT VOLTS
300 A=ATN(S/((1.0001-S^2)^.5))'FAKE ARC COS FUNCTION
310 A=(A*180/3.1416)-30'DELAY ANGLE
320 F=COS((1.1*A+39.3)*3.1416/180)'POWER FACTOR
330 GOTO 370
340 E=V*3*(1+C)/((2^.5)*3.1416)  'MODE 1 OUTPUT VOLTS
350 U=ATN(((1-C^2)^.5)/C)'MODE 1 OVERLAP
360 F=(1+COS(.95*U))/2'POWER FACTOR
370 D=(E-(I*((R3+R2+RL)*(H^2))))*T/(LL*H^2)'CURRENT INCREMENT
380 I=I+D'NEW LOAD CURRENT
```

TABLE C-1 continued

```
390 IF I<9000 GOTO 430'CHECK FOR START OF OH
400 P=E*I*1E-06+20*(I-9000)/3500'SUBTRACT OH POWER
410 I1=.78*I+.4*(I-9000)'GEN CURRENT WITH OH
420 GOTO 450
430 P=E*I*1E-06'POWER WITHOUT OH
440 I1=.78*I'RMS GEN CURRENT WITHOUT OH
450 J=J-P*T'NEW ROTATIONAL ENERGY
460 W=(J/M1)^.5'NEW SPEED
470 X9=X1-X2
480 VX=0
490 K=INT(N/T+.5)
500 DI(K)=D
510 FOR M=0 TO K
520 XX(M)=XX(M)+(X9-XX(M))*T/T3
530 VX=VX+DI(M)*XX(M)*.922*W
540 NEXT
545 VK=VX
550 VX=VX+I1*(X2-X3)*.922*W
560 Z=9410/(I1+1)'PER UNIT LOAD Z
570 R1=Z*F 'LOAD R
580 X6=Z*((1.0001-F^2)^.5)'LOAD X
582 X7=X1-X3
583 X8=X2-X3
590 T3=(X7*X8+X6*(X7+X8)+X6^2+R1^2)*T1'LOADED TIME CONSTANT NUMERATOR
600 T3=T3/(X7^2+2*X7*X6+X6^2+R1^2)'LOADED TIME CONSTANT DENOMINATOR
610 V=(((V1*W*14400)^2-(VX*F)^2)^.5-VX*(1.0001-F^2)^.5)'PHASOR ADD
620 GOTO 640'DELETE THIS STATEMENT FOR ED" OVER W CONSTANT
630 V=V1*W*14400
640 E=E-((R3+R2)*(H^2)*I)'GET COIL VOLTS BY SUBTRACTING IR DROP
650 N=N+T'INCREMENT TIME
660 IF N>2 GOTO 682
670 A$="#.##      ##.#     ######     ####    #.###     #####    #####"
680 PRINT USING A$;N;60*W;I*H;E/H;F;V;VK
681 GOTO 230
682 NEXT
683 END
```

BIBLIOGRAPHY

1. Witzke, R.L. et al, "Influence of A-C Reactance on Voltage Regulation of 6-Phase Rectifiers"; AIEE Transactions, Vol. 72 pt.1, 1953.

2. Witzke, R.L. et al, "Voltage Regulation of 12-Phase Double-Way Rectifiers"; AIEE Transactions, Vol.72, pt.1, 1953.

3. Bachtel, W.C. "Effect of Thyristor Loading on AC Generators"; Diesel and Gas Turbine Progress, April, 1975.

4. Praeg, W.F. "A Pulsed Power Supply For Tokamak Equilibrium Field Coils" IEEE Power Electronics Specialist Conference Record, 1977.

5. Fitzgerald, A.E., Kingsley, C., and Kusko, A. Electric Machinery McGraw-Hill, New York, 1971; section 6.3.

6. Kimbark, E.W. Power System Stability: Synchronous Machines , Dover New York, 1968; pages 40-69.

7. Blake, S.A.R.M., and Kassakian, J.G. A Physical Scale Model of the Alcator C Toroidal Field Power Supply; EPSEL Report #49, MIT Cambridge, Mass., 1977.

8. Umans, S.D., "Modeling of Solid Rotor Turbogenerators", PhD Thesis, MIT EE Dept. Cambridge, Mass., 1976.

9. Umans, S.D., and Wilson, G.L., Physical Scale Model of a Power System - A User's Guide; EPSEL Report #36 MIT , Cambridge, Mass. 1973.

10. McMurray, W. The Theory and Design of Cycloconverters, MIT Press, Cambridge Mass. 1972.

11. Wagner, C.F. Electrical Transmission and Distribution Handbook; Westinghouse Corp.

12. Haenen, G.H. "Evaluation of Mains Borne Harmonics Due to Phase Controlled Switching" Phillips Engineering Applications Bulletin Vol. 33 #1.